NATIONAL ADVISORY COMMITTEE FOR AERONAUTICS

TECHNICAL NOTE 3784

HANDBOOK OF STRUCTURAL STABILITY

PART IV - FAILURE OF PLATES AND COMPOSITE ELEMENTS

By George Gerard

New York University

Washington
August 1957

TABLE OF CONTENTS

Page

NATIONAL ADVISORY COMMITTEE FOR AERONAUTICS

TECHNICAL NOTE 3784

HANDBOOK OF STRUCTURAL STABILITY

PART IV - FAILURE OF PLATES AND COMPOSITE ELEMENTS

By George Gerard

SUMMARY

Available theories on failure of flat plates are reviewed. In terms of the results of these theories, available test data on the postbuckling behavior, effective width, and failure of flat and curved plates are correlated.

Test data on the crippling strength of various formed and extruded shapes are reviewed, from which a generalized method of crippling analysis is formulated. The effects upon the crippling strength of alclad coatings and the increased properties in the corners of formed sections are investigated by use of this analysis.

The generalized crippling analysis was applied to a variety of sections and materials in common use. It was found that the crippling strength of all the sections is governed in a simple manner by the developed length-thickness ratio and number of corners of the section.

INTRODUCTION

The present report is concerned with the failure of flat and curved plates and composite elements which are subject to buckling under compressive loads. For composite elements such as Z- or channel sections, the failure mode considered is that commonly referred to as crippling. Thus, the effective slenderness ratio of the composite elements is in the neighborhood of 20, a region in which variations in length result in negligible changes in the crippling strength.

In the section entitled "Basic Principles," the postbuckling behavior of columns, plates, and cylinders is briefly reviewed in order to determine those elements for which the failure load may considerably exceed the buckling load. Because of the mathematical complexities inherent in any theoretical treatment of the failure phenomenon, the available theories constitute an important contribution to the understanding of the factors operative at failure. Therefore, a comprehensive review of results obtained for hinged flanges is presented in the next section. This analysis serves as a reference frame from which semiempirical methods can be devised to treat failure of elements not amenable to theoretical solution.

In the next two sections, the postbuckling behavior, effective width, and failure of flat and curved plates are considered. Particular attention is devoted to the influence of the unloaded-edge boundary conditions upon failure of flat plates. The crippling strength of extruded and formed composite elements such as angle, Z-, channel, H-, and square-tube sections is treated in the following two sections. Various semiempirical methods are used to correlate the large mass of available test data. In particular, a generalized crippling analysis is presented which is both simple and nondimensional in form. By use of this analysis, the effect of the increased properties in the corners of formed sections has been investigated. Further, a method was studied for correcting for the alclad coating which may be present on formed sections.

In the section "Crippling of Sections of General Shape," the generalized crippling analysis was applied to unequal-flange, Z-, and channel sections, J-sections, lipped Z- and channel sections, hat sections, and other formed shapes. It was found that all available test data reported in the literature on various shapes and materials could be correlated according to the developed length-thickness ratio and the number of corners of the section.

In the appendix at the end of this report, the various results of importance in analysis and design are compiled for convenience. It is to be noted that failure of stiffened panels is treated in Part V of this Handbook (ref. 1). A discussion of failure of flat and curved tension-field members has been presented previously by Kuhn, Peterson, and Levin (ref. 2).

This survey was conducted under the sponsorship and with the financial assistance of the National Advisory Committee for Aeronautics.

SYMBOLS

A	area, sq in.
A_r	area of rib cross section, sq in.
a	length of plate, in.; also coefficient in equation (29)
b	width of plate, in.; also coefficient in equation (30)
$\bar{b}$	developed width or length of cross section, in.
b_e	effective width per edge, in.
b_f	width of flange, in.

b_w	width of web, in.
$C,\bar{C}$	coefficients
c	number of corners
E	elastic modulus, psi or ksi
E_s	secant modulus, psi
f	number of flanges; also ratio of total cladding thickness to total plate thickness
K	modified buckling coefficient, $\pi^2k/12(1 - \nu^2)$
K_c,k_c	buckling coefficients of curved plate, $K_c = \pi^2k_c/12(1 - \nu^2)$
k	buckling coefficient
L'	effective length of column, in.
m,n	exponents in stress equations
P	load, lb
R	radius, in.
t	thickness, in.
v,w	displacements, in.
x,y,z	coordinates
Z_b	curved plate parameter, $(b^2/Rt)(1 - \nu^2)^{1/2}$
α,β	coefficients
β_c	crippling coefficient for multicorner sections
ϵ	axial strain
$\bar{\eta}$	cladding reduction factor
ν	Poisson's ratio
ρ	radius of gyration, in.

σ axial stress, ksi

σ_{cl} cladding yield stress, ksi

σ_{cy} compressive yield stress, ksi

$\bar{\sigma}_{cy}$ average compressive yield stress in corner of formed section, ksi

$\bar{\sigma}_f$ failure or crippling stress, ksi

$\sigma_x, \sigma_y, \tau_{xy}$ membrane stresses

Subscripts:

av average

cr critical

e edge

f flange

o initial

p flat plate

r reduced value

w web

BASIC PRINCIPLES

In Part I of this Handbook (ref. 3), the elastic and plastic buckling of flat plates was considered, in Part II (ref. 4) buckling of composite elements was summarized, and in Part III (ref. 5) buckling of curved plates and shells was treated. In certain cases, buckling terminates the ability of the element to carry additional loads and, therefore, buckling and failure are essentially coincident. In other cases, primarily in flat and slightly curved plates which buckle elastically, failure occurs at loads considerably in excess of the buckling load. It is the purpose here to delineate the physical principles involved in the postbuckling behavior of various elements in order to examine in detail those elements for which the failure load may considerably exceed the buckling load.

Except for those cases in which the buckle form itself is unstable as discussed in reference 5, failure is generally a combination of large-deflection effects initiated at buckling and plasticity effects. Because of the nonlinearities associated with both large deflections and plasticity, the problem of determining the theoretical failing load of any buckled element is mathematically complex, if not intractable. However, since buckling initiates the processes leading to eventual failure, it is of utmost importance that analyses should exist for accurately predicting buckling stresses. Analyses presented in references 3 to 5 provide a key role in constructing a theory of failure, which, because of mathematical complexities, is often semiempirical in nature.

Failure in individual cases is coincident with, or occurs considerably after, buckling. Hence, it is important to examine the postbuckling behavior of various elements to determine the conditions under which the failure load can exceed the buckling load. For this purpose, figure 1 has been prepared. In figure 1(a) the schematic postbuckling behavior of flat plates, columns, and cylinders under axial compression is shown when elastic buckling occurs. Figure 1(b) indicates, schematically, the behavior of flat plates and columns after plastic buckling.

It can be observed from figure 1(a) that, for flat plates and columns, failure occurs at values of w/t well removed from the region where buckling initiates. Thus, small initial imperfections are unimportant. After buckling, the lateral deflection of the column is not restrained in any manner. Therefore, no transverse membrane stresses exist and the postbuckling behavior is represented by a horizontal line. Beyond a certain value of w/t, plasticity effects become important and the σ/σ_{cr} line decreases. Thus, failure occurs at the onset of significant plasticity effects.

For flat plates, the boundary constraints at the unloaded edges permit significant tension membrane stresses to develop after buckling which act to restrain lateral deflection. Thus, flat plates can support loads considerably in excess of the elastic buckling load. As for columns, failure occurs at the onset of significant plasticity effects.

By contrast with flat plates and columns, axially compressed cylinders develop transverse compressive membrane stresses after buckling and thus the buckle form itself is unstable. As discussed in some detail in reference 5, small initial imperfections are important in this case with the result that failure and buckling are essentially coincident. It is important to note that failure is due primarily to the instability of the buckle form rather than to the initiation of plasticity effects, which occurs at considerably larger values of w/t.

The postbuckling behavior of flat plates and columns which buckle plastically is shown schematically in figure 1(b). The general effect of

plasticity is to displace the large deflection curves of the elastic case downward. The nature of the transverse membrane stresses is relatively unimportant with the result that the failing load is very close to the buckling load in both cases.

FAILURE OF FLANGES

A hinged flange is the simplest element, from the standpoint of analysis, which can carry loads considerably in excess of the elastic buckling load. As compared with a column which is unsupported along the unloaded edges and thus deflects appreciably at buckling, the flange is supported along one unloaded edge. This boundary constraint tends to stiffen the flange during postbuckling rotation and permits supercritical loads to be carried.

Although the postcritical (nonlinear, large-deflection) behavior of various types of plates and shells has been investigated in considerable detail, such studies have been based on the assumption that the element followed Hooke's law. As such, the failure phenomenon cannot be observed, since failure is intimately associated with plasticity effects. Because of the nonlinearity of the postcritical behavior and the additional nonlinearities of plasticity, failure analyses of buckled elements are complex.

Fortunately, Stowell succeeded in conducting a failure analysis of a flange with a simply supported, straight, unloaded edge (ref. 6). The results of this investigation are of considerable importance because they supply quantitative data as to the failure mechanism. Furthermore, the analysis provides a reference frame from which semiempirical methods can be devised to treat other cases of failure for which complete analyses do not exist.

The method of analysis used by Stowell (ref. 6) which results in excellent agreement with test data (shown in fig. 2) is as follows:

(a) The strain distribution across the flange at any angle of twist is determined by means of a nonlinear finite-deflection analysis.

(b) This elastic strain distribution is assumed to persist into the plastic region. (Test data shown in fig. 3 tend to substantiate this assumption.)

(c) By use of deformation-type plasticity theory, the strain distribution is transformed into a stress distribution across the width of the flange.

(d) The load carried at successive increments of twist is obtained by graphical integration to determine when a maximum load is reached. Certain of the results of this analysis are presented in some detail in the following discussion.

Postbuckling Behavior

The large-deflection behavior of buckled elements is often conveniently represented by a relationship among the average $\bar{\sigma}$ and critical σ_{cr} stresses and the stress at the unloaded supported edge σ_e. For the hinged flange with the supported edge constrained to remain straight in the plane of the flange, such a relation is given by

$$\frac{\bar{\sigma}}{\sigma_{cr}} = \left(\frac{5}{9}\right) + \left(\frac{4}{9}\right)\left(\frac{\sigma_e}{\sigma_{cr}}\right) \tag{1}$$

For a material which follows Hooke's law, equation (1) can be written in terms of the strain ratios $\bar{\epsilon}/\epsilon_{cr}$ and ϵ_e/ϵ_{cr}. Stowell (ref. 6) assumed that equation (1) in terms of strain ratios could be extended to plastic strains. This assumption is justified by the data shown in figure 3.

After the flange has buckled, there are shear strains in the flange due to twisting in addition to the axial strains. By suitable combination of these strains, the pertinent value of the secant modulus E_s can be determined for a particular material. The compressive stress in the flange is then simply E_s times the compressive strain at that point. The average stress acting on the flange is finally obtained by integration of the stresses across the flange width.

Failure of Flanges

Failure occurs when the average stress reaches a maximum and begins to decrease with a further increase in strain. This is graphically depicted in figure 4. Up to the critical stress and strain, the distributions are uniform. Beyond critical, the distributions become successively less uniform as the twisting increases. Although the edge strain is continually increasing, the edge stress increases more slowly because of plasticity effects. Eventually, the edge stress ceases to increase and decreases with further straining. The maximum load, or failure, occurs just as the edge stress reaches a maximum.

The very significant physical fact which is brought out by this analysis is that the edge stress is intimately associated with failure. Apparently, failure occurs when the stress intensity at the edge reaches a value approximately equal to the compressive yield strength. This is

indicated by Stowell's analysis (ref. 6) where it is shown that for eight widely different hinged flanges the edge stress intensity is a constant within 1 percent and approximately equal to the compressive yield strength.

The results of the analysis which are important from a design standpoint are shown in figure 2. It can be observed that Stowell's theoretical curve is in good agreement with test data on 2024-T4 aluminum-alloy cruciform extrusions. In such sections, the opposed flanges constrain the simply supported unloaded edge to remain straight. For equal flange angles, however, the simply supported unloaded edges warp in the plane of the flange after buckling. Consequently, the test data of Needham on 2024-T3 formed angles (ref. 7) lie somewhat below Stowell's theoretical line which pertains to an undistorted edge. The significance of warping is discussed at some length in the section entitled "Failure of Compressed Flat Plates."

In order to have a convenient analytical representation of the theoretical and experimental data, the following semiempirical relationship is shown in figure 2. For simply supported flanges with straight unloaded edges, such as cruciforms,

$$\left.\begin{aligned} \frac{\bar{\sigma}_f}{\sigma_{cr}} &= 0.81\left(\frac{\sigma_{cy}}{\sigma_{cr}}\right)^{0.80} && \left(\bar{\sigma}_f \leqq 0.77\sigma_{cy}\right) \\ \bar{\sigma}_f &= \sigma_{cr} && \left(\bar{\sigma}_f > 0.77\sigma_{cy}\right) \end{aligned}\right\} \quad (2)$$

The second equation is used to represent the fact that beyond approximately $(3/4)\sigma_{cy}$ failure and buckling are essentially coincident.

For the formed equal flange angles,

$$\left.\begin{aligned} \frac{\bar{\sigma}_f}{\sigma_{cr}} &= 0.95\left(\frac{\sigma_{cy}}{\sigma_{cr}}\right)^{0.58} && \left(\bar{\sigma}_f \leqq 0.92\sigma_{cy}\right) \\ \bar{\sigma}_f &= \sigma_{cr} && \left(\bar{\sigma}_f > 0.92\sigma_{cy}\right) \end{aligned}\right\} \quad (3)$$

The fact that the second equation applies at a higher fraction of σ_{cy} for formed angles as compared with that for extruded cruciforms is attributed to the increased stress-strain characteristics in the corner of the formed angle. This factor is discussed further in the section entitled "Crippling of Formed Angle, Z-, and Channel Sections."

FAILURE OF COMPRESSED FLAT PLATES

It is well known that flat plates subject to compression (as well as to other types of loading) can carry loads considerably in excess of the elastic buckling load. A relatively large number of theoretical analyses, therefore, have been concerned with the postbuckling load-carrying ability of such plates. Such analyses, with one recent exception, are based on purely elastic considerations and while they yield valuable information on a limited range of postbuckling behavior, the important problem of failure requires the incorporation of plasticity theory into the large-deflection analysis.

As indicated previously, large-deflection analysis of buckled plates is mathematically complex because of nonlinearities in the strain-displacement relationships. The introduction of plasticity effects introduces another nonlinearity in the stress-strain relationships. By use of variational principles in conjunction with calculations performed on an electronic computer, Mayers and Budiansky were able to attack this difficult problem and obtained results related to failure of buckled plates (ref. 8).

Because of their importance in certain problems, the results of elastic analyses of postcritical behavior are reviewed. Certain of the results are considered in terms of effective width. The termination of load-carrying ability, or failure, is then discussed in terms of theory and available test data.

Postbuckling Behavior of Flat Plates

A bibliography of significant large-deflection analyses of buckled elastic plates under compressive loads is given by Mayers and Budiansky (ref. 8). The important results of these analyses have been summarized by Argyris and Dunne (ref. 9).

As discussed in the section "Failure of Flanges," the large-deflection behavior of buckled elements is conveniently represented by a relationship among the average $\bar{\sigma}$, critical σ_{cr}, and edge σ_e stresses. The various factors influencing this relationship include:

(a) Length of plate
(b) Edge rotational restraints
(c) Restraint of lateral expansion of plate
(d) Restraint of warping of unloaded edges in the plane of the plate

The first three of these factors affect the buckling stress as discussed in reference 3. The fourth factor becomes operative after buckling has occurred.

For values of σ_e/σ_{cr} less than approximately 3, the postcritical behavior of compressed flat plates can be given in the following form:

$$\frac{\bar{\sigma}}{\sigma_{cr}} = 1 - \beta + \left(\beta\sigma_e/\sigma_{cr}\right) \tag{4}$$

The values in table 1 for β were obtained from the book of Argyris and Dunne for long flat plates ($a/b > 3$, approximately) with simply supported edges (ref. 9). The restraint against lateral expansion is given by the ratio A_r/at as discussed in reference 3. In addition to the values of table 1, $\beta = 0.583$ for a long plate clamped along unloaded edges which are held straight.

One limiting case of restraint of the unloaded edges considered in table 1 is for straight unloaded edges such as would be obtained with flexurally rigid members along the unloaded edges of an infinite array of panels. The other case covers a stress-free unloaded edge in which in-plane warping is permitted as in a plate test with V-groove supports. The two limiting types of behavior are illustrated in figure 5.

For values of σ_e/σ_{cr} greater than approximately 3, significant changes in the buckle waveform occur and it is necessary to replace equation (4) by the following more accurate relations. For a square plate simply supported with unloaded edges held straight and free to move laterally $\left(A_r/at = 0\right)$

$$\frac{\bar{\sigma}}{\sigma_e} = 0.19 + 0.81\left(\frac{\sigma_{cr}}{\sigma_e}\right)^{1/2} \tag{5}$$

For long plates with rotationally restrained unloaded edges held straight and free to move laterally $\left(A_r/at = 0\right)$

$$\frac{\bar{\sigma}}{\sigma_e} = 1.2\left(\frac{\sigma_{cr}}{\sigma_e}\right)^{2/5} - 0.65\left(\frac{\sigma_{cr}}{\sigma_e}\right)^{4/5} + 0.45\left(\frac{\sigma_{cr}}{\sigma_e}\right)^{6/5} \tag{6}$$

Effective Width

The results of large-deflection analyses are often conveniently given in terms of the effective width of the plate acting at the edge stress. The average stress on the plate was defined as

$$\bar{\sigma} = P/bt \tag{7}$$

For the same load P, it is desired to find an effective width at each edge b_e acting at the edge stress:

$$P = \sigma_e 2b_e t \tag{8}$$

By substituting equation (8) into equation (7),

$$\frac{\bar{\sigma}}{\sigma_e} = \frac{2b_e}{b} \tag{9}$$

By rearranging equation (4) and by use of equation (9) the following effective width relation can be obtained for values of σ_e/σ_{cr} less than 3:

$$\frac{2b_e}{b} = \frac{\bar{\sigma}}{\sigma_e} = \frac{\sigma_{cr}}{\sigma_e}\left[1 - \beta + \beta\left(\sigma_e/\sigma_{cr}\right)\right] \tag{10}$$

For values of σ_e/σ_{cr} greater than 3, equations (5) and (6) may be used directly in conjunction with equation (9).

The effective width discussed in the foregoing comments is concerned with the load-carrying ability of the plate after buckling. A second type of effective width is associated with the stiffness of the plate against further compression. The reduced effective width is defined as

$$\left(\frac{2b_e}{b}\right)_r = \frac{d\bar{\sigma}}{d\sigma_e} \tag{11}$$

From equation (4), therefore

$$\left(\frac{2b_e}{b}\right)_r = \beta \tag{12}$$

For values of σ_e/σ_{cr} greater than 3, the reduced effective width can be found from equations (5) and (6) in the following forms: For the square plate:

$$\left(\frac{2b_e}{b}\right)_r = 0.19 + 0.405\left(\frac{\sigma_{cr}}{\sigma_e}\right)^{1/2} \tag{13}$$

and for the long plate:

$$\left(\frac{2b_e}{b}\right)_r = 0.72\left(\frac{\sigma_{cr}}{\sigma_e}\right)^{2/5} - 0.13\left(\frac{\sigma_{cr}}{\sigma_e}\right)^{4/5} - 0.09\left(\frac{\sigma_{cr}}{\sigma_e}\right)^{6/5} \tag{14}$$

As indicated in figure 1, the effects of small initial imperfections are confined primarily to the region of the theoretical buckling stress for flat plates. Thus, small initial imperfections lower somewhat the values of effective width as compared with those for a perfect plate up to approximately $\sigma_e/\sigma_{cr} = 2$. Beyond this, the effects are negligible.

Since the reduced effective width depends upon the derivative as indicated by equation (11), the effect of small initial imperfections is to lower significantly the values of reduced effective width as compared with those of perfect plates below the theoretical buckling stress. Beyond this, the effects are negligible and the values for a perfect plate may be safely used.

All the foregoing results on effective width are based on analyses which assume the plate to be elastic in behavior after buckling. Mayers and Budiansky introduced plasticity effects in the postbuckling analysis and computed the effective width of flat plates of 2024-T3 aluminum alloy that buckled at 0.3, 0.4, 0.5, and 0.6 of the compressive yield strength (ref. 8).

The results of this analysis indicate that the effect of plasticity is to reduce the effective width as compared with that derived from elastic theory for values of ϵ_e/ϵ_{cr} (edge strain/critical strain) up to approximately 3. Beyond this, elastic theory yields somewhat conservative values.

Failure of Flat Plates

The termination of load-carrying ability of flat plates appears to be dependent upon the boundary conditions along the unloaded edges. As discussed in the section "Failure of Flanges," failure of a flange is intimately associated with the highest attainable value of edge stress which in turn is a function of the edge-stress intensity. Thus, variations in edge-stress intensities due to differing boundary conditions may be expected to result in variations in the failure behavior.

In discussing the failure of flat plates, it is necessary, therefore, to identify carefully small differences in boundary conditions which by themselves may not cause a difference in buckling stress. For this purpose, the discussion will be concerned with the failure of flat plates for which:

(a) The unloaded edges do not warp and thus remain straight in the plane of the plate (v = Constant) (fig. 5(a)).

(b) The unloaded edges are free to warp in the plane of the plate ($\sigma_y = 0$)(fig. 5(b)).

(c) The unloaded edges are supported by columns of solid cross section.

The load-carrying capacities of flat plates with straight edges constrained to remain straight have been computed by Mayers and Budiansky for 2024-T3 plates that buckle elastically at 0.3, 0.4, 0.5, and 0.6 of the compressive yield strength (ref. 8). Although the average compressive stress did not have a maximum value in the range of end shortening considered (up to 0.010) the curves were very flat from a strain of approximately 0.006 on. Thus, the average compressive stress at a strain of 0.010 was taken as an indication of failure.

The results of this analysis, together with experimental data on failure of flat plates with various boundary conditions of Anderson and Anderson (ref. 10), Botman (ref. 11), and Besseling (ref. 12), are shown by the lower curve and test points in figure 6. A very significant fact brought out by the theoretical analysis is that the load-carrying ability of plates with straight unloaded edges may be significantly higher than that of plates with unloaded edges which are free to warp.

Plates tested in V-groove supporting fixtures are free to warp. In addition, out-of-plane displacements at the unloaded edges are not entirely prevented after buckling because of lateral shortening in the central region of the plates as shown in figure 5. Similarly, the post-buckling behavior of compressed square tubes closely follows that of plates tested in V-groove supports. For the tubes, both warping and out-of-plane displacements of the corners are evident after failure.

The importance of the boundary conditions in relation to failure is further supported by experimental data of Botman (ref. 11) and Besseling (ref. 12) on wide plates divided into three bays by a series of opposed knife edges running longitudinally. It can be observed in figure 6 that these data lie between experimental data on plates with warped edges and theoretical results on plates with straight edges. Since the outside edges in the three-bay tests are free to warp, it is possible that higher strengths would be achieved in tests of plates with a greater number of bays.

It is convenient to use a semiempirical relationship in order to unify the theoretical results of Mayers and Budiansky (ref. 8) and the experimental data. For this purpose, the following equations are assumed to apply:

$$\left.\begin{aligned} \frac{\bar{\sigma}_f}{\sigma_{cr}} &= \alpha\left(\frac{\sigma_{cy}}{\sigma_{cr}}\right)^n \qquad \left(\sigma_{cr} \leqq (\alpha)^{1/n}\sigma_{cy}\right) \\ \bar{\sigma}_f &= \sigma_{cr} \qquad \left(\sigma_{cr} > (\alpha)^{1/n}\sigma_{cy}\right) \end{aligned}\right\} \tag{15}$$

This is the same equation used in the section "Failure of Flanges" to fit the data for hinged flanges.

From the logarithmic plots shown in figure 6, the values of α and n were determined and are given in table 2. It is to be noted that the theoretical results cover a small although sufficient range to permit a reasonably precise estimate of the α and n values. The data for square tubes presented in figure 6 cluster for the most part in a narrow region. However, the line drawn for the V-groove test data fits the square-tube data well. The square-tube data are discussed at some length in the section "Crippling of Formed Angle, Z-, and Channel Sections."

It is interesting to note that the slope of the lines drawn through all of the test data has a value of 0.58 as compared with the theoretical value of 0.80. Apparently, in the three-bay plate tests, the effects of the outside edges, which are free to warp, are still sufficiently pronounced to cause the plate to act more in the manner of the V-groove plate than in that of the theoretical straight-edge plate.

These results serve to indicate that although V-groove and square-tube tests may be representative of complex wing structures as far as buckling is concerned, they may or may not yield conservative data on failure depending upon the compression cover-supporting structure. For example, in a multiweb wing design, the continuity of adjacent panels tends to prevent warping of the unloaded panel edges. In such cases, it is possible that the failure relation will lie between the theoretical relationship as an upper bound and the three-bay plate data as a lower bound.

The test data for V-groove plates and square tubes are also shown in an alternate form in the upper curve of figure 6. This form of presentation is used extensively throughout the remainder of this report and therefore it is convenient to have the flat-plate failure data in this form. The buckling stress of a long, flat, simply supported plate is given by

$$\sigma_{cr} = KE(t/b)^2 \tag{16}$$

By substituting equation (16) into equation (15) and rearranging terms,

$$\frac{\bar{\sigma}_f}{\sigma_{cy}} = \alpha K^{1-n}\left[\frac{t}{b}\left(\frac{E}{\sigma_{cy}}\right)^{1/2}\right]^{2(1-n)} \tag{17}$$

In a simplified form

$$\frac{\bar{\sigma}_f}{\sigma_{cy}} = \beta\left[\frac{t}{b}\left(\frac{E}{\sigma_{cy}}\right)^{1/2}\right]^{m} \tag{18}$$

The test data in the upper curve of figure 6 are plotted according to the parameters of equation (18) and it can be observed that for $\bar{\sigma}_f/\sigma_{cy} < 0.9$ the data correlate within ±10 percent limits. The values of β and m in equation (18) were computed from the α and n values obtained from table 2 as follows:

$$\left.\begin{aligned} \beta &= \alpha(3.12)^{0.425} = 1.42 \\ m &= 2(1 - n) = 0.85 \end{aligned}\right\} \tag{19}$$

From the section "Failure of Flanges" it is known that the failure load of the flange is directly related to the stress intensity at the supported unloaded edge. It is reasonable to assume, therefore, that failure of the flat plate is related to the edge stress intensity.

A qualitative estimate of the edge stress intensity in the post-buckled plate can be obtained from figure 5. For the plate with straight unloaded edges, the value of the membrane stress σ_x at the edge is approximately the same at the center as at the ends, with the value of the membrane stress σ_y varying along the length. For the plate with distorted unloaded edges, however, the value of σ_x at the edge increases appreciably toward the center as compared with that at the ends.

The value of the edge stress intensity depends primarily upon the value of σ_x and only secondarily upon σ_y and τ_{xy} which arise after buckling has occurred. Therefore, it appears that the edge stress intensity at the center of the plate with distorted unloaded edges may be appreciably higher for a given value of average compressive stress $\bar{\sigma}_x$ than in the corresponding plate with straight edges. In conjunction with the fact that in the V-groove and square-tube tests some lateral bending of the edges may occur, the differences in edge stress intensities between the two types of plates could account for the data presented in figure 6.

If the unloaded edges of the plates are supported by columns which fail at a value of edge stress below that associated with failure of the plate in a V-groove or three-bay test, for example, then the data presented in figure 6 cannot be used. In its place, the load-carrying ability of the plate may be estimated by use of equations (4) to (6) in which σ_e now represents the strength of the column.

The problem of failure of stiffened panels under compressive loads is treated at length in reference 1. The failure of stiffened panels under shear loads has been thoroughly presented by Kuhn, Peterson, and Levin in their development of tension-field theory (ref. 2).

POSTBUCKLING BEHAVIOR AND FAILURE OF COMPRESSED CURVED PLATES

As discussed in reference 5, the buckling behavior of curved plates under axial compressive loads is governed by the curvature parameter Z_b. At values of Z_b less than 10, approximately, the buckling stress of curved plates is essentially the same as that of flat plates with comparable boundary conditions. In the region of Z_b between 10 and roughly 1,000, the transition between flat-plate and complete-cylinder behavior occurs. In this region, the boundary conditions along both the loaded and unloaded edges exert significant influences upon the buckling stresses. Beyond values of Z_b of roughly 1,000, long-cylinder behavior predominates, in which boundary conditions are insignificant.

Curved plates which are characterized by Z_b values beyond the flat-plate region exhibit discontinuities after buckling such as shown in figure 1(a) for cylinders. This behavior is typical of curved elements under compressive loadings. At values of Z_b in the neighborhood of 10, this discontinuity is relatively small and such plates can carry loads considerably in excess of the buckling load. As Z_b increases, the discontinuity becomes so large that the postbuckling loads are always below the buckling load. In such cases, buckling and failure are coincident. Experimental evidence indicates this to be true for compressed cylinders and curved plates of large values of Z_b.

In this section, the postbuckling behavior of curved plates which fall in the transition region is reviewed. Experimental data on effective width and failure are presented from which generalized empirical formulas are derived.

Postbuckling Behavior

Cox and Pribram have considered the postbuckling behavior of long, clamped, curved plates with negligible lateral restraint (ref. 13). Based on a semiempirical approach, the data shown in figure 7(a) were presented for curved plates ($Z_b < 60$) with relatively small initial imperfections. Somewhat larger initial imperfections alter the shapes of the curves in the region of buckling although they cause insignificant changes in the postbuckling behavior.

In figure 7(a), the dashed lines are used to indicate schematically the behavior of the curved plate at buckling in an ideal controlled-deformation-type testing machine. This region is most sensitive to initial imperfections as well as to the elasticity of the testing machine.

Furthermore, various interpretations can be used to define the buckling load under different loading systems. As a consequence, the dashed lines are to be viewed as an indication of the behavior of the curved plate at buckling and not as an attempt to define the buckling load itself.

Since it is somewhat difficult to define the buckling load precisely, the data displayed in figure 7 are in terms of $E(t/b)^2$ instead of σ_{cr} as used for flat plates. This has the advantage of avoiding the use of the buckling coefficient k_c and permits presentation of the results directly in terms of E and the geometric parameters of the curved plate. Thus,

$$\frac{\sigma_{cr}12(1 - \nu^2)}{\pi^2 k_c} = E\left(\frac{t}{b}\right)^2 \tag{20}$$

A further advantage of this method of presentation lies in the experimental fact that the buckling load tends to decrease significantly under successive loadings. Test data of Cox and Clenshaw (ref. 14) and of Jackson and Hall (ref. 15) indicate that the buckling region is significantly affected upon reloading although the postbuckling region appears to undergo negligible change.

The same data also indicate that in the postbuckling region plasticity effects become important soon after buckling with the result that the postbuckling curves generally have concave-downward characteristics.

Effective Width

In figure 7(b), the effective width of curved plates has been calculated from the data of figure 7(a). These curves are intended to indicate schematically that the effective-width behavior of slightly curved plates is not significantly different from that of flat plates. The only important difference is that a discontinuity may appear in the effective-width data for curved plates at values of Z_b greater than 30, approximately. The magnitude of the discontinuity is associated with the jump which occurs at buckling and is significantly affected by the magnitude of the initial imperfections.

A theoretical analysis of the effective width of long, simply supported plates of slight curvature (Z_b less than 10) has been conducted by Levy (ref. 16). It was concluded that when the buckle depth becomes comparable with the sheet thickness, the effect of initial curvature on the load carried in axial compression becomes negligible. The results indicate that when the edge stress is approximately twice the buckling stress of the corresponding flat plate, the effective widths are substantially the same. These results are in agreement with figure 7(b) for values of Z_b less than 10.

Because of the limited range of this theoretical investigation both from the standpoint of the low values of Z_b (0, 5, and 10) and the relatively small range of $2b_e/b$ considered (1 to 0.5), it is necessary to adopt an empirical approach to this problem.

The available test data are for long, clamped, curved plates. Ramberg, Levy, and Fienup (ref. 17) tested multiple-bay curved panels of 2024-T3 aluminum alloy stiffened by sturdy lipped Z-extrusions which provided clamped boundary conditions along the unloaded edges of the plates. The data for which the edge strain was below the proportional limit fall into two Z_b groups of 0 to 8 and 24 to 31 and are shown in figure 8.

Additional test data on 2017-T3 aluminum-alloy plates clamped along the unloaded edges were presented by Jackson and Hall (ref. 15). The data shown in figure 8 are from the second series of tests and include flat plates $(Z_b = 0)$ and curved plates with Z_b values ranging from 4 to 125.

A study of the data presented in figure 8 reveals that an apparent discontinuity occurs in the region of $\bar{\sigma}/\sigma_e$ $(= 2b_e/b)$ between 0.5 and 0.4. The data of Ramberg, Levy, and Fienup (ref. 17) indicate that, for the Z_b ranges of 0 to 10 and 24 to 32, the effective-width range from 1 to 0.45 can be represented by the following equation within ±10 percent limits:

$$\frac{2b_e}{b} = K_c^{1/2} \frac{t}{b} \left(\frac{E}{\sigma_e}\right)^{1/2} \tag{21}$$

for $2b_e/b > 0.45$. The buckling coefficient K_c is that of the curved plate and may be determined from reference 5:

$$K_c = \frac{\pi^2 k_c}{12(1 - \nu^2)} \tag{22}$$

Equation (21) also represents the Jackson and Hall data (ref. 15) on flat and curved plates.

Below effective-width values of approximately 0.45, the test data of Jackson and Hall (ref. 15) appear to follow the trend of the failure lines for flat and curved plates. The failure lines are obtained from figure 9 as discussed in the next subsection. The equation for the line passing through the effective-width test data for both flat and curved plates $(0 \leqq Z_b \leqq 125)$ as shown in figure 8 is

$$\frac{2b_e}{b} = K_p^{0.43} \left[\frac{t}{b} \left(\frac{E}{\sigma_e}\right)^{1/2}\right]^{0.85} \tag{23}$$

for $2b_e/b < 0.45$. The buckling coefficient K_p is for the flat plate. In this case, for a long clamped flat plate, $K_p = 6.3$ as indicated in figure 8.

Since equations (21) and (23) are based on test data which cover a rather limited range of Z_b values, they should be used with some caution beyond Z_b values of approximately 30. It does appear, however, that the effective width of flat plates tends to act as a lower limit for curved plates. This is substantiated not only by the experimental data for figure 8 but also by figure 7(b) and the failure data of figure 9.

Beyond Z_b values of 30, figure 7(b) indicates that large discontinuities may appear in the effective width curves immediately after buckling. For values of Z_b large enough for the curved plate to act as a complete cylinder, the discontinuity can be expected to drop directly to the failure line, since in this case buckling and failure are coincident.

Failure of Curved Plates

The only reliable data on failure of curved plates with well-defined boundary conditions are from Jackson and Hall's second series of tests (ref. 15). The jigs used for these tests not only clamped the unloaded edges but also tended to restrain any in-plane warping of the curved plates after buckling.

As mentioned previously in this section, it is not advantageous to present test results for curved plates in terms of the buckling stress, as used in the sections "Failure of Flanges" and "Failure of Compressed Flat Plates" for flat plates. This is due to the difficulty of precisely defining the buckling stress because of sensitivity to initial imperfections. Furthermore, K_c is not constant but is a function of Z_b and may change appreciably upon successive loadings. Thus, it is desirable to use the alternate form of presentation given in the section "Failure of Compressed Flat Plates" and used for the V-groove-plate test data.

As shown in the preceding sections, the failure strength of flat plates which buckle elastically can be expressed in the following form:

$$\frac{\bar{\sigma}_f}{\sigma_{cr}} = \alpha\left(\frac{\sigma_{cy}}{\sigma_{cr}}\right)^n \tag{24}$$

Multiplying both sides of equation (24) by σ_{cr}/σ_{cy}

$$\frac{\bar{\sigma}_f}{\sigma_{cy}} = \alpha\left(\frac{\sigma_{cr}}{\sigma_{cy}}\right)^{1-n} \tag{25}$$

The buckling stress of a curved panel is given by

$$\sigma_{cr} = K_c E \left(\frac{t}{b}\right)^2 \tag{26}$$

By substituting equation (26) into equation (25)

$$\frac{\bar{\sigma}_f}{\sigma_{cy}} = \alpha K_c^{1-n} \left[\frac{t}{b}\left(\frac{E}{\sigma_{cy}}\right)^{1/2}\right]^{2(1-n)} \tag{27}$$

In a simplified form this becomes equation (18).

Equation (18) is equivalent to equation (24), although it is in a more convenient form for correlating Jackson and Hall's test data on failure of curved plates (ref. 15). These test data are shown in figure 9 according to the parameters of equation (18). It is to be noted that the values of σ_{cy} were taken as 85 percent of the tension yield strengths since only the latter were given. The data were divided into several Z_b ranges and are shown in figure 9.

Within approximately ±10-percent limits, equation (18) fits the test data in the following form:

$$\frac{\bar{\sigma}_f}{\sigma_{cy}} = 2.01 \left[\frac{t}{b}\left(\frac{E}{\sigma_{cy}}\right)^{1/2}\right]^{0.85} \qquad \text{for } \frac{\bar{\sigma}_f}{\sigma_{cy}} < \frac{3}{4} \tag{28}$$

The range of validity of equation (28) probably applies for values of $\bar{\sigma}_f/\sigma_{cy}$ less than 3/4, a value obtained in the preceding sections. No test data on curved plates are available to establish this limit.

Equation (28) apparently gives a reasonable fit to all the test data for values of Z_b between 10 and 125. The data for the Z_b range between 0 and 10 consistently fall on the lower 10-percent limit. For this range, it is suggested that a value of $\beta = 1.79$ be used in equation (28).

CRIPPLING OF EXTRUDED Z-, CHANNEL, AND H-SECTIONS

The failure following local buckling of stiffening elements is variously referred to as maximum average strength, ultimate strength, crushing strength, or crippling strength. The last term is in common use in the aircraft industry and is associated with the short-column region (L'/ρ less than approximately 20) where the strength does not vary significantly with the length of the stiffener. The term crippling strength is used in this sense herein.

From the standpoint of local buckling (ref. 4), the stiffener cross section is envisioned as an assemblage of plate elements. The boundary conditions along the unloaded edges of each of the individual plate elements at a common junction are associated with rotational restraints provided by adjoining plate elements. The junction may be the filleted corner of an extrusion or the bend line of a formed section.

Early attempts to determine the crippling strength of stiffening elements were based upon the buckling behavior of the elements. In such analyses, the crippling load was taken as the sum of the buckling loads of each of the plate elements comprising the stiffener cross section. Such analyses are typified by methods presented in the book of Sechler and Dunn (ref. 18).

Based on the knowledge that the failure load of a flat plate can appreciably exceed the elastic buckling load, later analyses attempted to refine the method of calculation of stiffener crippling strengths. Such methods are in wide use in the aircraft industry for sections of general shape and differ possibly only in minor details from that presented by Crockett (ref. 19).

For equal flange stiffeners such as Z- or H-extrusions, extensive test data are available for several materials. The sharp corners and relatively uniform stress-strain characteristics in the cross sections of extrusions has permitted a synthesis of these data in a simple form. A relationship involving the buckling stress of the section and the compressive yield strength of the material is related directly to the crippling strength.

For formed Z- and channel sections, the relationship among buckling stress, compressive yield strength, and crippling strength appears to be influenced by additional factors. These include the finite radius of the rounded corner and the increase in compressive yield properties in the corner due to the forming process.

These effects have recently led Needham to propose a revised method of analysis for formed sections of general shape (ref. 7). In this method, the crippling load of the stiffener is obtained by summing the failure loads of each of the corner elements comprising the stiffener cross section.

In this section of the report, a semiempirical analysis is presented based upon the knowledge gained from the preceding sections on failure of flanges and flat plates. This analysis serves to unify test results on various types of stiffening elements and also provides some physical insight as to the factors operative at failure. Available crippling test data on Z-, H-, and channel extrusions are reviewed in this section. Formed angle, channel, and Z-sections are reviewed in the following

section and methods of analysis for sections of general shape are presented in section after next.

Semiempirical Analysis of Crippling

From the flat-plate analysis presented in the section "Failure of Compressed Flat Plates," it can be expected that the following factors will influence the postbuckling behavior of stiffened elements:

(a) The degree of rotational restraints at the unloaded edges
(b) The degree of warping and lateral bending of the unloaded edges

In addition, it can be anticipated that the following factors will influence crippling of the stiffener:

(c) The corner configuration
(d) The stress-strain characteristics of the material and in particular nonuniformity of stress-strain characteristics in the cross section such as occurs in formed sections

Theoretical postbuckling analyses of flanges and flat plates indicate a definite relationship among the average stress, the critical stress, and the stress at the unloaded edge of the element. The principal effect of small initial imperfections is to replace the discontinuity between prebuckling and postbuckling behavior, which occurs at the critical stress, with a continuous relation. In such cases, the theoretical relationships between average, critical, and edge stresses can be quite accurately fitted by an equation of the following type:

$$\frac{\bar{\sigma}}{\sigma_{cr}} = a\left(\frac{\sigma_e}{\sigma_{cr}}\right)^n \tag{29}$$

where a and n reflect the large-deflection behavior of the element as given by conditions (a) and (b) above for postbuckling behavior.

From the theoretical analysis of failure of flanges given in the section "Failure of Flanges," it was observed that the maximum average stress $\bar{\sigma}_f$ is attained when the edge stress reaches a relatively large fraction of the compressive yield strength of the material. Thus, it appears plausible to assume that failure occurs when

$$\sigma_e = b\sigma_{cy} \tag{30}$$

where b is a function of the stress-strain characteristics of the material and the edge stress intensity in the element. The coefficient b presumably reflects the influence of items (b), (c), and (d).

By substituting equation (30) into equation (29),

$$\frac{\bar{\sigma}_f}{\sigma_{cr}} = ab^n\left(\frac{\sigma_{cy}}{\sigma_{cr}}\right)^n \tag{31}$$

Letting $\alpha = ab^n$, equation (31) becomes equation (24).

Equation (24) has been used in the preceding sections to fit the theoretical data on failure of flanges and flat plates with undistorted unloaded edges. In both cases, a value of $n = 4/5$ gave a good fit to the theory and available test data.

The usefulness of equation (24) has been demonstrated to some extent in the preceding sections where theoretical data are available. In subsequent sections, it will be shown to be of considerable value as a means of correlating test data on elements of complex cross section for which theoretical failure analyses do not exist.

The usefulness of equation (24) was demonstrated by Schuette in correlating an extensive amount of test data on formed and extruded equal flange stiffeners (ref. 20). The analysis in this section follows in broad outline that of Schuette in an interpretation of the test data. The recent publication of theoretical analyses of the failure of flanges and flat plates, as reviewed herein, has provided data which substantiate some of the assumptions and lend confidence in the approach.

Analysis of Z-, Channel-, and H-Extrusion Data

An extensive amount of test data on equal-flange Z-, channel, and H-extrusions of various aluminum and magnesium alloys has been correlated on the basis of equation (24) by Heimerl (ref. 21) and Schuette (ref. 20). The extrusions tested were characterized by sharp filleted corners with relatively uniform stress-strain characteristics over the cross section.

Test data for H-, Z-, and channel extrusions are shown in figure 10 for four aluminum alloys and one magnesium alloy. The data were taken from the references listed in the reports of Heimerl and Schuette. These data were fitted according to equation (24) with the values of α and n given in table 3 for values of σ_{cr}/σ_{cy} less than 3/4, approximately. It is to be noted that, for all extrusions, values of b_w/t ranged from 18 to 23.

In preparing the specimens for these tests, the Z- and channel sections were obtained by removing flanges from the H-extrusions. Consequently these data are from specimens of very similar properties and can be used to obtain a reliable estimate of the various factors influencing

failure as discussed under items (a) to (d) in the subsection "Semi-empirical Analysis of Crippling."

The degree of rotational restraint at the unloaded edge of the flange (the element in the cross section which buckled first in these tests) is influenced by the corner configuration and the relative dimensions of the flange and web. The corner configuration was substantially the same for all specimens and, therefore, no estimate of this effect can be obtained from these tests.

The degree of rotational restraint at the unloaded edge, item (a), varied between simple support and clamped as influenced by the relative flange and web dimensions b_f/b_w. A range of values of b_f/b_w between 0.55 and 0.83 was covered in the H-extrusion tests. An analysis of the data did not reveal any systematic variation in the α values with this parameter. Apparently, the influence of the rotational edge restraints is accounted for in determining the critical stress of the section and does not have any further effect upon the crippling strength.

The stress-strain characteristics of the material, item (d), do appear to have a slight effect upon the value of α. This can be ascribed to the influence of the value of b as given in equation (30). From the value of α listed in table 3, it can be observed that there is a consistent trend for all three sections. Aluminum alloy 2014-T4 has the highest values of α, alloys 7075-T6 and 0-1HTA have the lowest, and alloys 2024-T4 and R303-T have approximately the same values which are intermediate to the other values.

The influence of warping and lateral bending of the unloaded edges, item (b), is clearly evident from the difference in n values between the H-sections and the Z- and channel sections. The value of $n = 0.8$ obtained for the H-sections is the same as that for flanges and flat plates with undistorted unloaded edges. Evidently, the opposed flanges of the H-section prevent any warping of the flanges at the corner. In fact, the values of α for the H-section and hinged flange agree closely.

For the Z- and channel sections, the absence of an opposing flange at the junction to the web permits some warping and possibly some lateral bending to occur. Thus, the value of $n = 0.72$ for Z- and channel sections is less than that for H-sections. This is in agreement with the trend observed for flat plates in which the value of n for plates with warped edges was less than for those with undistorted edges. For extruded Z- and channel sections, apparently the web and filleted corner act so as to prevent some warping of the supported unloaded edge of the flange. This can be judged by the value of $n = 0.72$ for the Z- and channel sections which is intermediate to $n = 0.80$ for undistorted edges and $n = 0.65$ obtained for flat plates with edges free to warp.

Design Data for Z-, Channel, and H-Extrusions

For design purposes, it may not be necessary to use the rather precise values of n and α given in table 3. Heimerl has suggested the following formulas for values of σ_{cr} less than $(3/4)\sigma_{cy}$ (ref. 21):

(a) For H-sections:

$$\bar{\sigma}_f = 0.80\sigma_{cr}^{0.20}\sigma_{cy}^{0.80} \tag{31}$$

(b) For Z- and channel sections:

$$\bar{\sigma}_f = 0.77\sigma_{cr}^{0.20}\sigma_{cy}^{0.80} \tag{32}$$

In an analysis of the same test data, Schuette has recommended for Z-, channel, and H-sections (ref. 20)

$$\bar{\sigma}_f = 0.80\sigma_{cr}^{0.25}\sigma_{cy}^{0.75} \tag{33}$$

The differences among these formulas is considerably less numerically than the scatter of all the test data when variations due to material properties and section configuration are not considered.

All of the formulas considered thus far, (eqs. (24) and (31) to (33)) apply for values of σ_{cr} less than approximately $(3/4)\sigma_{cy}$. This generally corresponds to cases where buckling is elastic. For cases where σ_{cr} exceeds $(3/4)\sigma_{cy}$, buckling generally occurs in the plastic range and failure occurs slightly beyond buckling as shown in figure 11.

From an analysis of test data, Schuette has proposed for values of σ_{cr}/σ_{cy} greater than 3/4 (ref. 20)

$$\bar{\sigma}_f = 1.04\sigma_{cr} \tag{34}$$

where σ_{cr} is computed according to methods given in reference 4 using the appropriate plasticity-reduction factor.

From the same test data, Heimerl (ref. 21) suggested an extension of the secant-modulus method of Gerard (ref. 22). In this case, for values of σ_{cr}/σ_{cy} greater than 3/4,

$$\bar{\sigma}_f = \frac{k_w\pi^2 E_s}{12\left(1 - \nu^2\right)}\left(\frac{t_w}{b_w}\right)^2 \tag{35}$$

Heimerl and Roberts (ref. 23) investigated the short-time behavior of aluminum-alloy H-sections at elevated temperatures up to 600° F. The test data are shown in figure 12, from which it can be observed that the relationships established at room temperature are satisfactory for short-time loading at elevated temperatures.

CRIPPLING OF FORMED ANGLE, Z-, AND CHANNEL SECTIONS

The various factors influencing crippling of extruded sections, as discussed in the preceding section, also pertain to formed sections. Several additional factors such as the rounded corner and increased stress-strain characteristics in the corner region as a result of forming indicate the desirability of discussing formed sections separately from extrusions in this presentation. Furthermore, stiffening elements are often formed of alclad sheet and it is necessary to consider the effect of the cladding upon the crippling strength.

A mass of test data on Z- and channel sections formed of 2017-T3 and 2024-T3 aluminum alloys was analyzed by Schuette (ref. 20) on the basis of equation (24). It was found that a value of $n = 3/4$ fitted the test data well but that there was a systematic variation of the coefficient α with the parameter b_w/t which ranged between 18 and 43. Since α appeared to be constant for extruded Z- and channel sections, the variation in α for formed sections was attributed to the increased stress-strain properties in the corners.

In an analysis of the same test data used by Schuette plus data on FS-1h formed Z-sections, Gallaher (ref. 24) found that a simple correlation of the form $\bar{\sigma}_f = f(A/t^2)$, where A is the cross-sectional area of the stiffener, gave a good fit with the test data. Recently, Needham (ref. 7) presented test data on formed angles and channels of alclad 2024-T3, 2024-T3, and alclad 7075-T6 aluminum alloys and obtained good correlation on the basis of

$$\bar{\sigma}_f = C(t^2/A)^m \tag{36}$$

A value of $m = 3/4$ gave a good fit with all of Needham's test data. In fact, a replot of Gallaher's data on the basis of equation (36) with $m = 3/4$ resulted in excellent agreement with the test data.

Semiempirical Analysis of Angles and Square Tubes

The interesting fact evident from the foregoing discussion is that there are apparently two different correlative schemes which are each in good agreement with test data. The Gallaher-Needham method is the simplest since, for a given material, the crippling strength is a simple function of the geometric properties of the cross section t^2/A, or $t/\bar{b}$ where $\bar{b}$ is the developed length of the cross section. However, it is not directly evident how to generalize equation (36) in terms of the physical properties such as E and σ_{cy} of the material. Furthermore, equation (36) is valid only for values of $\bar{\sigma}_f/\sigma_{cy}$ less than approximately 3/4 as in the case of extrusions. This fact is often disregarded when the data are presented according to equation (36).

The Schuette form of correlation involves computation of the buckling stress, and, therefore, is not so simple as the above method. Primarily, the simplicity is lost for Z- and channel sections because α in equation (24) is not a constant but is a function of b_w/t. The advantages of the Schuette method, however, include the fact that the results are in a generalized form for various materials since the values of E (in σ_{cr}) and σ_{cy} appear in the semiempirical relationship. Furthermore, the range of validity of the relationship in terms of $\bar{\sigma}_f/\sigma_{cy}$ is readily evident.

In preparing this review, it became evident that certain relations must exist between the two correlative schemes which would permit a generalized approach. It is desirable to retain the simplicity of the Gallaher-Needham method, although in a nondimensionalized form, with the range of validity of the formula readily evident. The last two features are contained in the Schuette method of correlation.

The following analysis presupposes that the available test data for a particular stiffener shape which buckles elastically have been correlated on the basis of the two methods discussed above. From the Gallaher-Needham method equation (36) holds and from the Schuette method for $\bar{\sigma}_f \leqq \alpha^{1/n}\sigma_{cy}$, there is equation (24) or

$$\bar{\sigma}_f = \alpha\sigma_{cr}^{1-n}\sigma_{cy}^{n} \tag{37}$$

It is assumed that the values of C, α, m, and n can be established from test data.

At this point, the expression σ_{cr} is to be introduced into equation (37). Although this can be done in a generalized manner, it is

convenient to consider those cases in which the buckling coefficient k is constant (such as for equal flange angles and square tubes) separately from cases where k is a function of the geometric parameters of the cross section:

$$\sigma_{cr} = \bar{\eta} \frac{\pi^2 kE}{12(1 - \nu^2)}\left(\frac{t}{b}\right)^2 = \bar{\eta} KE\left(\frac{t}{b}\right)^2 \tag{38}$$

where $\bar{\eta}$ is the cladding reduction factor discussed in reference 3. By substituting equation (38) into equation (37)

$$\bar{\sigma}_f = \alpha(K\bar{\eta}E)^{1-n}\left(\frac{t}{b}\right)^{2(1-n)}\sigma_{cy}{}^n \tag{39}$$

Also, for equal flange angles and square tubes, the parameter t^2/A can be replaced by t/b with the resultant change in equation (36):

$$\bar{\sigma}_f = \bar{C}(t/b)^m \tag{40}$$

By equating equations (39) and (40)

$$\alpha(K\bar{\eta}E)^{1-n}\left(\frac{t}{b}\right)^{2(1-n)}\sigma_{cy}{}^n = \bar{C}\left(\frac{t}{b}\right)^m \tag{41}$$

By rearranging terms and defining a new parameter β, the following relationship exists:

$$\beta = \alpha K^{1-n}\left(\frac{t}{b}\right)^{2(1-n)-m} = \bar{C}\Big/(\bar{\eta}E)^{1-n}\sigma_{cy}{}^n \tag{42}$$

By virtue of equation (40) and since t/b is proportional to $(\sigma_{cr})^{1/2}$,

$$\bar{\sigma}_f \propto \sigma_{cr}{}^{m/2} \tag{43}$$

From equation (37), however,

$$\bar{\sigma}_f \propto \sigma_{cr}{}^{1-n} \tag{44}$$

Therefore, for equal flange angles and square tubes the exponents of σ_{cr} must be related in one of the following ways:

$$\left.\begin{aligned} 1 - n &= \frac{m}{2} \\ \frac{1 - n}{m} &= \frac{1}{2} \\ 2(1 - n) - m &= 0 \end{aligned}\right\} \tag{45}$$

By use of equations (45), equation (42) simplifies to

$$\beta = \alpha K^{1-n} = \frac{\bar{C}}{(\bar{\eta}E)^{m/2}\sigma_{cy}^{1-(m/2)}} \tag{46}$$

Finally, equations (39) and (40) become

$$\frac{\bar{\sigma}_f}{\sigma_{cy}} = \beta\left[\left(\frac{t}{b}\right)\left(\frac{\bar{\eta}E}{\sigma_{cy}}\right)^{1/2}\right]^m \tag{47}$$

The range of validity of equation (47) follows from equation (24). Since equation (24) is valid for

$$\frac{\bar{\sigma}_f}{\sigma_{cy}} \leq \alpha^{1/n} \tag{48}$$

it follows from equation (46) that in terms of β

$$\frac{\bar{\sigma}_f}{\sigma_{cy}} \leq \left(\frac{\beta}{K^{1-n}}\right)^{1/n} \tag{49}$$

For values of $\bar{\sigma}_f/\sigma_{cy}$ greater than those given by equation (49)

$$\bar{\sigma}_f = \sigma_{cr} \tag{50}$$

The application of this method of generalized analysis will be demonstrated by correlating data on square tubes and equal flange angles.

Crippling of Square Tubes and Equal Flange Angles

A sufficient, although not extensive, amount of available test data on crippling of extruded square tubes of several aluminum alloys has been summarized by Needham (ref. 7). The data for tubes for which $\bar{\sigma}_f/\sigma_{cy}$ was less than approximately 3/4 were correlated according to the Gallaher-Needham method, Schuette method, and the generalized method presented herein.

From test data shown in figure 13, it can be observed that $m = 0.85$ fits the data according to the Gallaher-Needham method and $n = 0.575$ fits the data according to the Schuette method. According to equation (45), the relation between m and n is satisfied without any adjustment in these values. In terms of the generalized correlation for the square tubes

$$\frac{\bar{\sigma}_f}{\sigma_{cy}} = 1.42\left[\left(\frac{t}{b}\right)\left(\frac{E}{\sigma_{cy}}\right)^{1/2}\right]^{0.85} \tag{51}$$

for $\frac{\bar{\sigma}_f}{\sigma_{cy}} \leq 0.7$. Also included in figure 13 are some data on rectangular tubes of 2024-T3. It can be observed that the data are in agreement with equation (51) which is the same equation obtained for V-groove plates in the section "Failure of Compressed Flat Plates."

Needham has conducted tests on crippling of equal flange angles formed of 2024-T3, alclad 2024-T3, and alclad 7075-T6 aluminum alloys in the -T condition to an inside radius approximately equal to 3t (ref. 6). The test data for each material were correlated by Needham according to

$$\bar{\sigma}_f = \bar{C}(t/b)^{3/4} \tag{52}$$

As pointed out by Needham, an exponent of $m = 3/4$ gave a satisfactory fit, although not necessarily the best fit, to the test data. The values of $\bar{C}$ as well as the physical properties of the materials are tabulated in table 4.

Although alcald angles were tested by Needham (ref. 6), the buckling stresses for a large majority of the test points were well below the proportional limit of the cladding. In such cases, no correction for the cladding, as discussed in reference 3, is required. The few test points which theoretically do require a correction were not revised because of the minor nature of the correction in this case.

In order to provide additional data for use with the generalized crippling formula, Needham's test data for the 2024-T3 equal angles were plotted according to the Schuette method in figure 2. Although there is some scatter in this plot, which also exists in Needham's data plotted according to equation (52), the following relation fits reasonably well as shown in figure 2 and by equation (3):

$$\frac{\bar{\sigma}_f}{\sigma_{cr}} = 0.95\left(\frac{\sigma_{cy}}{\sigma_{cr}}\right)^{0.575} \qquad \text{for } \frac{\bar{\sigma}_f}{\sigma_{cy}} \leq 0.92 \tag{53}$$

Thus, a value of $m = 3/4$ was used by Needham and a value of $n = 0.575$ was obtained from equation (53). According to equation (45),

however, $2(1 - n) = m$, a relationship which is not satisfied in this case. The discrepancy is apparently due to the fact that the scatter of the data permitted some latitude in personal judgment in fitting the data according to equations (30) and (40).

To resolve this discrepancy, all of Needham's test data for angles were plotted as shown in figure 14, according to equation (47). The average generalized crippling formula for formed angles which fits the data within ±10-percent limits is

$$\frac{\bar{\sigma}_f}{\sigma_{cy}} \doteq 0.665\left[\left(\frac{t}{b}\right)\left(\frac{\bar{\eta}E}{\sigma_{cy}}\right)^{1/2}\right]^{0.85} \tag{54}$$

for $\bar{\sigma}_f/\sigma_{cy} \leqq 0.92$. This formula is valid for materials with strain-hardening characteristics similar to those of 2024-T3 alloy and with a bend radius of approximately $3t$ formed in the -T condition. For materials such as 7075-T6 alloy which have lower strain-hardening characteristics than 2024-T3 alloy, the test data appear to be consistently lower than the average curve in figure 14. Therefore, a value of $\beta = 0.630$ should be used in equation (54) for such materials.

Needham has also conducted tests on alclad 2024-T3 unequal flange angles (ref. 7). By defining the term t/b as $2t/(b_1 + b_2)$ where b_1 and b_2 represent the flange widths, Needham obtained satisfactory correlation with equation (52) using the value of $\bar{C}$ given in table 4 for alclad 2024-T3 equal flange angles. These data are also shown in figure 14. Apparently, equation (54) is in reasonably good agreement with these data.

Semiempirical Analysis of Z- and Channel Sections

As in the cases of angles and square tubes, the analysis for Z- and channel sections presupposes that the available test data for sections which buckle elastically have been correlated on the basis of the two methods. For the Gallaher-Needham method equation (36) holds true and for the Schuette method there is equation (37).

For equal flange, Z-, and channel sections, the buckling stress may be determined from the following equation and buckling coefficients presented in reference 4:

$$\sigma_{cr} = \bar{\eta}\,\frac{\pi^2 k_w E}{12(1 - \nu^2)}\left(\frac{t}{b_w}\right)^2 = \bar{\eta}K_w E\left(\frac{t}{b_w}\right)^2 \tag{55}$$

By substituting equation (55) into equation (37)

$$\bar{\sigma}_f = \alpha K_w^{1-n} \left(\frac{t}{b_w}\right)^{2(1-n)} (\bar{\eta}E)^{1-n} \sigma_{cy}^{\ n} \tag{56}$$

For Z- and channel sections of constant thickness,

$$\frac{A}{t^2} = \left(\frac{b_w}{t}\right)\left[1 + \left(\frac{2b_f}{b_w}\right)\right] \tag{57}$$

where b_w and b_f are the web and flange widths, respectively. By substituting equation (57) into equation (36)

$$\bar{\sigma}_f = C\left(\frac{t}{b_w}\right)^m \left(1 + \frac{2b_f}{b_w}\right)^m \tag{58}$$

By equating equations (56) and (58), rearranging terms, and defining the parameter β in a manner similar to that used for angles and square tubes,

$$\beta = \alpha K_w^{1-n} \left(1 + \frac{2b_f}{b_w}\right)^m \left(\frac{t}{b_w}\right)^{2(1-n)-m} = \frac{C}{(\bar{\eta}E)^{1-n}\sigma_{cy}^{\ n}} \tag{59}$$

Finally, by substituting equation (59) into equation (36), the generalized crippling formula is obtained

$$\frac{\bar{\sigma}_f}{\sigma_{cy}} = \beta\left[\left(\frac{t^2}{A}\right)\left(\frac{\bar{\eta}E}{\sigma_{cy}}\right)^{1-n/m}\right]^m \tag{60}$$

which is valid if equation (48) is satisfied.

Note that, in this case, a direct relation between the exponents m and n cannot be established theoretically as in the case of equal-element sections such as angles and square tubes. For the latter, the buckling coefficient is a constant and t^2/A can be replaced directly by t/b. For the Z- and channel sections, the buckling coefficient and the t^2/A parameters are different functions of b_f/b_w.

Crippling of Z- and Channel Sections

Schuette has analyzed test data on 2017-T3 and 2024-T3 channel and Z-sections formed in the -T condition to an inside bend radius of 3t (ref. 20). In all cases the flange buckled elastically. It was quite

conclusively established that a value of $n = 3/4$ in equation (37) gave the best fit to the test data. This value is practically the same as that obtained for extruded Z- and channel sections. The test data for the extrusions covered the narrow b_w/t range from 18 to 23 and therefore a fixed value of $\alpha = 0.80$ (eq. (33)) was used to correlate the data. The formed sections, however, covered a b_w/t range between 18 and 43 and, consequently, a variation of α with the parameter b_w/t was obtained.

The test data for the 2017-T4 sections are shown in figure 15(a). In figures 15(b) and 15(c), the test data for the 2024-T4 sections are given. Additional test data of Gallaher (ref. 24) on FS-1h magnesium-alloy Z-sections formed in the -h condition to an inside bend radius of $4.3t$ are shown in figure 15(d). In all these cases, $n = 3/4$ and the values of α listed in table 5 provided a good fit to the test data.

The same test data were correlated according to equation (36) and are presented in figure 15(e) in terms of $\bar{\sigma}_f$ and A/t^2. It can be observed that all data for each material lie along a single line of slope $m = 0.75$. There is no systematic variation of the data with the parameter b_w/t as occurs in figures 15(a) to 15(d). Thus, correlation according to equation (36) is evidently simpler and more direct than according to equation (37).

Now that the values of the exponents $n = 0.75$ and $m = 0.75$ have been established from figure 15, generalized crippling formula (60) becomes

$$\frac{\bar{\sigma}_f}{\sigma_{cy}} = \beta\left[\left(\frac{t^2}{A}\right)\left(\frac{\bar{\eta}E}{\sigma_{cy}}\right)^{1/3}\right]^{0.75} \tag{61}$$

All available test data for formed Z- and channel sections of 2017-T3, 2024-T3, and FS-1h alloys are plotted in nondimensional form according to equation (61) in figure 16. It can be observed that a value of $\beta = 4.00$ in equation (61) fits the 2017-T3 and 2024-T3 data within a ±5-percent scatter band. The FS-1h data appear to be somewhat lower with a value of $\beta = 3.78$. The lower value of β is attributed to the lower strain-hardening characteristics of FS-1h alloy, which result in a smaller increase in yield properties in the corners as compared with those of the two aluminum alloys. This effect is considered in detail in a later portion of this section.

For values of m and n equal to 0.75, the relations among β, α, and C become, from equation (59),

$$\beta = \alpha K_w^{0.25}\left(1 + \frac{2b_f}{b_w}\right)^{0.75}\left(\frac{b_w}{t}\right)^{0.25} = \frac{C}{(\bar{\eta}E)^{0.25}\sigma_{cy}^{0.75}} \tag{62}$$

An interesting sidelight on the variation of α with the parameter b_w/t can be obtained from the calculation presented in table 6. The values of K_w as a function of b_f/b_w were obtained from reference 4. It can be seen that the parameter listed in table 6 is reasonably constant over the b_f/b_w range of the majority of the test data. By use of the values listed in table 6, equation (62) simplifies to:

$$\beta = 2.14\alpha\left(\frac{b_w}{t}\right)^{0.25} \tag{63}$$

In order to confirm equation (63) by use of the values of α listed in table 5, it is convenient to rearrange equation (63) in the form

$$\alpha = \left(\frac{\beta}{2.14}\right)\left(\frac{b_w}{t}\right)^{-0.25} \tag{64}$$

In figure 17, the data of table 5 are plotted and shown in relation to equation (64). A value of $\beta = 4.05$ fits the data reasonably well within a scatter band of ±3 percent. This value of β was determined independently of that obtained from figure 16. Both values of β are in close agreement.

Also shown in figure 17 is the value of $\alpha = 0.80$ which was obtained from equation (33) for extruded Z- and channel sections. Since the extruded sections tested covered only a b_w/t range from 18 to 23, no experimental variation of α was observed. However, from the relation between β and α as given by equation (59), it is reasonable to expect an α variation for extrusions as well as for formed sections. The dashed line in figure 17 appears to be a reasonable estimate of this variation.

It is interesting to note that the extrusion line falls below that for formed sections. This is ascribed to the increased stress-strain characteristics in the corners of the formed sections. Apparently, the strain-hardening due to forming has little, if any, influence upon the value of n. Its only effect is to increase the value of α, presumably by increasing the edge stress at failure as reflected in equation (30).

As indicated by equation (48), equation (61) is valid below values of $\alpha^{1/n}$. By use of equation (64), the values of the cutoffs shown in figure 16 can be readily established. Beyond these cutoffs, extensive test data correlated by Heimerl (ref. 21) indicate that

$$\bar{\sigma}_f = \frac{\pi^2 k_w E_s}{12(1-\nu^2)}\left(\frac{t}{b_w}\right)^2 \tag{65}$$

where k_w can be determined from reference 4.

Cladding Correction

The cladding which may be present on formed sections acts to reduce the value of the buckling stress as indicated in equation (55). The post-buckling load-carrying ability of the section is adequately accounted for by use of the pertinent stress-strain data for the clad materials. The principal effects of the cladding, therefore, include a decrease in the buckling stress as reflected in the cladding reduction factor $\bar{\eta}$ and a slight decrease in E and σ_{cy} as compared with those of the core material.

Needham has presented a considerable amount of test data on channel sections of alclad 2024-T3 and alclad 7075-T6 formed in the -T condition with an inside bend radius of $3t$. The data of figure 16 on 2024-T3 Z- and channel sections can thus be used as a standard of comparison with the alclad 2024-T3 data of Needham (ref. 7) to substantiate the method of correcting for the cladding.

The cladding correction factor $\bar{\eta}$ can be computed from the following formula given in reference 3

$$\bar{\eta} = \frac{1 + 3(\sigma_{cl}/\sigma_{cr})f}{1 + 3f} \tag{66}$$

where f is the ratio of total cladding thickness to total thickness ($f = 0.10$ for alclad 2024-T3 and $f = 0.08$ for alclad 7075-T6 alloys). Since data for the individual test points were not given by Needham (ref. 7), an overall correction based on a value of $\sigma_{cl}/\sigma_{cr} = 1/2$ was used for the alclad 2024-T3 data and $\sigma_{cl}/\sigma_{cr} = 1/3$ for the alclad 7075-T6 data. The values of σ_{cl}/σ_{cr} selected were based on an estimated average value of σ_{cr} for the range of test data presented. These values of $\bar{\eta}$ tend to undercorrect at the higher values of $\bar{\sigma}_f$ and overcorrect at the lower values of $\bar{\sigma}_f$. However, since the correction is of a minor nature, this approach appears to be acceptable.

Needham's test data are presented in a generalized form in figure 18. Equation (54) is compared with the alclad 2024-T3 data by using the value of $\beta = 4.00$ obtained from the 2024-T3 data of figure 16. It can be seen that the data fall within the ±10-percent scatter band. Such scatter was previously observed also for the data on formed angles, figure 14. Inasmuch as Needham's data scattered within ±10-percent limits when correlated according to equation (36), the scatter in figure 18 cannot be attributed to the generalized correlation method in this case. Therefore, the method of correcting for the alclad coating appears to be satisfactory.

The alclad 7075-T6 data in figure 18 fall consistently below the alclad 2024-T3 data. These data are fitted within ±10-percent limits by equation (61) with a value of $\beta = 3.42$. The lower strain-hardening characteristics of alclad 7075-T6 appear to be responsible for the lower value of β.

Increased Corner Properties of Formed Sections

The increased stress-strain properties of sections which are formed in the -T condition have been discussed briefly at various points in this section. Now that the values of β in equation (61) have been established for formed Z- and channel sections of several different materials, it is possible to examine quantitatively the effects of the increased corner properties on crippling.

The average compressive yield strength $\bar{\sigma}_{cy}$ of the corners of Z- and channel sections as compared with that of the unformed sheet has been investigated by Heimerl and Roy for 2017-T3 (ref. 25), Heimerl and Woods for 2024-T3 (ref. 26), Woods and Heimerl for alclad 7075-T6 aluminum alloy (ref. 27), and Gallaher for FS-1h alloy (ref. 24). The ratios of the average compressive yield strengths of the corner $\bar{\sigma}_{cy}$ to the yield strengths of the unformed sheet σ_{cy} for these materials are presented in table 7. The data are for sheets formed in the -T condition with the bend line parallel to the grain direction.

In order to correlate the crippling strengths with the increased corner properties of formed sections, the pertinent values of β and $\bar{\sigma}_{cy}/\sigma_{cy}$ are presented in table 8.

The values of β as a function of $\bar{\sigma}_{cy}/\sigma_{cy}$ are plotted in figure 19 from which a fairly consistent trend is evident. The values in the last column of table 8 are based on the fact that the crippling stress for Z- and channel sections is proportional to β and $\sigma_{cy}^{0.75}$. Thus, in attempting to estimate the value of β for sections which do not have increased corner properties (sections formed in the annealed condition and subsequently heat-treated, e.g.) the values calculated in the last column were averaged and are shown in figure 19. This average value is within ±5 percent of the computed values of table 8 and is based upon the assumption that the crippling strength depends primarily upon the compressive yield strength of the corner. The data except for the 2024-T3 material appear to substantiate this assumption.

Figure 19 also includes the value of $\beta = 3.64$ for extruded Z- and channel sections. When compared with the estimated value of $\beta = 3.30$

at $\bar{\sigma}_{cy}/\sigma_{cy} = 1.00$, it appears that the filleted corner of the extrusion is responsible for approximately a 10-percent increase in crippling strength.

CRIPPLING OF SECTIONS OF GENERAL SHAPE

In the section entitled "Crippling of Extruded Z-, Channel, and H-Sections" crippling strength data for extruded Z-, channel, and H-sections were analyzed and in the next section extruded tubes and formed angle, Z-, and channel sections were considered. Although such sections are in common use, many other sections such as J-, hat, lipped Z-, and channel sections are widely used. Furthermore, the included angle between various elements in the cross section may be considerably different from 90° and the flanges of a Z- or channel section, for example, may be of unequal dimensions. Thus, it is necessary to review available test data on sections not treated previously in order to consider extension of the semi-empirical methods of the two preceding sections to more general shapes.

Empirical methods are in wide use in the aircraft industry for calculating the crippling strength of sections of general shape. Typical of these methods is that presented by Crockett (ref. 19) in which the failing strengths of the various flat and curved plate elements comprising the cross section are summed to determine the crippling load of a section of general shape. Curves for various materials in which the failing strength is given as a function of b/t or R/t have been presented for plates with one edge free and those with no edge free.

Recently, Needham proposed a method of calculating crippling strengths of formed sections in which the cross section is divided into a series of equivalent angles with one-edge-free and no-edge-free conditions (ref. 7). Data for the failing strength as a function of A/t^2 of the equivalent angles were obtained from tests on channel and square-tube sections such as discussed in the preceding section. The crippling load of sections of general shape is obtained by summing the failing loads of the various equivalent-angle elements of the cross section.

Needham stated that an advantage of this method is its inclusion of the influence upon crippling of the increased yield properties in the corners of sections formed in the heat-treated condition (ref. 7). Further, the division of the cross section into angle rather than plate elements places the "cut" in the least sensitive region of the plate.

Although the last argument appears to be rather abstract, focussing attention on the corner by considering the equivalent angle does appear to be of considerable significance. As discussed in the section "Failure of Compressed Flat Plates," failure of an element which buckles elastically

is intimately associated with the stress intensity at the unloaded edge. Since the corner provides the support for the unloaded edge, the number of corners in a section of general shape should have a significant influence upon the crippling strength.

Indeed, the analysis of available test data to be presented in this section suggests that only two geometric parameters are required to determine the crippling strength of many sections of general shape for a particular material. One parameter is A/t^2, which, for a section of constant thickness, is the developed length-thickness ratio. The other parameter is the number of corners c which subdivide the developed length into a series of plate elements.

In order to indicate the influence of the number of corners upon crippling strength, the general shapes to be considered in this section are treated according to this parameter. Thus, one-corner elements include equal- and unequal-flange-angle, T-, and cruciform sections. Two-corner elements include equal- and unequal-flange, Z-, channel, and J-sections. Sections with a number of corners greater than two include lipped angles, lipped Z- and channel sections, and hat and lipped hat sections.

One-Corner Elements

A generalized formula for determining the crippling strength of equal and unequal flange formed angles was obtained in the preceding section based on the analysis of a mass of test data. From equation (54),

$$\frac{\bar{\sigma}_f}{\sigma_{cy}} = \beta_f \left[\left(\frac{ft^2}{A} \right) \left(\frac{\bar{\eta} E}{\sigma_{cy}} \right)^{1/2} \right]^{0.85} \tag{67}$$

where f is the number of flanges and the parameter ft^2/A has been substituted for t/b. Needham first demonstrated that for equal and unequal angles with the same value of the parameter A/ft^2, the crippling strengths were the same within experimental error (ref. 7).

For alclad 2024-T3 angles formed in the -T condition $\beta_f = 0.665$ and for alclad 7075-T6 angles $\beta_f = 0.630$. These values were established from a considerable amount of test data and are probably quite reliable. In an attempt to estimate the value of β_f for extruded angles, the data of Crockett (ref. 19) and of Ramberg and Levy (ref. 28) listed in table 9 were used and are shown in figure 20. Equation (67) with a value of $\beta_f = 0.565$ was used to fit the data. Because of the meager amount of data, this value of β_f can be regarded as only a first approximation.

In the sections "Failure of Flanges" and "Failure of Compressed Flat Plates," it was shown that the degree of warping of the unloaded edge, or

corner in this case, has a strong influence on failure. Thus, angles which are relatively free to warp have lower crippling strengths than cruciforms which have straight unloaded edges by virtue of their opposed flanges.

The crippling strength of extruded cruciforms according to equation (2) is

$$\frac{\bar{\sigma}_f}{\sigma_{cr}} = 0.81\left(\frac{\sigma_{cy}}{\sigma_{cr}}\right)^{0.80} \tag{68}$$

Multiplying both sides of equation (68) by σ_{cr}/σ_{cy},

$$\frac{\bar{\sigma}_f}{\sigma_{cy}} = 0.81\left(\frac{\sigma_{cr}}{\sigma_{cy}}\right)^{0.20} \tag{69}$$

The buckling stress of a long simply supported flange for $\nu = 0.3$ is

$$\sigma_{cr} = 0.388E\left(\frac{t}{b}\right)^2 = 0.388E\left(\frac{ft^2}{A}\right)^2 \tag{70}$$

By substituting equation (70) into equation (69), the generalized crippling formula of extruded cruciform sections becomes

$$\frac{\bar{\sigma}_f}{\sigma_{cy}} = 0.670\left[\left(\frac{ft^2}{A}\right)\left(\frac{E}{\sigma_{cy}}\right)^{1/2}\right]^{0.40} \tag{71}$$

Equation (71) is shown in comparison with equation (67) in figure 20.

An extruded T-section is a common shape in the category of one-corner flanged elements. It has a pair of opposed flanges such as in a cruciform and can be considered as one-half of an H-section. Some of the test data of Crockett (ref. 19) and Ramberg and Levy (ref. 28) for T-sections listed in table 9 are shown in figure 20. (For Crockett's data in table 9, the value $\sigma_{cy} = 43$ ksi was obtained from ref. 28.) It can be observed that equation (71) is in reasonable agreement with the few available test points.

Two-Corner Elements

A generalized crippling-strength formula for equal-flange, Z- and channel sections was obtained in the preceding section based on a large mass of test data. From equation (61)

$$\frac{\bar{\sigma}_f}{\sigma_{cy}} = \beta\left[\left(\frac{t^2}{A}\right)\left(\frac{\bar{\eta}E}{\sigma_{cy}}\right)^{1/3}\right]^{0.75} \tag{72}$$

Values of β for extruded and formed sections of several different aluminum and magnesium alloys are shown in figure 19.

For sections of general shape, the angle between adjacent plate elements is often different from 90°. Since all of the sections considered thus far were composed of right-angle elements, it is pertinent to consider available test data of Roy and Schuette on equal-flange Z-sections where the bend angle was the only systematically varied parameter (ref. 30).

Test data for a typical Z-section are shown in figure 21 as a function of the bend angle. It may be concluded that the buckling and crippling stresses are independent of the bend angle provided that the radius of gyration of the section is not reduced sufficiently to result in primary instability.

In equal-flange Z- and channel sections, the stress conditions at each corner are identical because of certain symmetrical properties of the sections. For unequal-flange Z- or channel sections, the buckling stresses of the flanges are different and consequently the stress conditions at each corner may be different.

In figure 22, two-corner elements tested by Needham (ref. 7) and Crockett (ref. 19) are shown. The crippling data of the unequal-flange channel and Z-sections and the J-sections which are considered as two-corner elements are given in table 10. The sections were formed in the heat-treated condition of alclad 2024-T3 and alclad 2024-T36 aluminum alloys.

The test data for these sections are presented in nondimensional form according to equation (72) in figure 23. The cladding-correction according to equation (66) was based on the estimated buckling stress of the section. Shown for comparison is equation (72) with a value of $\beta = 4.00$ obtained for 2024-T3 and alclad 2024-T3 equal-flange Z- and channel sections. The data for the various two-corner sections presented in figure 23 lie within a ±10-percent scatter band.

Although this relatively simple method of analysis requires substantiation by considerably more test data than were presented here, the available test data indicate that two-corner elements tend to behave in the same manner regardless of their shape. Should the proposed method be confirmed by additional tests, a considerable simplification in determining the crippling strength of two-corner elements will be achieved over methods in current use.

As a possible explanation for the behavior of two-corner elements it is suggested that for unequal-flange elements the following averaging process may be operative. Under a uniform-end-shortening type of test, the corner of the wider flange reaches a value of edge stress corresponding

to failure of the corner first. This corner does not carry any additional load under the continued end shortening required to fail the second corner. The crippling stress is therefore a weighted average of the failure stress of each corner. For equal-flange sections, the crippling stress is the failing stress of each corner. Therefore, unequal-flange sections tend to have an average crippling strength equal to the crippling strength of an equal-flange section having the same value of A/t^2.

In accordance with observations of data on equal-flange Z- and channel sections, equation (72) applies when buckling of the first element in the cross section is elastic. The cutoffs given in figure 16 pertain to figure 23 also. Beyond the cutoffs,

$$\bar{\sigma}_f = \sigma_{cr} \tag{73}$$

where σ_{cr} can be determined with sufficient accuracy by use of buckling coefficients for equal-flange Z- and channel sections given in reference 4.

Multicorner Elements

For convenience, all sections with more than two corners are designated as multicorner elements. Typical sections are shown in figure 24. For the three-corner elements shown, calculations indicated that the flange generally buckled first. For those sections with four or more corners, a web element in the cross section was always responsible for buckling. Since the behavior of the latter closely resembles that of square and rectangular tubes, an attempt was made to correlate available test data on multicorner elements according to the generalized crippling formula for tubes, equation (51):

$$\frac{\bar{\sigma}_f}{\sigma_{cy}} = \beta \left[\left(\frac{t^2}{A} \right) \left(\frac{\bar{\eta} E}{\sigma_{cy}} \right)^{1/2} \right]^{0.85} \tag{74}$$

If this method of correlation were not successful, the value of m would be different from 0.85 and the exponent of the $\sigma_{cy}/\bar{\eta}E$ term would tend to differ from 1/2.

Available test data of Needham on multicorner sections of alclad 2024-T3 formed in the -T condition (ref. 7) and of Crockett on formed alclad 2024-T3 and alclad 2024-T36 (ref. 19) were correlated according to the parameters of equation (74). The shapes of the various sections are shown in figure 24 and the dimensions and crippling data are given in tables 11 and 12. The cladding correction according to equation (66) was based on the estimated buckling stress of the section.

The available test data are shown in figure 25. Lines of slope, m = 0.85, fit the data well according to equation (74), even for the

three-corner elements in which the flange buckled first. The values of β appear to depend only upon the number of corners c and are shown in figure 26. It is a remarkable coincidence that the value of β is almost equal to the number of corners.

This dependence of β upon the number of corners led to the further generalization of equation (74) in the following form:

$$\frac{\bar{\sigma}_f}{\sigma_{cy}} = \beta_c \left[\left(\frac{ct^2}{A} \right) \left(\frac{\bar{\eta} E}{\sigma_{cy}} \right)^{1/2} \right]^{0.85} \tag{75}$$

The test data are shown in the form of equation (75) in figure 27. A value of $\beta = 1.30$ fits all the data within ±5-percent limits. It is interesting to note that these limits are one-half those previously used when correlating Needham's data on formed angle and channel sections.

Again, as for the two-corner elements, a considerable amount of additional test data are required before the proposed method of crippling analysis can be used with complete confidence. In the form of equation (75), the method of analysis for multicorner elements is remarkably simple.

Lips and Bulbs

In estimating the number of corners for sections containing flanges which are stiffened by formed lips or extruded bulbs, certain ambiguities may arise. There is little, if any, test data available on the specific influence of the lip and bulb dimensions on failure of a flange. Therefore, it is advantageous to consider the influence of such stiffening elements upon buckling of a flange since such data were presented in reference 4.

From the charts presented in reference 4, it is relatively simple to determine the necessary lip or flange dimensions which will cause the flange to act as a web from the standpoint of buckling. If the stiffened flange acts as a web, then the lip-flange or bulb-flange junction acts as an additional corner. If the lip or bulb are insufficient to stiffen the flange so that it acts as a web, then the lip flange or bulb flange acts as a stiffened flange without the addition of a corner.

Although these criteria have theoretical justification from the standpoint of the buckling behavior of the stiffened flange, test data on failure of stiffened flanges are required to substantiate the suggested approach.

Research Division, College of Engineering
New York University,
New York, N. Y., April 7, 1955.

APPENDIX A

APPLICATION SECTION

In this application section, the results which may be of importance to the failure of plates and composite elements from the standpoint of analysis and design are summarized.

Flat and Curved Plates

Effective width.- For values of σ_e/σ_{cr} less than 3, the effective width of flat plates may be determined by use of equation (10) in conjunction with the values listed in table 1. These values were theoretically derived and are for long, simply supported flat plates with the following boundary conditions:

(1) Unloaded edges held straight

(2) Unloaded edges free to warp in plane of plate

(3) Various degrees of restraint upon the lateral motion of the plate

For values of σ_e/σ_{cr} greater than 3, the effective width of long flat plates with rotationally restrained unloaded edges held straight and free to move laterally may be determined from equation (5).

The effective-width formulas of long curved plates are based on test data and are, therefore, semiempirical in nature. For effective-width values greater than 0.45, test data on long, clamped curved plates for the range of available test data, $0 \leqq Z_b \leqq 31$, are represented by equation (21)

$$\frac{2b_e}{b} = K_c^{1/2} \frac{t}{b}\left(\frac{E}{\sigma_e}\right)^{1/2} \tag{21}$$

where K_c is the buckling coefficient of the curved plate as determined from reference 5.

For effective-width values less than 0.45, test data for the range of available test data $0 \leqq Z_b \leqq 125$ are represented by equation (23)

$$\frac{2b_e}{b} = K_p 0.43\left[\frac{t}{b}\left(\frac{E}{\sigma_e}\right)^{1/2}\right]^{0.85} \tag{23}$$

where K_p is the flat-plate buckling coefficient.

Failure.- Both theoretical results and test data on the failure strength of long simply supported flat plates can be represented by the following formulas:

$$\frac{\bar{\sigma}_f}{\sigma_{cr}} = \alpha\left(\frac{\sigma_{cy}}{\sigma_{cr}}\right)^n \quad \text{for} \quad \sigma_{cr} \leqq \alpha^{1/n}\sigma_{cy} \tag{A1}$$

$$\bar{\sigma}_f = \sigma_{cr} \quad \text{for} \quad \sigma_{cr} > \alpha^{1/n}\sigma_{cy} \tag{A2}$$

The values of α and n depend upon the restraint of in-plane warping of the unloaded edges as indicated in table 2.

Test data on failure of V-groove plates and long, clamped, flat and curved plates in the range $0 \leqq Z_b \leqq 125$ can be represented in the alternate form

$$\frac{\bar{\sigma}_f}{\sigma_{cy}} = \beta\left[\frac{t}{b}\left(\frac{E}{\sigma_{cy}}\right)^{1/2}\right]^{0.85} \tag{A3}$$

The values of β depend upon the type of edge support and curvature of the plate as follows:

(1) V-groove flat plates: $\beta = 1.42$

(2) Flat clamped plates: $\beta = 1.79$

(3) Curved clamped plates; $10 \leqq Z_b \leqq 125$: $\beta = 2.01$

Although complete data are not available, it is believed that equation (A3) is valid for $\sigma_{cr} < 0.9\sigma_{cy}$ approximately. For $\sigma_{cr} > 0.9\sigma_{cy}$, equation (A2) can be expected to apply.

Crippling

The generalized crippling analyses of test data indicate that, for a given material, the crippling strength depends upon the developed length-thickness ratio and the number of corners of the section:

$$\frac{\bar{\sigma}_f}{\sigma_{cy}} = \beta\left[\frac{t^2}{A}\left(\frac{\bar{\eta}E}{\sigma_{cy}}\right)^{(1/3 \text{ or } 1/2)}\right]^m \quad \text{for} \quad \frac{\bar{\sigma}_f}{\sigma_{cy}} \leqq \alpha^{1/n} \tag{A4}$$

$$\bar{\sigma}_f = \sigma_{cr} \quad \text{for} \quad \frac{\bar{\sigma}_f}{\sigma_{cy}} > \alpha^{1/n} \tag{A5}$$

For formed sections, the additional effects of the alclad coating and the increased properties in the corners require consideration.

As shown in the section entitled "Crippling of Formed Angle, Z-, and Channel Sections," the effects of the alclad coating can be adequately accounted for by use of the cladding reduction factor, as given in equation (66):

$$\bar{\eta} = \frac{1 + 3\left(\sigma_{cl}/\sigma_{cr}\right)f}{1 + 3f} \tag{66}$$

This factor was derived in reference 3 and is based on the buckling stress of the section σ_{cr}. Since the value of $\bar{\eta}$ affects equation (A4) in a relatively minor manner, only a rough estimate of σ_{cr} may be required in most applications.

The value of β in equation (A4) depends upon the increased yield properties $\bar{\sigma}_{cy}$ in the corners of formed sections. As discussed in the above-mentioned section and shown in figure 19, β appears to be proportional to $\left(\bar{\sigma}_{cy}/\sigma_{cy}\right)^{[1-(m/2)]}$ or $\left(\bar{\sigma}_{cy}/\sigma_{cy}\right)^{[1-(m/3)]}$. This follows from equation (A4). Therefore, all values of β determined for one, two, and multicorner elements are shown in figure 28 as a function of $\bar{\sigma}_{cy}/\sigma_{cy}$.

One-corner elements.- The available test data on formed angles and extruded-angle, T-, and cruciform sections are adequately represented by the following generalized crippling formula:

$$\frac{\bar{\sigma}_f}{\sigma_{cy}} = \beta_f \left[\frac{ft^2}{A} \left(\frac{\bar{\eta} E}{\sigma_{cy}} \right)^{1/2} \right]^m \tag{A6}$$

Sections with opposed flanges appear to have greater crippling strengths than those with supported unloaded edges subjected to in-plane warping. This effect is discussed in the sections "Failure of Flanges," "Failure of Compressed Flat Plates," and "Crippling of Extruded Z-, Channel, and H-Sections."

Values of m and β_f for use with equation (A6) are given in table 13 and figure 28.

Equation (A6) is valid for values of $\bar{\sigma}_f/\sigma_{cy} < 0.92$ for formed angles for which $\bar{\sigma}_{cy}/\sigma_{cy} > 1.25$. Test data on cruciforms indicate that equation (A6) is valid for $\bar{\sigma}_f/\sigma_{cy} < 3/4$. In the absence of other test data, this cutoff should be used for all other cases listed in table 13. Beyond the cutoff, equation (73) can be expected to apply:

$$\bar{\sigma}_f = \sigma_{cr} \tag{73}$$

Two-corner elements.- The available test data on formed and extruded Z-, J-, and channel sections are represented by the following generalized crippling formula (61):

$$\frac{\bar{\sigma}_f}{\sigma_{cy}} = \beta \left[\frac{t^2}{A} \left(\frac{\bar{\eta} E}{\sigma_{cy}} \right)^{1/3} \right]^{0.75} \tag{61}$$

Values of β are given in table 14 and figure 28. The range of validity of equation (61) follows from equations (48) and (64):

$$\frac{\bar{\sigma}_f}{\sigma_{cy}} \leq \left[\frac{\beta}{2.14} \left(\frac{t}{b_w} \right)^{0.25} \right]^{4/3} \tag{A7}$$

For an average value of $\beta = 3.6$, equation (A7) reduces to

$$\frac{\bar{\sigma}_f}{\sigma_{cy}} \leq 2 \left(\frac{t}{b_w} \right)^{1/3} \tag{A8}$$

Beyond this cutoff value, equation (73) applies.

An H-extrusion is a special type of two-corner element. Test data for H-extrusions for the range $18 \leqq b_w/t \leqq 23$ are in good agreement with equation (31) for $\bar{\sigma}_f/\sigma_{cr} \leqq 3/4$:

$$\bar{\sigma}_f = 0.80\sigma_{cr}^{0.20}\sigma_{cy}^{0.80} \tag{31}$$

Beyond the cutoff, equation (73) applies.

Multicorner elements.- The available test data on extruded square tubes and formed sections of various shapes as shown in figure 24 are all represented by

$$\frac{\bar{\sigma}_f}{\sigma_{cy}} = \beta_c\left[\frac{ct^2}{A}\left(\frac{\bar{\eta}E}{\sigma_{cy}}\right)^{1/2}\right]^{0.85}$$

Values of β_c are given in table 15 and figure 28.

The range of validity of equation (31) for square tubes is $\bar{\sigma}_f/\sigma_{cy} \leqq 0.7$, as shown in figure 13. From figure 27, it appears that a suitable cutoff for $\beta_c = 1.3$ would be $\bar{\sigma}_f/\sigma_{cy} \leqq 0.9$. There are insufficient test data to establish cutoff values for other values of β_c. However, for $\bar{\sigma}_f/\sigma_{cy} \leqq 3/4$, equation (73) probably is of sufficient accuracy for most cases.

REFERENCES

1. Gerard, George: Handbook of Structural Stability. Part V - Compressive Strength of Flat Stiffened Panels. NACA TN 3785, 1957.

2. Kuhn, Paul, Peterson, James P., and Levin, L. Ross: A Summary of Diagonal Tension. Part I - Methods of Analysis. NACA TN 2661, 1952.

3. Gerard, George, and Becker, Herbert: Handbook of Structural Stability. Part I - Buckling of Flat Plates. NACA TN 3781, 1957.

4. Becker, Herbert: Handbook of Structural Stability. Part II - Buckling of Composite Elements. NACA TN 3782, 1957.

5. Gerard, George, and Becker, Herbert: Handbook of Structural Stability. Part III - Buckling of Curved Plates and Shells. NACA TN 3783, 1957.

6. Stowell, Elbridge Z.: Compressive Strength of Flanges. NACA TN 2020, 1950.

7. Needham, Robert A.: The Ultimate Strength of Aluminum-Alloy Formed Structural Shapes in Compression. Jour. Aero. Sci., vol. 21, no. 4, Apr. 1954, pp. 217-229.

8. Mayers, J., and Budiansky, Bernard: Analysis of Behavior of Simply Supported Flat Plates Compressed Beyond the Buckling Load into the Plastic Range. NACA TN 3368, 1955.

9. Argyris, J. H., and Dunne, P. C.: Structural Principles and Data. Part 2, Structural Analysis. Handbook of Aero., no. 1, fourth ed., Sir Isaac Pitman & Sons, Ltd. (London), 1952.

10. Anderson, Roger A., and Anderson, Melvin S.: Correlation of Crippling Strength of Plate Structures with Material Properties. NACA TN 3600, 1956.

11. Botman, M.: De experimentele bepaling van de meedragende breedte van vlakke platen in het elastische en het plastische gebied (deel II). (The Experimental Determination of the Effective Width of Flat Plates in the Elastic and Plastic Range (part II).) Rep. S.438, Nationaal Luchtvaartlaboratorium, Jan. 1954.

12. Besseling, J. F.: De experimentele bepaling van de meedragende breedte van vlakke platen in het elastische en het plastische gebied. (The Experimental Determination of the Effective Width of Flat Plates in the Elastic and Plastic Range.) Rep. S.414, Nationaal Luchtvaartlaboratorium, Feb. 1953.

13. Cox, H. L., and Pribram, E.: The Elements of the Buckling of Curved Plates. Jour. R.A.S., vol. 52, no. 453, Sept. 1948, pp. 551-565.

14. Cox, H. L., and Clenshaw, W. J.: Compression Tests on Curved Panels of Thin Sheet Duralumin. R. & M. No. 1894, British A.R.C., 1941.

15. Jackson, K. B., and Hall, A. H.: Curved Plates in Compression. Rep. AR-1, Nat. Res. Council, 1947.

16. Levy, Samuel: Large-Deflection Theory of Curved Sheet. NACA TN 895, 1943.

17. Ramberg, Walter, Levy, Samuel, and Fienup, Kenneth L.: Effect of Curvature on Strength of Axially Loaded Sheet-Stringer Panels. NACA TN 944, 1944.

18. Sechler, Ernest E., and Dunn, Louis G.: Airplane Structural Analysis and Design. John Wiley & Sons, Inc., 1942.

19. Crockett, Harold B.: Predicting Stiffener and Stiffened Panel Crippling Stresses. Jour. Aero. Sci., vol. 9, no. 13, Nov. 1942, pp. 501-509.

20. Schuette, E. H.: Observations of the Maximum Average Stress of Flat Plates Buckled in Edge Compression. NACA TN 1625, 1949.

21. Heimerl, George J.: Determination of Plate Compressive Strengths. NACA TN 1480, 1947.

22. Gerard, George: Secant Modulus Method for Determining Plate Instability Above the Proportional Limit. Jour. Aero. Sci., vol. 13, no. 1, Jan. 1946, pp. 38-44, 48.

23. Heimerl, George J., and Roberts, William M.: Determination of Plate Compressive Strengths at Elevated Temperatures. NACA Rep. 960, 1950. (Supersedes NACA TN 1806.)

24. Gallaher, George L.: Plate Compressive Strength of FS-1h Magnesium-Alloy Sheet and a Maximum-Strength Formula for Magnesium-Alloy and Aluminum-Alloy Formed Sections. NACA TN 1714, 1948.

25. Heimerl, George J., and Roy, J. Albert: Column and Plate Compressive Strengths of Aircraft Structural Materials. 17S-T Aluminum-Alloy Sheet. NACA WR L-20, 1945. (Formerly NACA ARR L5F08.)

26. Heimerl, George J., and Woods, Walter: Effect of Brake Forming on the Strength of 24S-T Aluminum-Alloy Sheet. NACA TN 1072, 1946.

27. Woods, Walter, and Heimerl, George J.: Effect of Brake Forming in Various Tempers on the Strength of Alclad 75S-T Aluminum-Alloy Sheet. NACA TN 1162, 1947.

28. Ramberg, Walter, and Levy, Samuel: Instability of Extrusions Under Compressive Loads. Jour. Aero. Sci., vol. 12, no. 4, Oct. 1945, pp. 485-498.

29. Templin, R. L., Hartmann, E. C., and Paul, D. A.: Typical Tensile and Compressive Stress-Strain Curves for Aluminum Alloy 24S-T, Alclad 24S-T, 24S-RT, and Alclad 24S-RT Products. Tech. Paper No. 6, Aluminum Res. Lab., Aluminum Co. of Am., 1942.

30. Roy, J. Albert, and Schuette, Evan H.: The Effect of Angle of Bend Between Plate Elements on the Local Instability of Formed Z-Sections. NACA WR L-268, 1944. (Formerly NACA RB I4I26.)

31. Coan, J. M.: Large-Deflection Theory for Plates With Small Initial Curvature Loaded in Edge Compression. Jour. Appl. Mech., vol. 18, no. 2, June 1951, pp. 143-151.

TABLE 1.- VALUES OF β FOR EFFECTIVE WIDTH OF LONG SIMPLY SUPPORTED FLAT PLATES

[Data from reference 8]

A_r/at	Unloaded edges held straight, v = Constant	Unloaded edges free to move in plane of plate, $\sigma_y = 0$
0	0.500	0.408
.25	.548	.458
.5	.580	.494
1	.621	.540
2	.665	.590
4	.696	.613
∞	.746	.684

TABLE 2.- VALUES OF α AND n FOR FLAT PLATES

Element	α	n
Theory for straight unloaded edges	0.78	0.80
V-groove test data	.80	.58
Three-bay plate test data	.80	.65

TABLE 3.- VALUES OF α AND n FOR VARIOUS EXTRUDED SECTIONS AND MATERIALS

Material	Values of α for -		
	H-section, n = 0.80	Z-section, n = 0.72	Channel section, n = 0.72
2014-T4	0.83	0.85	0.85
2024-T4	.80	.81	.81
R303-T	.80	.83	.81
7075-T6	.77	.80	.79
0-1 HTA	.78	.82	.79
	[a].80	[a].82	[a].81

[a]Average.

TABLE 4.- CRIPPLING OF FORMED EQUAL FLANGE ANGLES

Material	$\bar{C}$, ksi	σ_{cy}, ksi	E, ksi
2024-T3	225.0	45.1	10,500
Alclad 2024-T3	200.1	42.0	10,000
Alclad 7075-T6	259.0	66.2	10,000

TABLE 5.- VALUES OF α FOR CRIPPLING OF FORMED Z- AND CHANNEL SECTIONS

Material	Section	$(b_w/t)_{av}$	α
2017-T3	Z, channel	25.5	0.85
		31.7	.82
2024-T3	Z	18.8	.89
		23.1	.87
		26.7	.85
		31.9	.77
		38.7	.74
2024-T3	Channel	24.5	.87
		29.5	.84
		34.2	.80
		43.2	.74
FS-1h	Z	29	.81
		35	.77

TABLE 6.- VALUES OF K_w AS A FUNCTION OF b_f/b_w FOR Z- AND CHANNEL SECTIONS

b_f/b_w	K_w	$K_w^{0.25}\left[1 + \left(2b_f/b_w\right)\right]^{0.75}$
0.4	3.37	2.11
.6	2.00	2.14
.8	1.25	2.17

TABLE 7.- INCREASED CORNER PROPERTIES

FOR FORMED SECTIONS

Sheet material	t, in.	R/t	$\bar{\sigma}_{cy}/\sigma_{cy}$
2017-T3	0.125	3	1.23
2024-T3	.125	3	1.35
Alclad 7075-T6	.102	6	1.06
FS-1h	.102	4.3	1.15

TABLE 8.- VARIATION OF β WITH $\bar{\sigma}_{cy}/\sigma_{cy}$ FOR

Z- AND CHANNEL SECTIONS

Material	R/t	$\bar{\sigma}_{cy}/\sigma_{cy}$	β	$\beta/\left(\bar{\sigma}_{cy}/\sigma_{cy}\right)^{3/4}$
2017-T3	3	1.23	4.00	3.42
2024-T3	3	1.35	4.00	3.19
Alclad 2024-T3	3	1.35	4.00	3.19
Alclad 7075-T6	3	[a]1.09	3.42	3.14
FS-1h	4.3	1.15	3.78	3.42
				[b]3.30
All extrusions	1 (filleted)	1.00	3.64	

[a]Estimated value.

[b]Average value.

TABLE 9.- TEST DATA ON EXTRUDED ANGLE AND T-SECTIONS

[LS shapes are from data of Crockett (ref. 19); shapes 6 and 7 are from data of Ramberg and Levy (ref. 28).]

Shape	t, in.	b_1, in.	b_2, in. [a]	A/t^2	$\frac{A}{ft^2}\left(\frac{\sigma_{cy}}{E}\right)^{1/2}$	$\bar{\sigma}_f$, ksi	σ_{cy}, ksi [b]	$\bar{\sigma}_f/\sigma_{cy}$
[c]Angle sections								
LS 208	0.125	0.875	1.75	21	0.67	32.4	43	0.754
LS 209	.051	.50	.625	22	.70	30.7	43	.737
LS 210	.125	1.00	1.75	22	.70	32.8	43	.764
6	.064	1.00	2.00	46.1	1.44	----	42.4	[d].43
[c]T-sections								
LS 236	0.065	1.00	1.50	38.5	0.82	31.0	43	0.721
[e]LS 247	.040	.75	1.25	50	1.06	29.2	43	.680
[e]LS 248	.050	1.00	1.50	50	1.06	28.0	43	.652
[e]LS 249	.064	1.00	1.50	39	.83	32.2	43	.750
7	.100	3.00	2.00	49.6	1.09	----	40.4	[d].65

[a]For T-sections, b_2 is total width of opposed flanges.

[b]For Crockett's data (ref. 19), σ_{cy} = 43 ksi as obtained by Templin, Hartmann, and Paul (ref. 29).

[c]In extrusion fillets for angles, $0 < R/t < 1/2$; for T-sections, $1/2 < R/t < 1$.

[d]Values of $\bar{\sigma}_f/\sigma_{cy}$ correspond to $L'/\rho = 20$.

[e]The b_1 flange had a 1/16-in.-radius bulb at free edge.

TABLE 10.- TEST DATA ON TWO-CORNER ELEMENTS

Shape (a)	t, in.	A/t^2	$\frac{A}{t^2}\left(\frac{\sigma_{cy}}{\bar{\eta}E}\right)^{1/3}$	$\bar{\sigma}_f$, ksi	σ_{cy}, ksi (b)	$\bar{\sigma}_f/\sigma_{cy}$
E1	0.0252	136.7	22.10	15.8	42	0.376
E2	.0253	87.2	14.10	22.6	42	.538
E3	.0504	67.6	10.92	24.7	42	.588
E4	.0255	95.5	15.45	21.0	42	.500
X785-C	.025	103	16.52	19.6	41	.478
	.040	64.5	10.68	26.2	41	.639
	.064	40.3	6.93	37.7	41	.920
	.025	103	16.67	22.0	51	.431
	.040	64.5	11.47	29.2	51	.573
	.064	40.3	7.45	43.5	51	.853
XLS-165	.025	99.4	15.94	20.7	41	.505
	.040	62.1	10.28	26.6	41	.648
	.025	99.4	17.12	25.6	51	.502
	.040	62.1	11.02	34.7	51	.680
LS-160	.025	80.8	12.97	23.7	41	.578
	.040	50.5	8.36	32.4	41	.790
	.025	80.8	13.92	25.9	51	.507
	.040	50.5	8.98	35.9	51	.704
LS-161	.025	93.6	15.03	21.5	41	.525
	.040	58.5	9.68	29.3	41	.715
	.025	93.6	16.15	23.2	51	.455
	.040	58.5	10.40	30.4	51	.596

[a]See figure 22 for dimensions of sections.

[b]For Crockett's data (ref. 19), values of σ_{cy} were obtained from Templin, Hartmann, and Paul (ref. 29).

TABLE 11.- DIMENSIONS OF MULTICORNER SECTIONS

[See figure 24 for explanation of notation]

Shape	a, in.	b, in.	c, in.	d, in.	e, in.	t, in.	A/t^2
Three-corner elements							
A1	1.000	1.000	0.434	0.434	-----	0.0250	107.6
A2	1.568	1.568	.437	.437	-----	.0315	119.8
F3	1.788	.953	.443	.438	-----	.0500	67.2
G1	.977	1.561	.881	.422	-----	.0318	111.2
G2	.936	2.457	.863	.425	-----	.0255	175.7
Four-corner elements							
C1	2.457	0.980	0.980	0.449	0.449	0.0200	247.0
C2	2.487	.987	.987	.414	.414	.0315	158.4
C3	2.412	.892	.892	.408	.408	.0382	129.7
C4	2.236	1.262	1.262	.428	.428	.0505	104.1
C5	1.813	.862	.862	.425	.425	.0258	157.0
F1	2.331	.856	1.241	.424	.424	.0318	155.5
F2	2.118	.976	1.266	.732	.442	.0318	163.7
D1	1.231	2.260	.853	.443	.443	.0203	239.0
D2	1.255	2.195	.875	.429	.429	.0382	128.1
D3	.847	1.887	.847	.431	.431	.0258	160.8
D4	1.244	1.950	1.244	.423	.423	.0252	198.5
D5	1.250	1.904	1.250	.415	.415	.0383	127.1
X785-D	.625	1.250	.750	-----	-----	.025	167.5
X785-D	.625	1.250	.750	-----	-----	.040	104.7
Five-corner elements							
H	3.668	1.528	0.393	0.943	-----	0.0318	191.7
LS-152	2.500	1.312	.250	.562	-----	.040	126.5
LS-153	3.250	1.437	.187	.562	-----	.051	101.6
Six-corner elements							
B1	1.205	1.340	1.236	0.447	-----	0.0255	282.0
B2	1.198	1.610	1.001	.445	-----	.0320	199.5

TABLE 12.- TEST DATA ON MULTICORNER SECTIONS

Shape (a)	c	$\frac{A}{t^2}\left(\frac{\sigma_{cy}}{\bar{\eta}E}\right)^{1/2}$	$\bar{\sigma}_f$, ksi	σ_{cy}, ksi (b)	$\bar{\sigma}_f/\sigma_{cy}$
A1	3	7.30	26.2	42	0.624
A2	3	8.21	22.9	42	.545
F3	3	4.91	35.0	42	.839
G1	3	7.32	26.2	42	.624
G2	3	11.56	17.8	42	.424
C1	4	16.25	17.3	42	.412
C2	4	10.42	24.1	42	.574
C3	4	8.46	27.5	42	.655
C4	4	7.30	31.4	42	.748
C5	4	10.32	24.0	42	.571
F1	4	10.35	23.9	42	.569
F2	4	10.78	23.8	42	.567
D1	4	15.70	17.4	42	.414
D2	4	8.78	28.2	42	.671
D3	4	10.58	23.3	42	.555
D4	4	13.07	19.0	42	.452
D5	4	8.72	27.7	42	.659
X785-D	4	10.72	22.0	41	.537
X785-D	4	7.03	31.1	51	.760
X785-D	4	11.97	24.3	41	.477
X785-D	4	7.83	36.2	51	.710
H	5	13.00	25.0	42	.595
LS-152	5	9.50	39.5	51	.775
LS-153	5	7.75	44.1	51	.864
B1	6	19.15	20.8	42	.495
B2	6	13.70	27.1	42	.645

[a]See figure 24 and table 11 for shapes and dimensions.

[b]For Crockett's data (X785-D, LS-152, LS-153) (ref. 19), values of σ_{cy} were obtained from Templin, Hartmann, and Paul (ref. 29).

TABLE 13.- ONE-CORNER ELEMENTS

Element	m	$\bar{\sigma}_{cy}/\sigma_{cy}$	β_f	Remarks
Formed angles	0.85	1.0	0.59	
		1.1	.62	
		1.2	.65	Estimated
		>1.25	.66	
Extruded angles	.85	-----	.57	R/t = 1/2
		-----	.60	Estimated for R/t = 1
T-extrusions	.40	-----	.67	Based on limited test data
Cruciform extrusions	.40	-----	.67	

TABLE 14.- TWO-CORNER ELEMENTS

Element	$\bar{\sigma}_{cy}/\sigma_{cy}$	β	Remarks
Formed angles	1.0	3.3	Estimated
	1.1	3.5	
	1.2	3.8	
	>1.25	4.0	
Extruded angles		3.6	R/t = 1

TABLE 15.- MULTICORNER ELEMENTS

Elements	$\bar{\sigma}_{cy}/\sigma_{cy}$	β_c	Remarks
Formed angles	1.0 1.1 >1.25	1.1 1.2 1.3	Estimated Estimated
Extruded angles	-----	1.2	Estimated for R/t = 1
Extruded square tubes	-----	1.4	

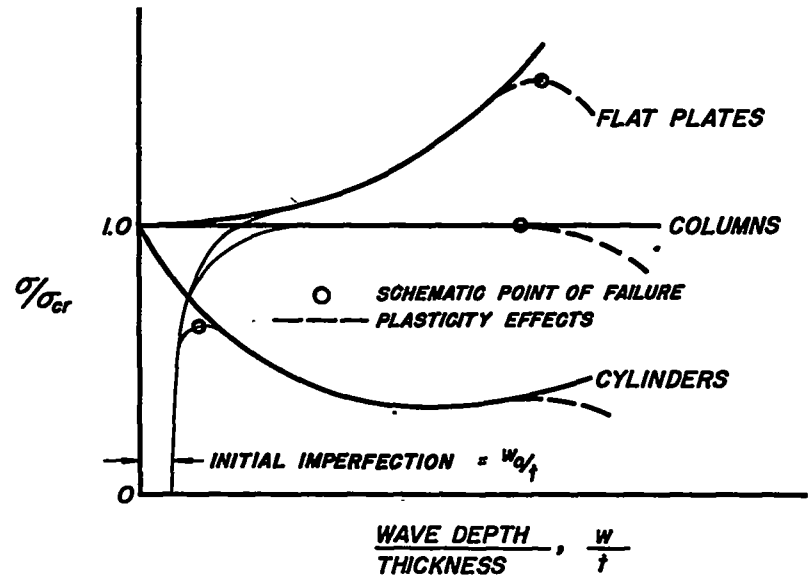

(a) Elastic buckling.

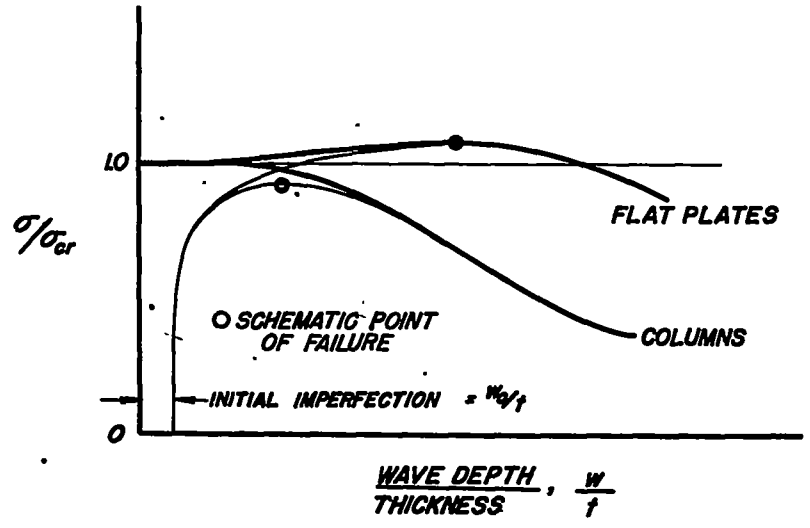

(b) Plastic buckling.

Figure 1.- Schematic postbuckling behavior of various axially compressed elements.

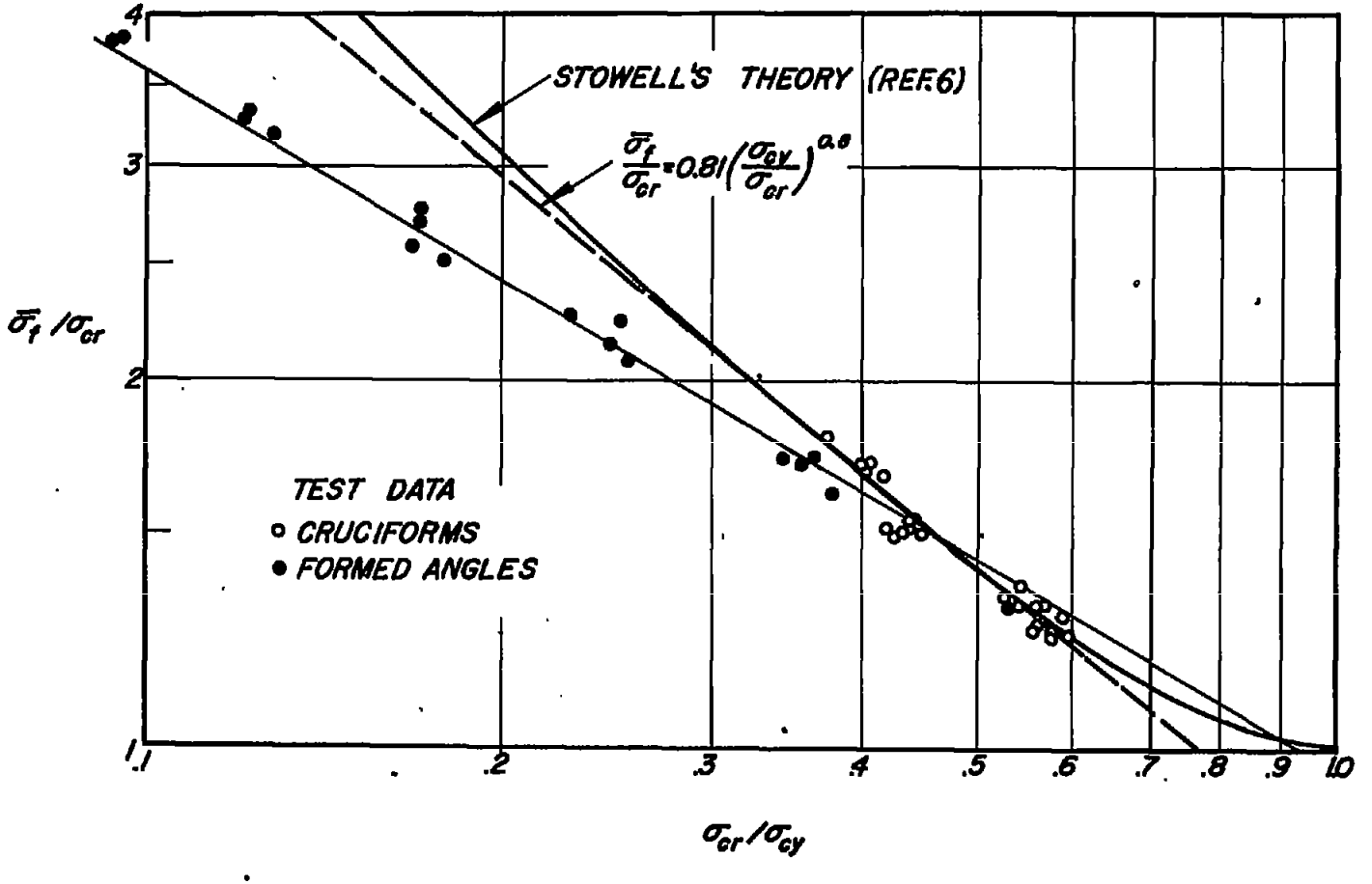

Figure 2.- Comparison of theoretical failure analysis with test data on 2024-T4 aluminum-alloy cruciform sections and 2024-T3 formed angles.

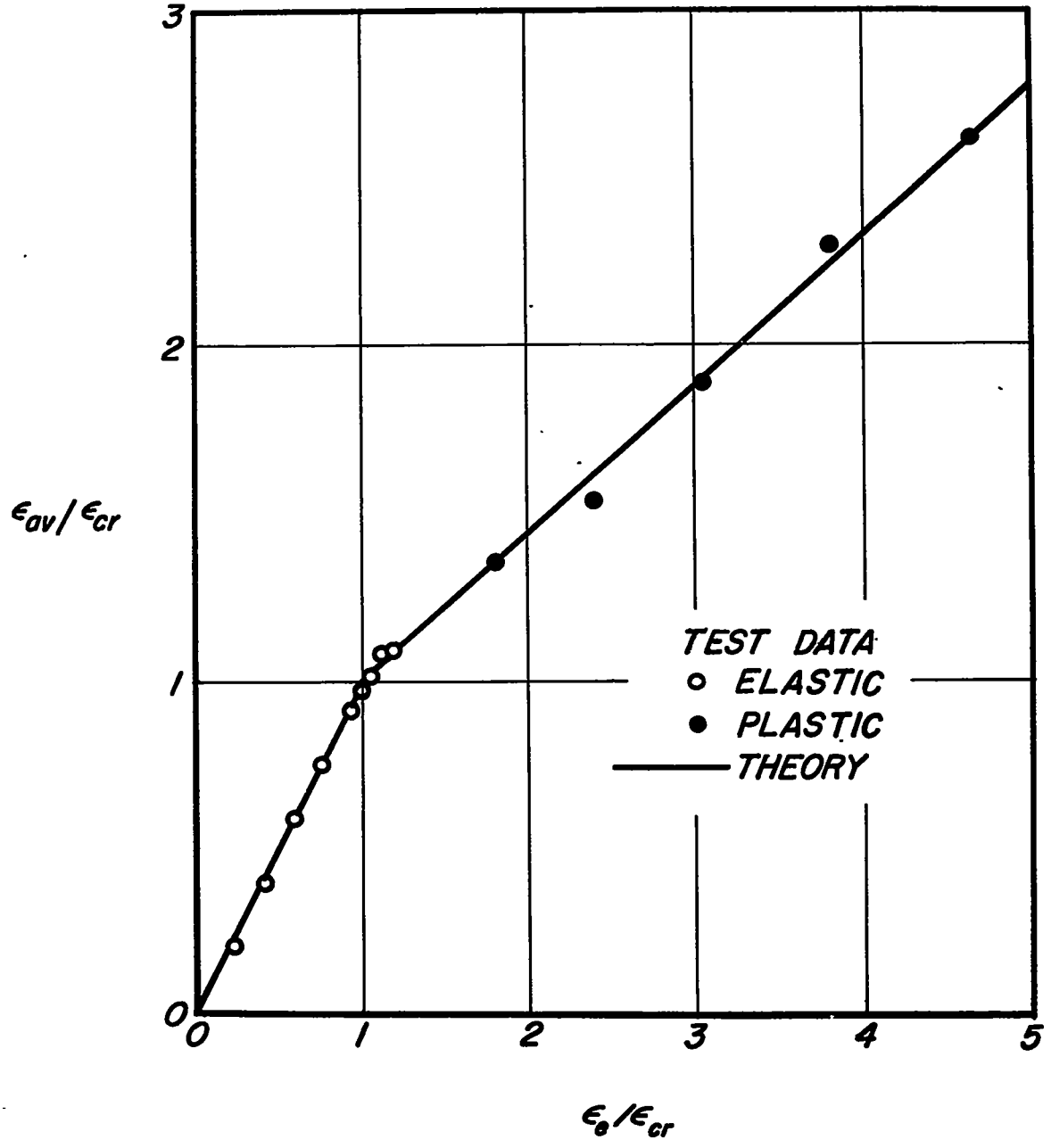

Figure 3.- Comparison of experimental data with theory for postcritical behavior of hinged flange.

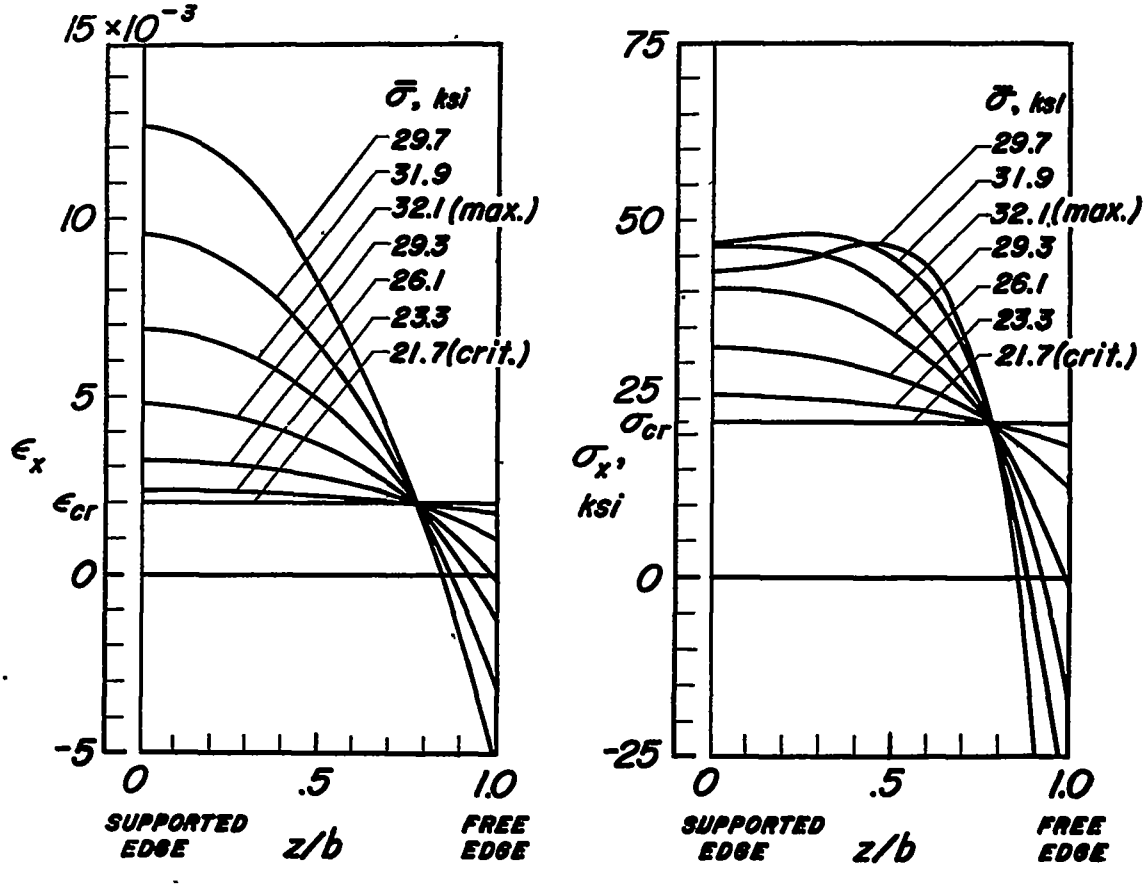

(a) Strain distribution. (b) Stress distribution.

Figure 4.- Theoretical strain and stress distribution across a hinged flange of 2024-T4 aluminum alloy (data from Stowell, ref. 6).

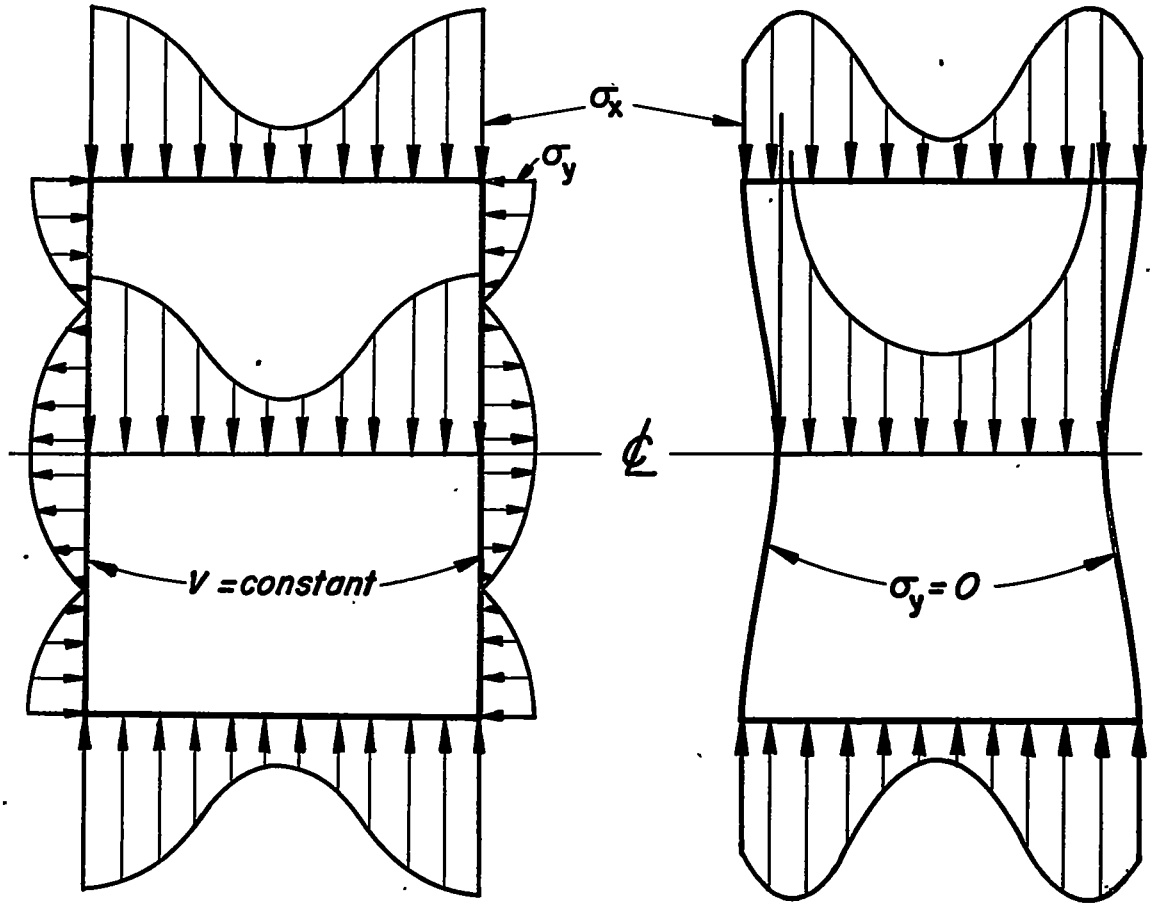

(a) Straight unloaded edges.

(b) Stress-free unloaded edges free to warp in plane of plate.

Figure 5.- Stresses and displacements of flat plates after buckling under conditions of uniform end shortening (see ref. 31).

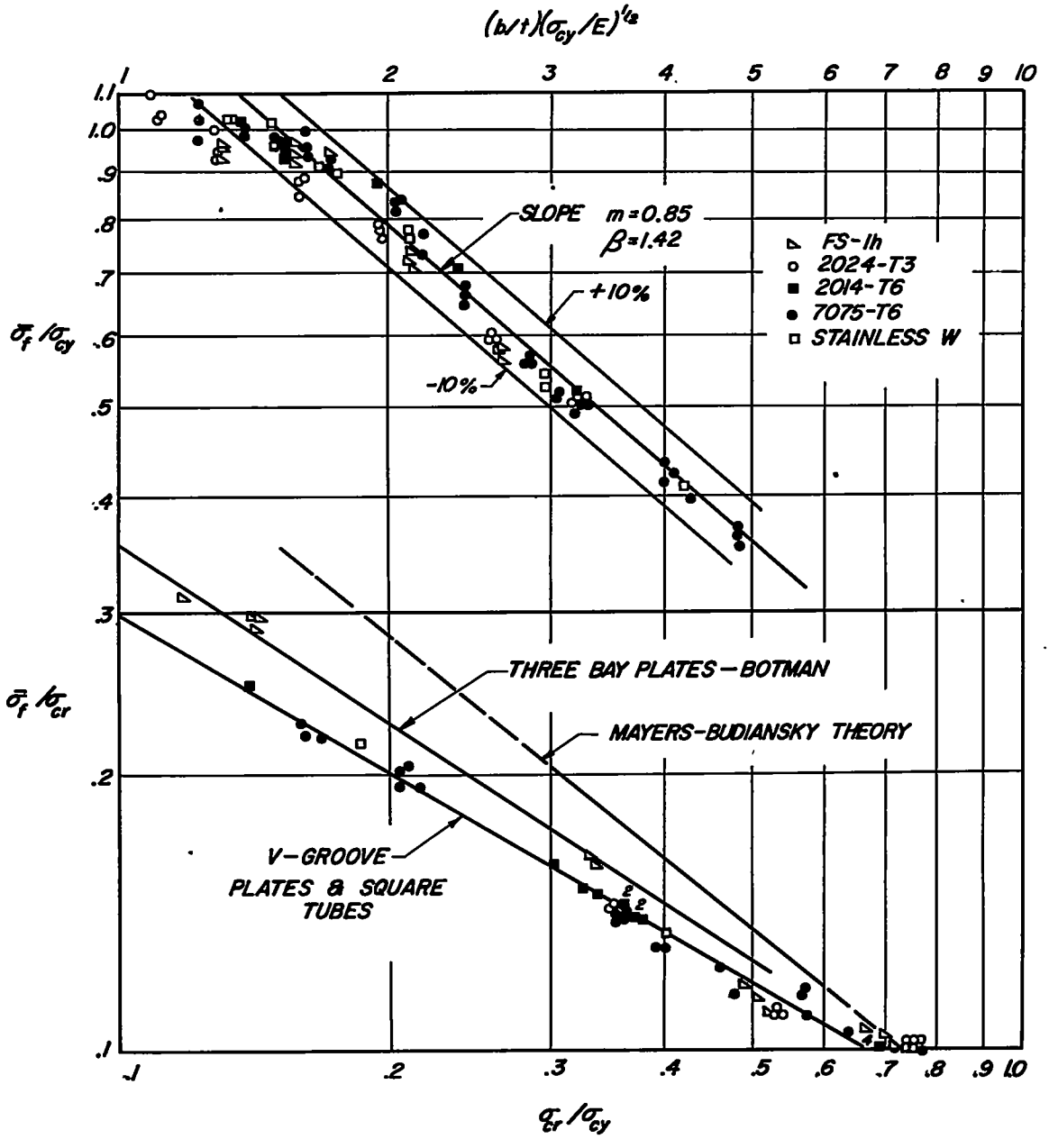

Figure 6.- Results of theoretical failure analysis of compressed flat plates with straight unloaded edges and test data on various plate elements.

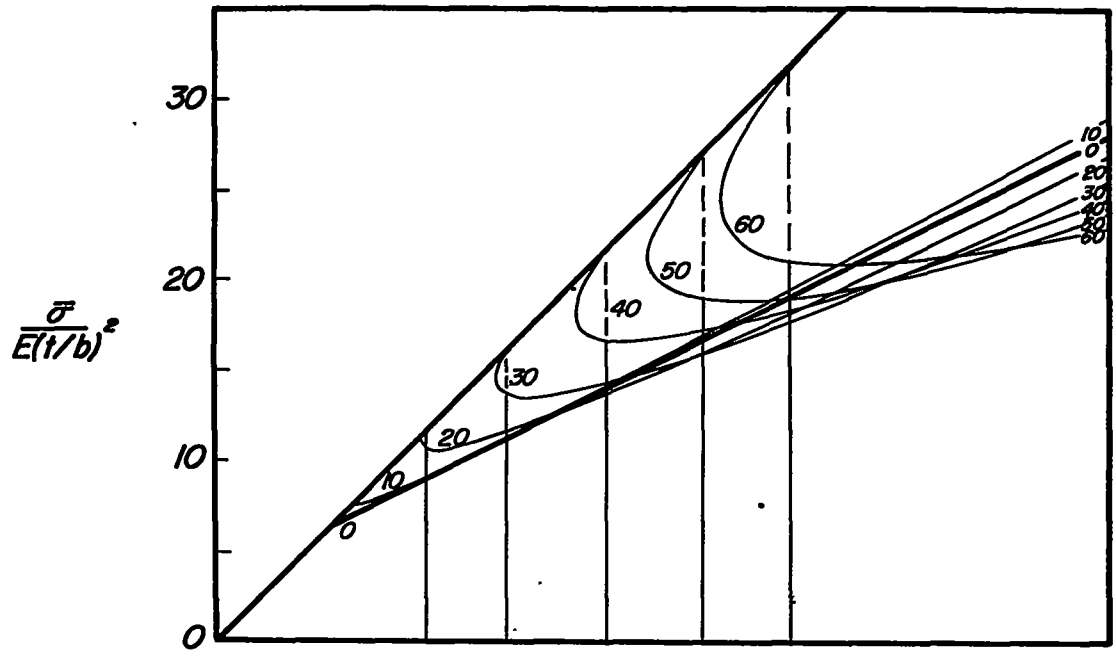

(a) Elastic postbuckling behavior.

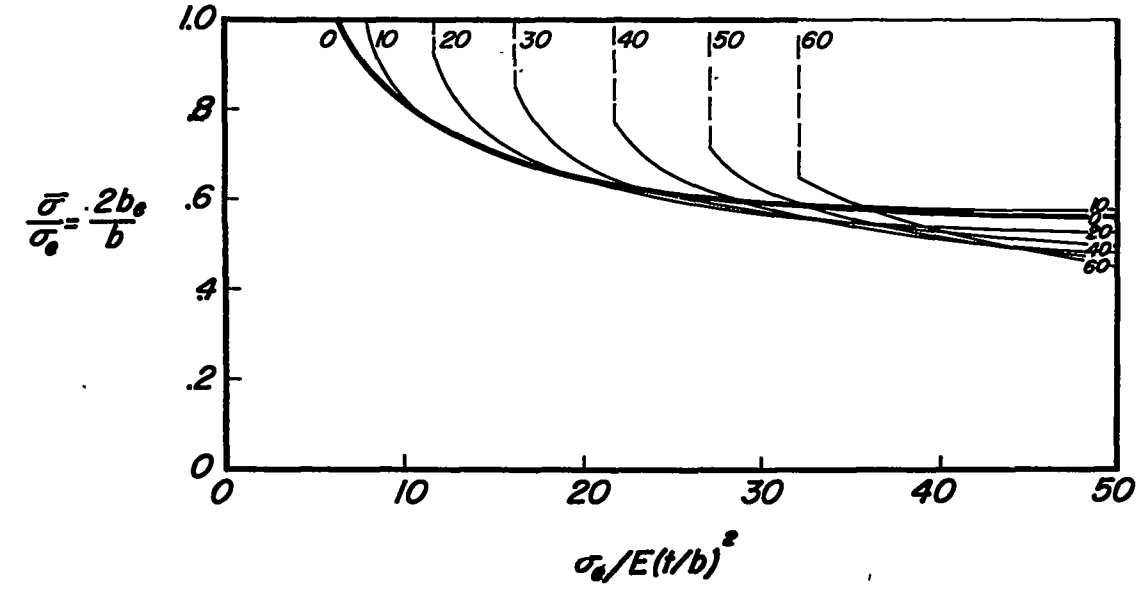

(b) Effective width.

Figure 7.- Data for long, clamped, curved plates. Numbers indicate values of $\frac{b^2}{Rt} = Z_b\left(1 - \nu^2\right)^{-1/2}$.

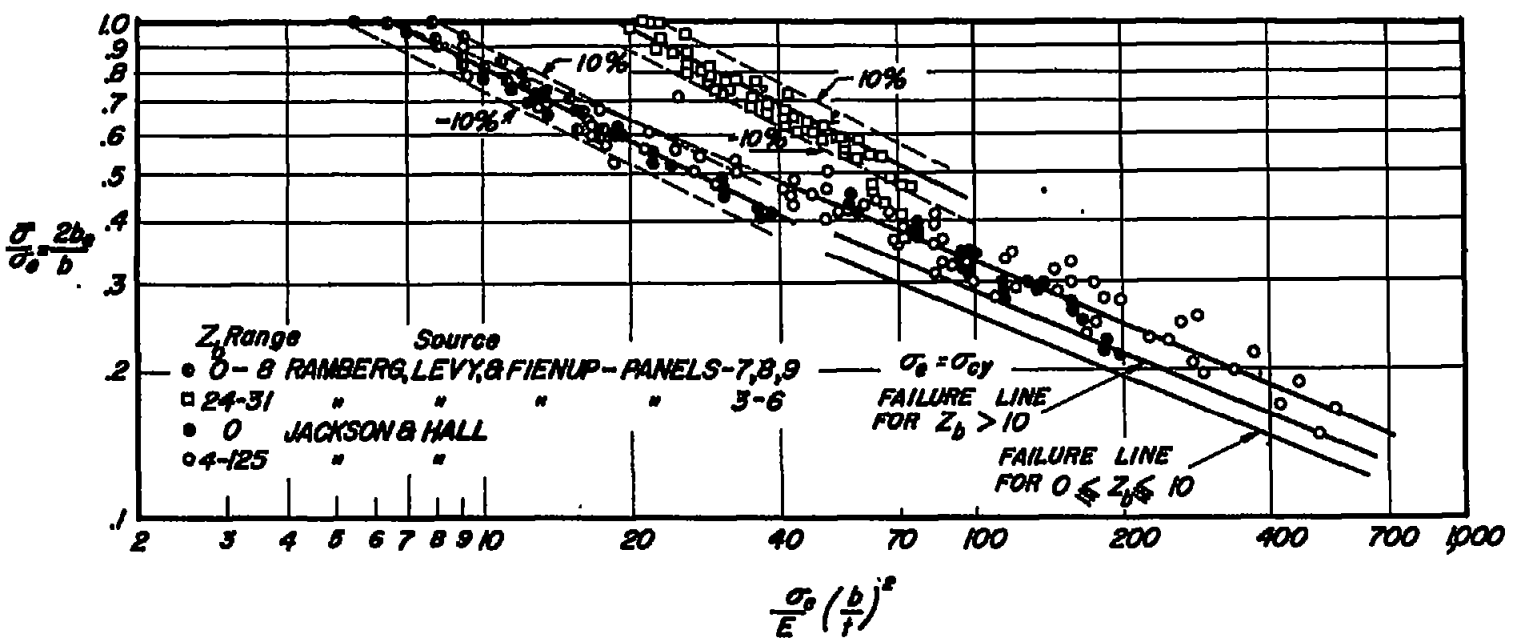

Figure 8.- Experimental data on effective width of long, clamped, curved plates. Ramberg, Levy, and Fienup, reference 17; Jackson and Hall, reference 15.

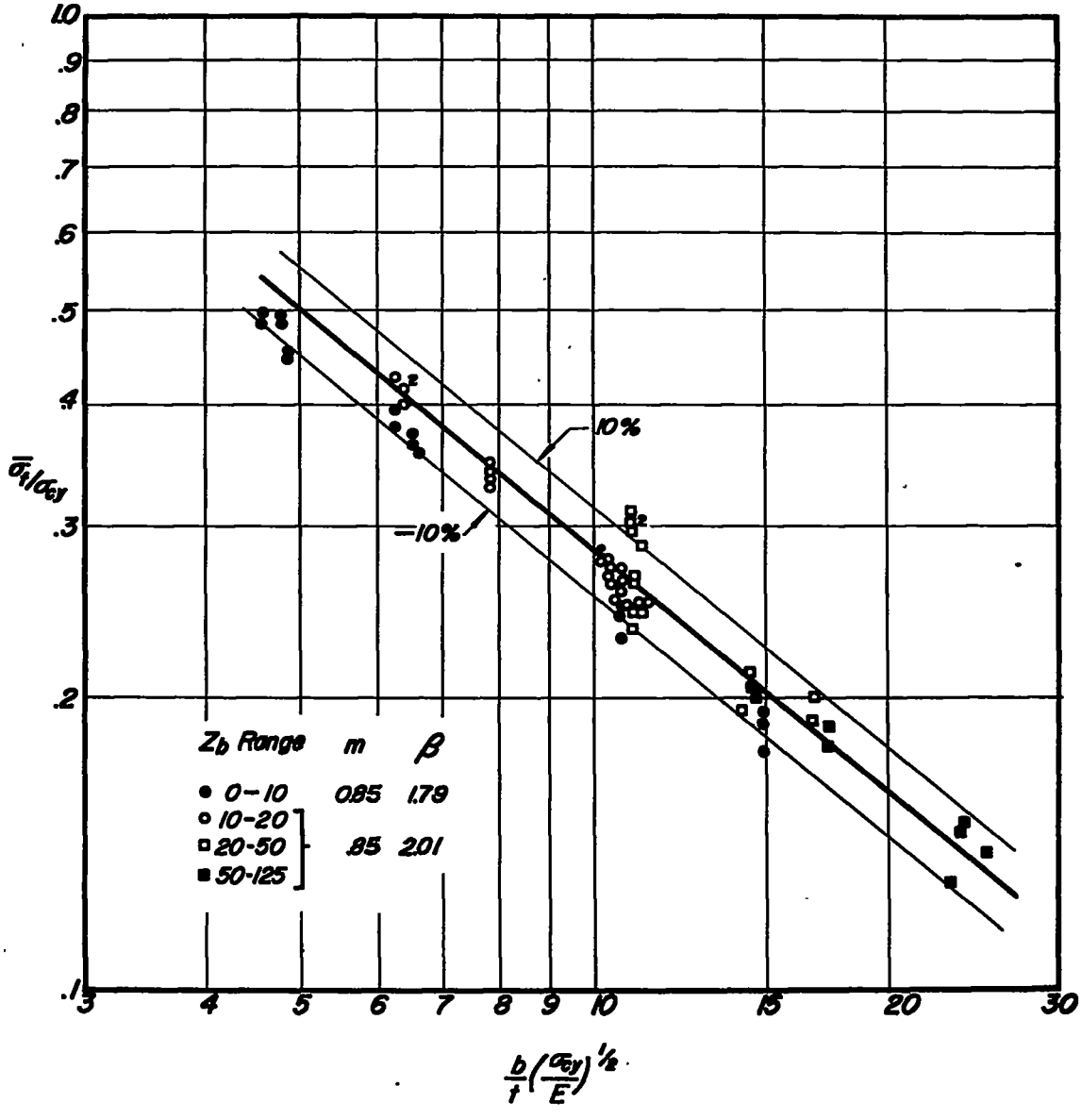

Figure 9.- Experimental data on failure of long, clamped, flat and curved plates.

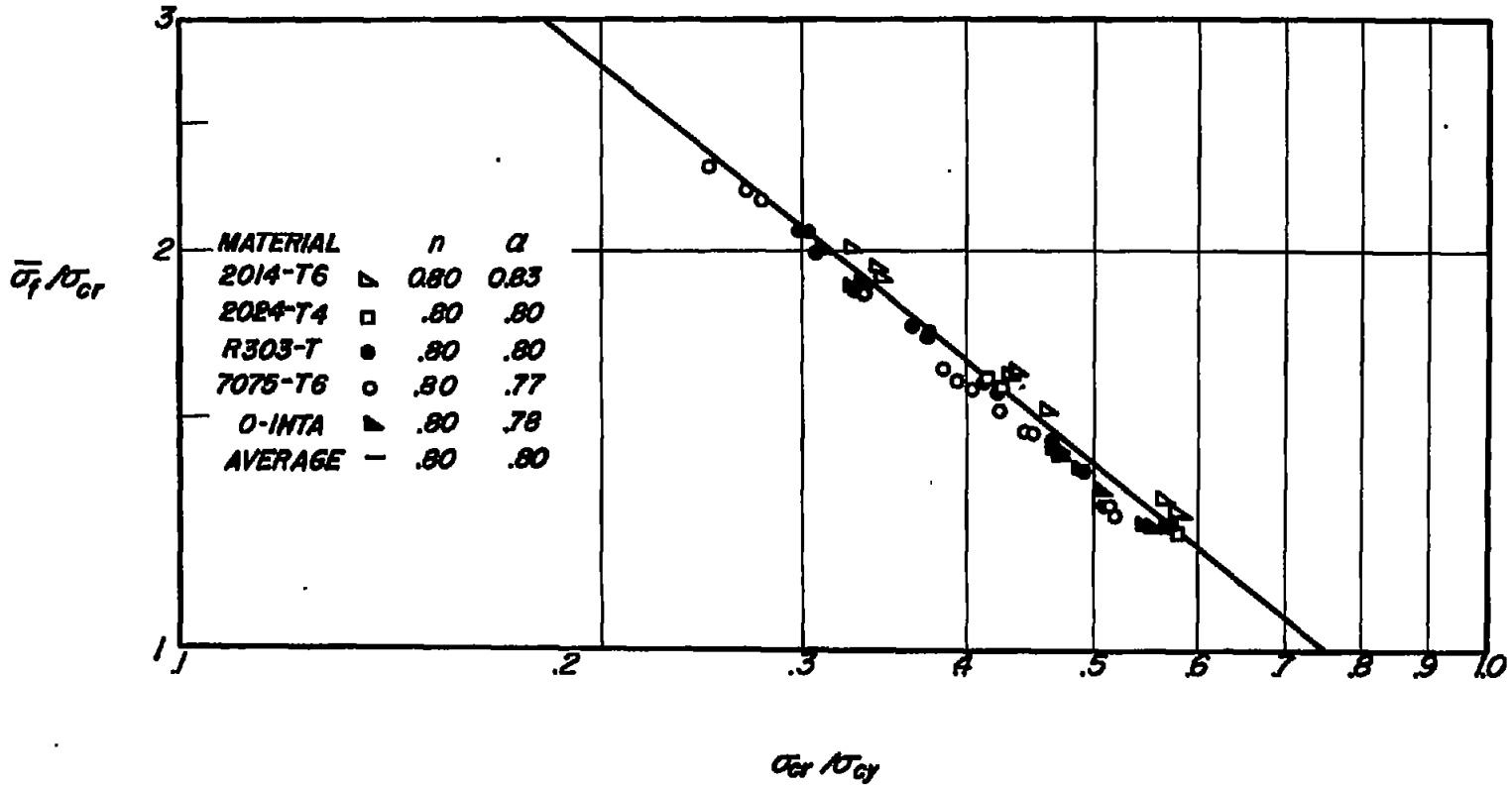

(a) H-extrusions.

Figure 10.- Crippling data for various extrusions.

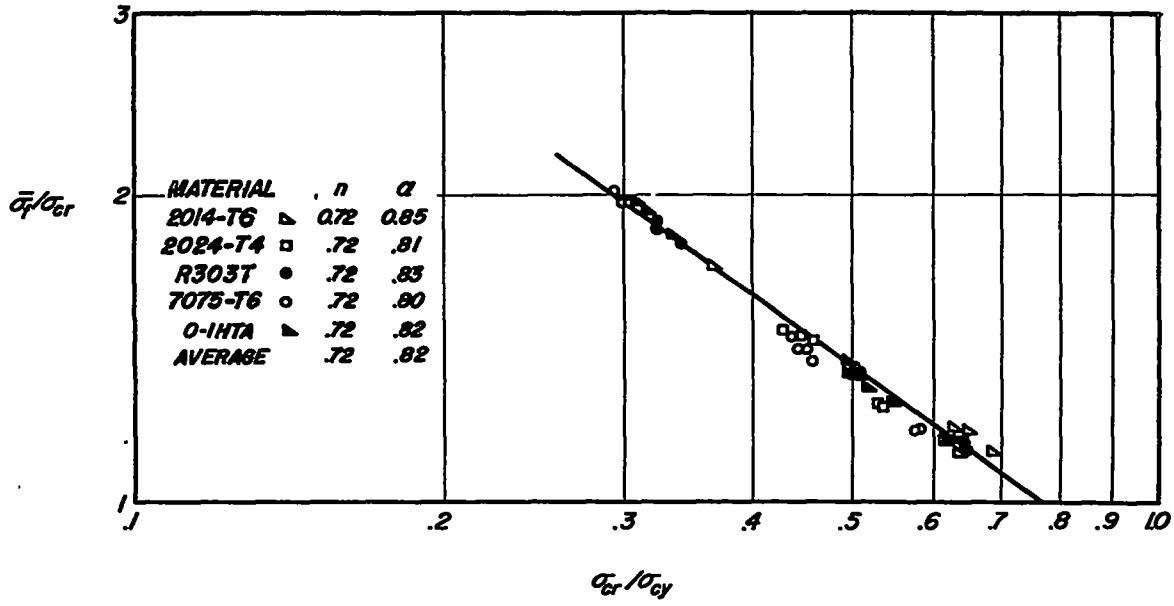

(b) Z-extrusions.

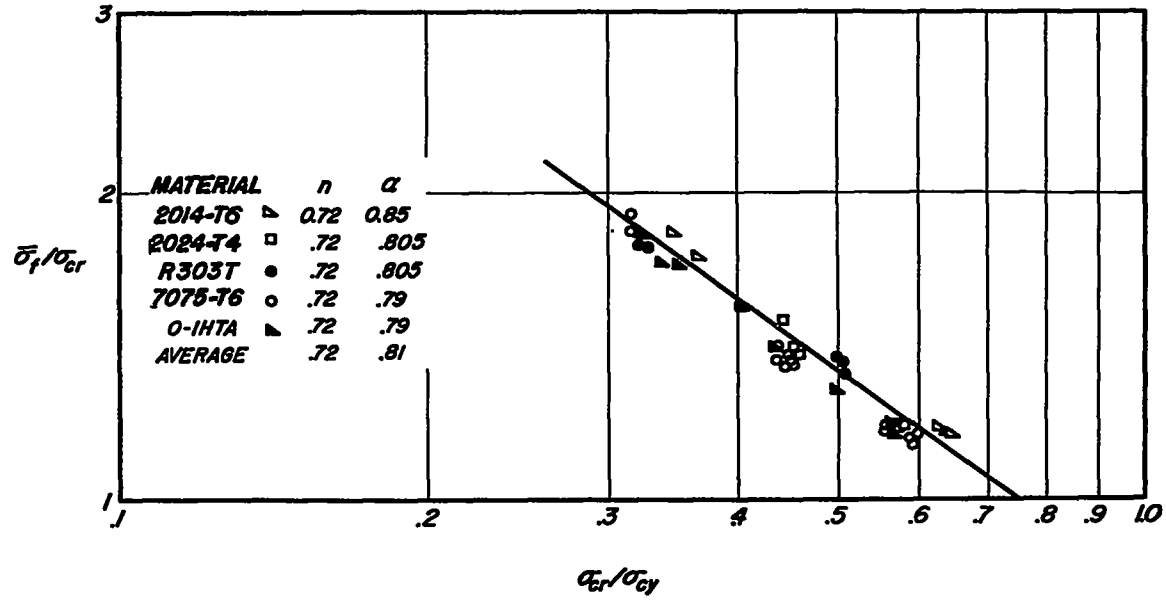

(c) Channel extrusions.

Figure 10.- Concluded.

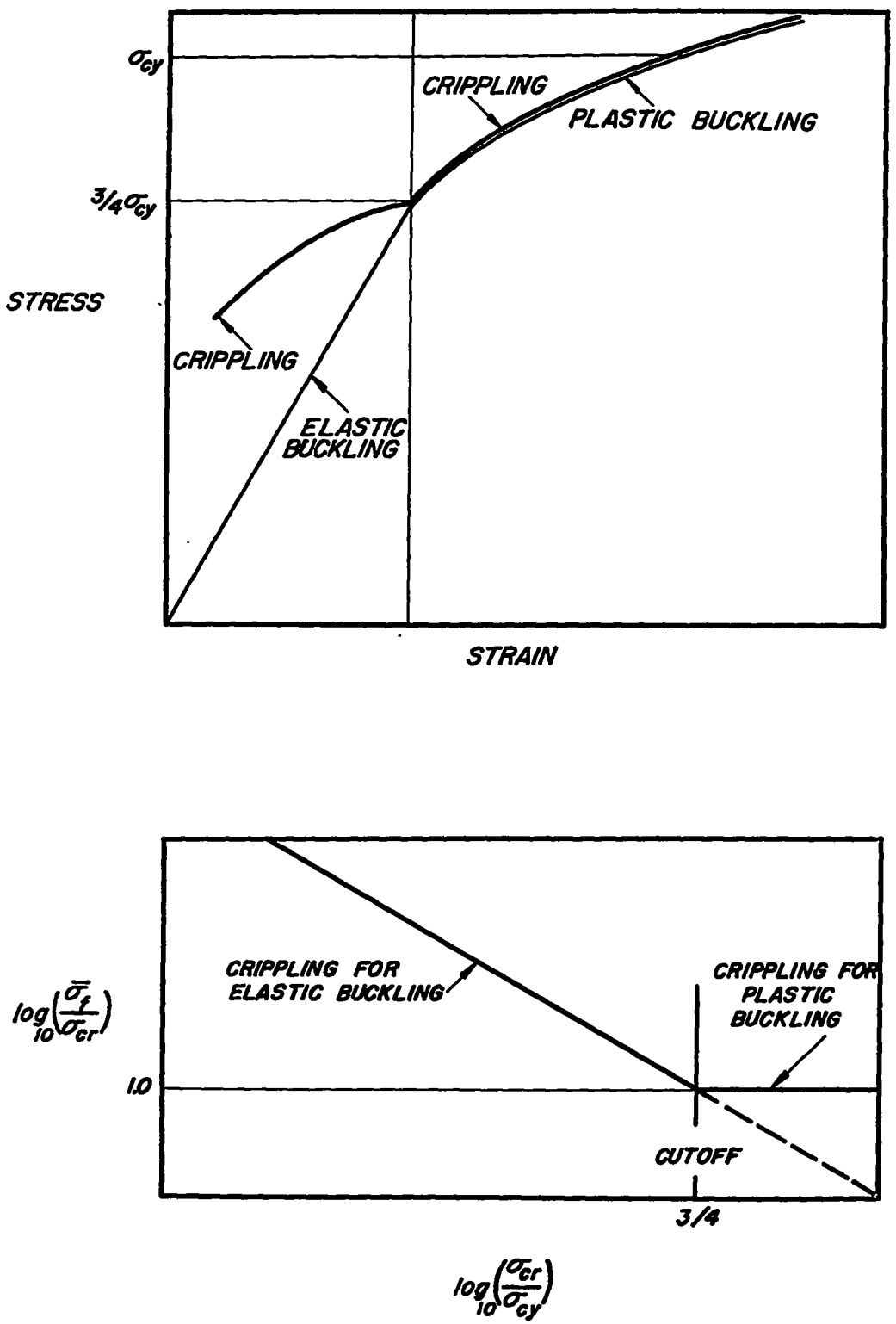

Figure 11.- Relation between buckling and crippling of extruded sections.

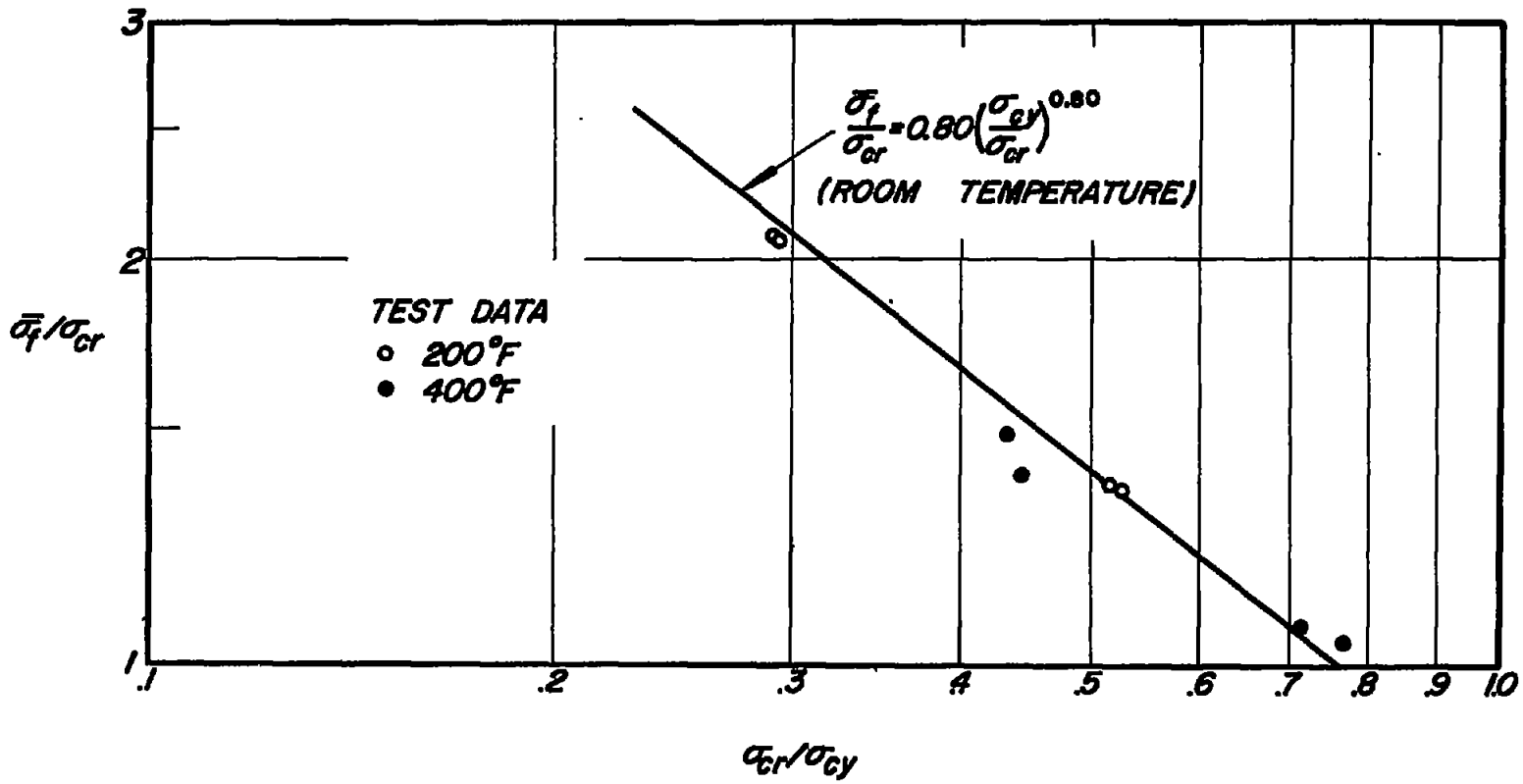

Figure 12.- Short-time crippling data on H-extrusions at elevated temperatures. Data from reference 23.

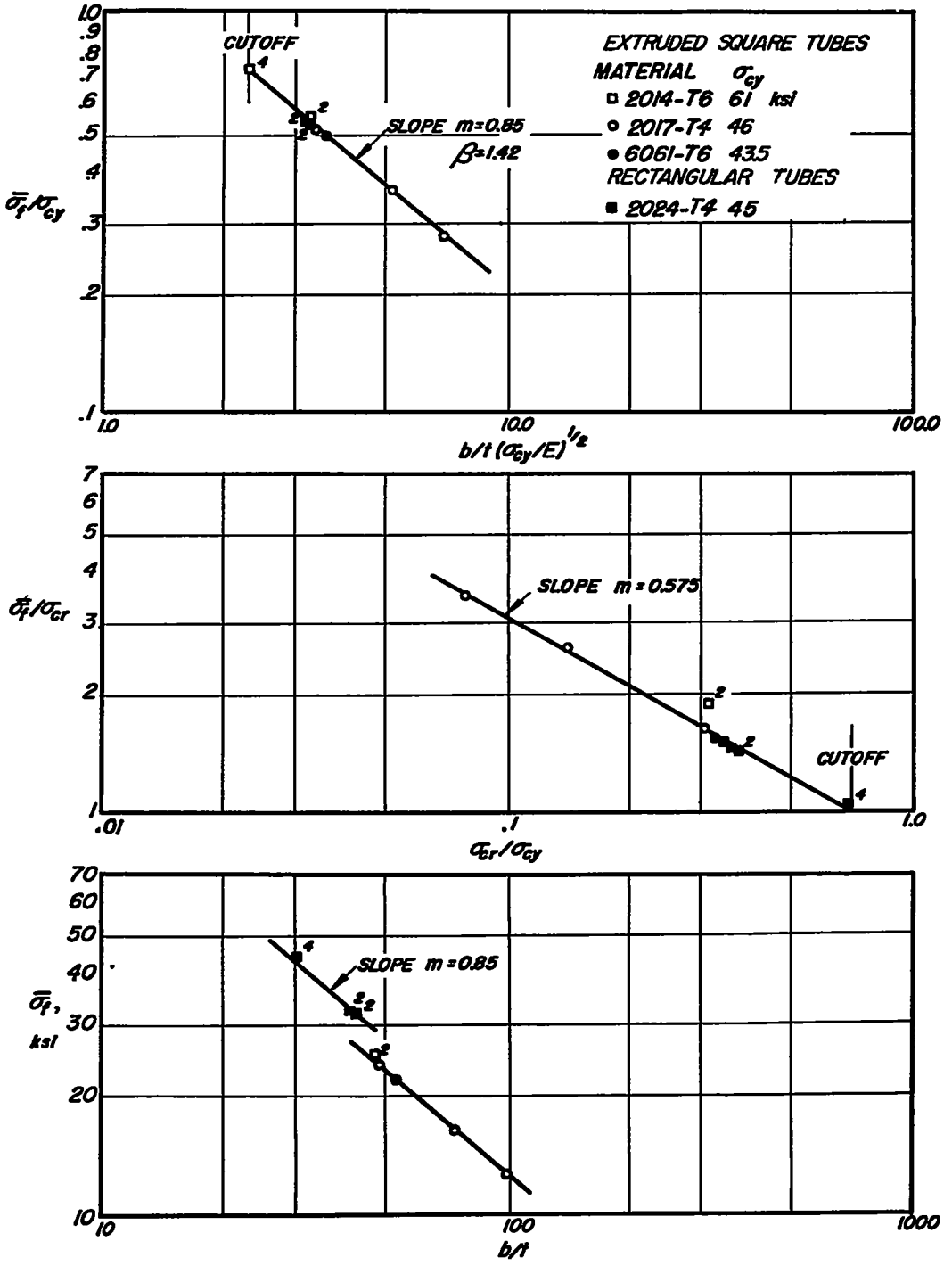

Figure 13.- Crippling data on extruded tubes according to various correlation methods. b/h = 0.583; b/t = (b + h)/2t for rectangular tubes.

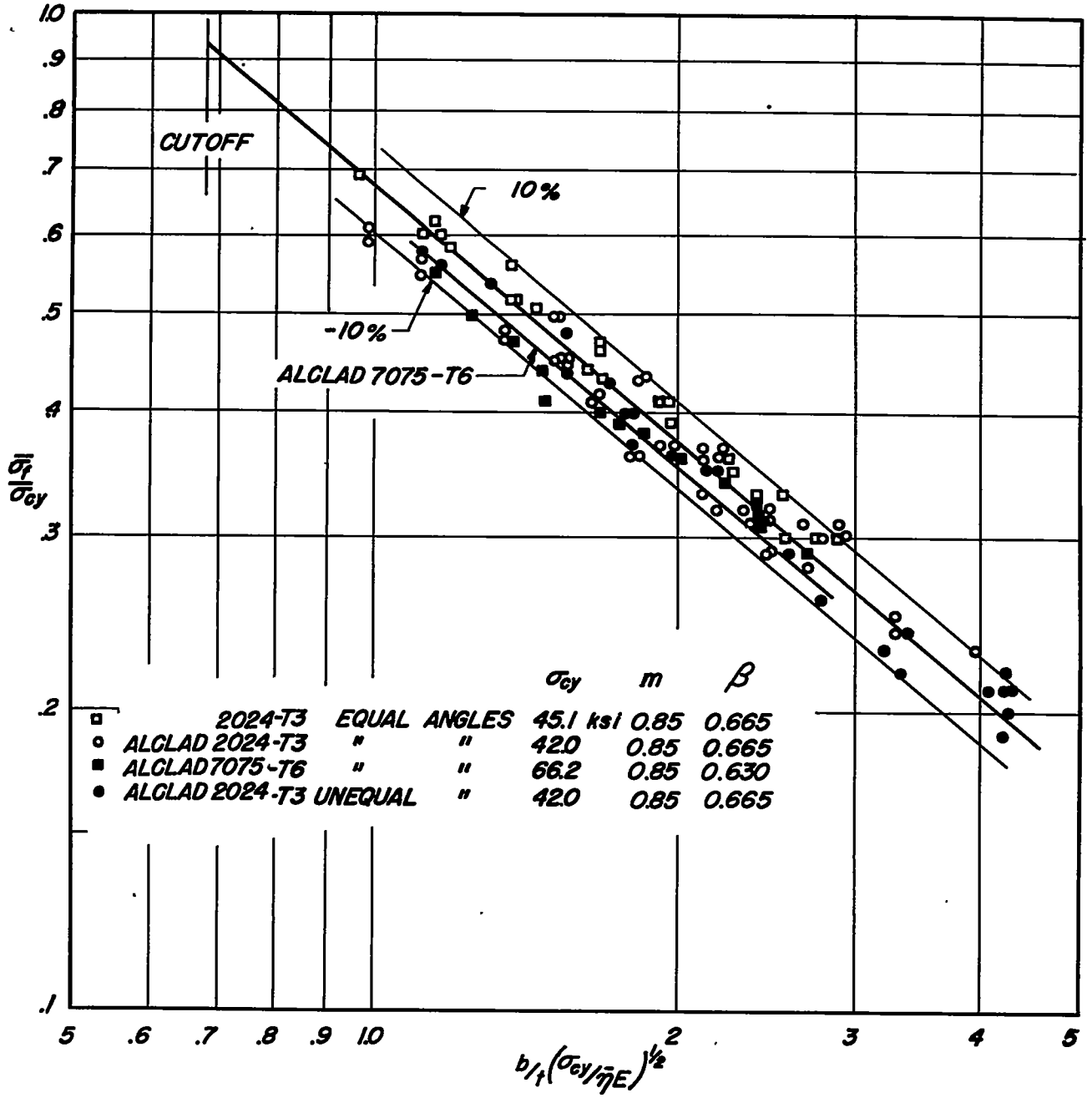

Figure 14.- Generalized crippling analysis of formed angles.

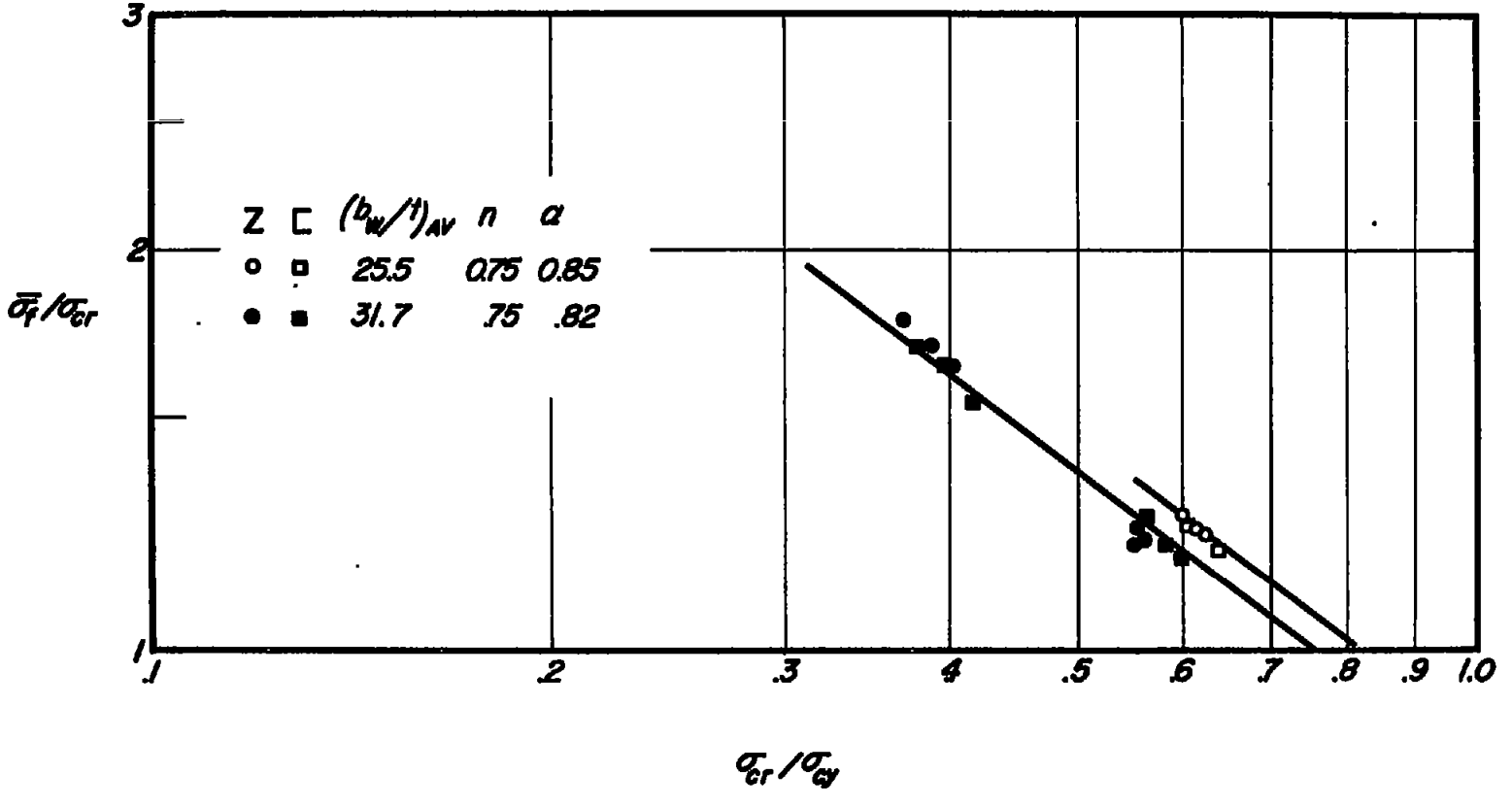

(a) Formed Z- and channel sections of 2017-T3 aluminum alloy.

Figure 15.- Crippling data on formed sections.

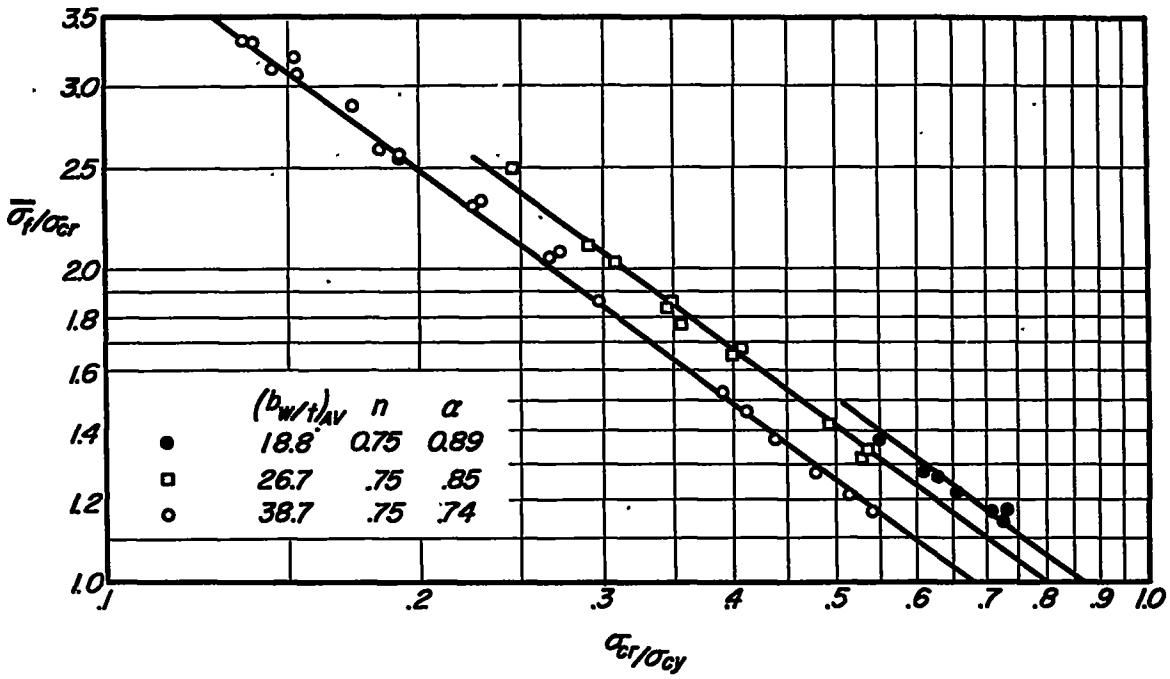

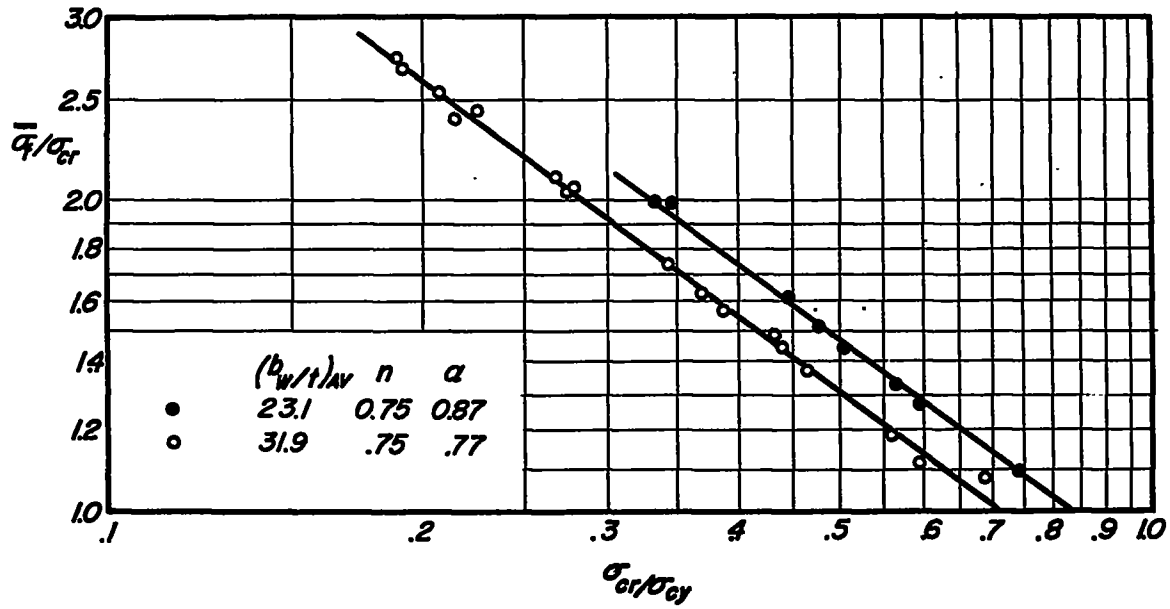

(b) Formed Z-sections of 2024-T3 aluminum alloy.

Figure 15.- Continued.

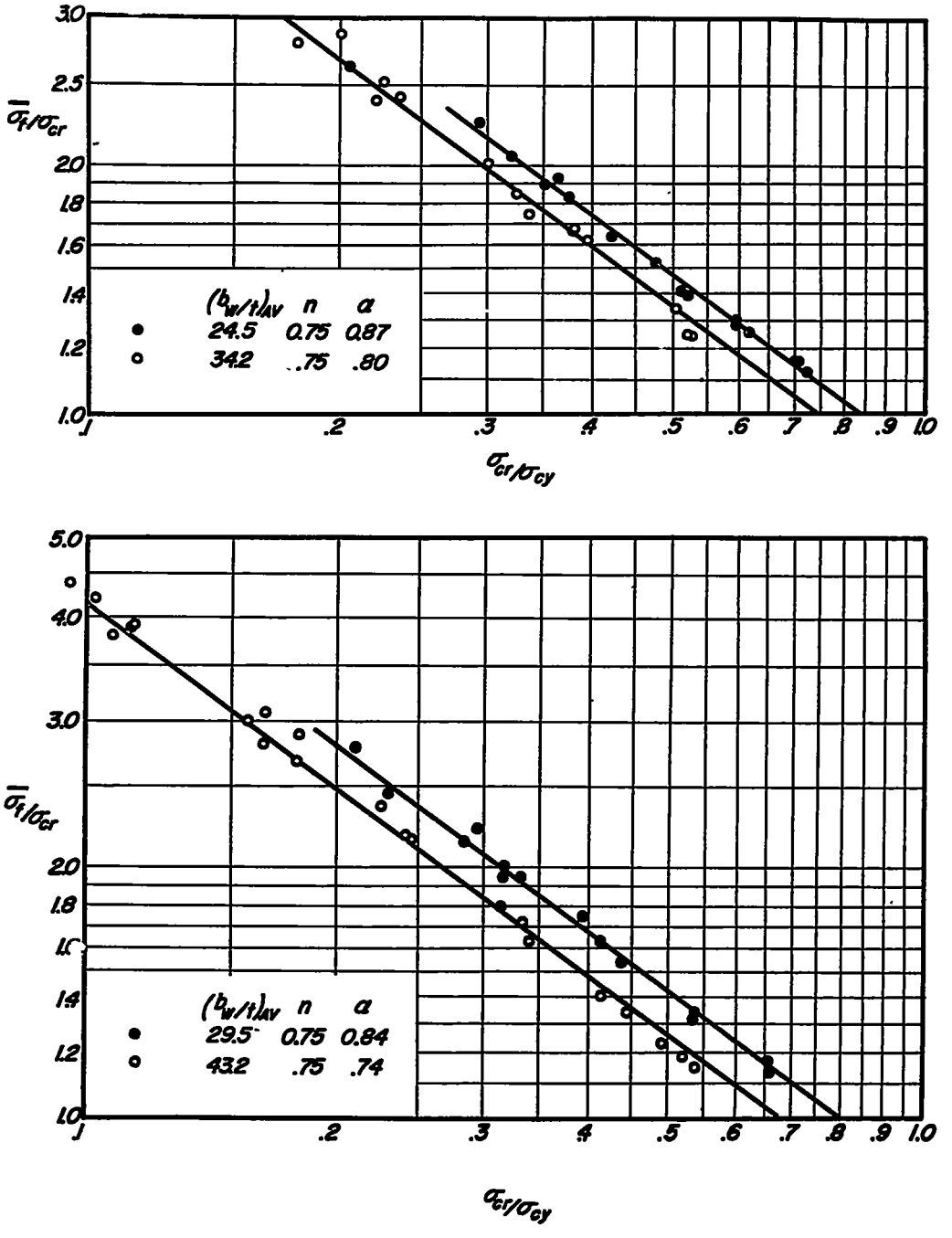

(c) Formed channel sections of 2024-T3 aluminum alloy.

Figure 15.- Continued.

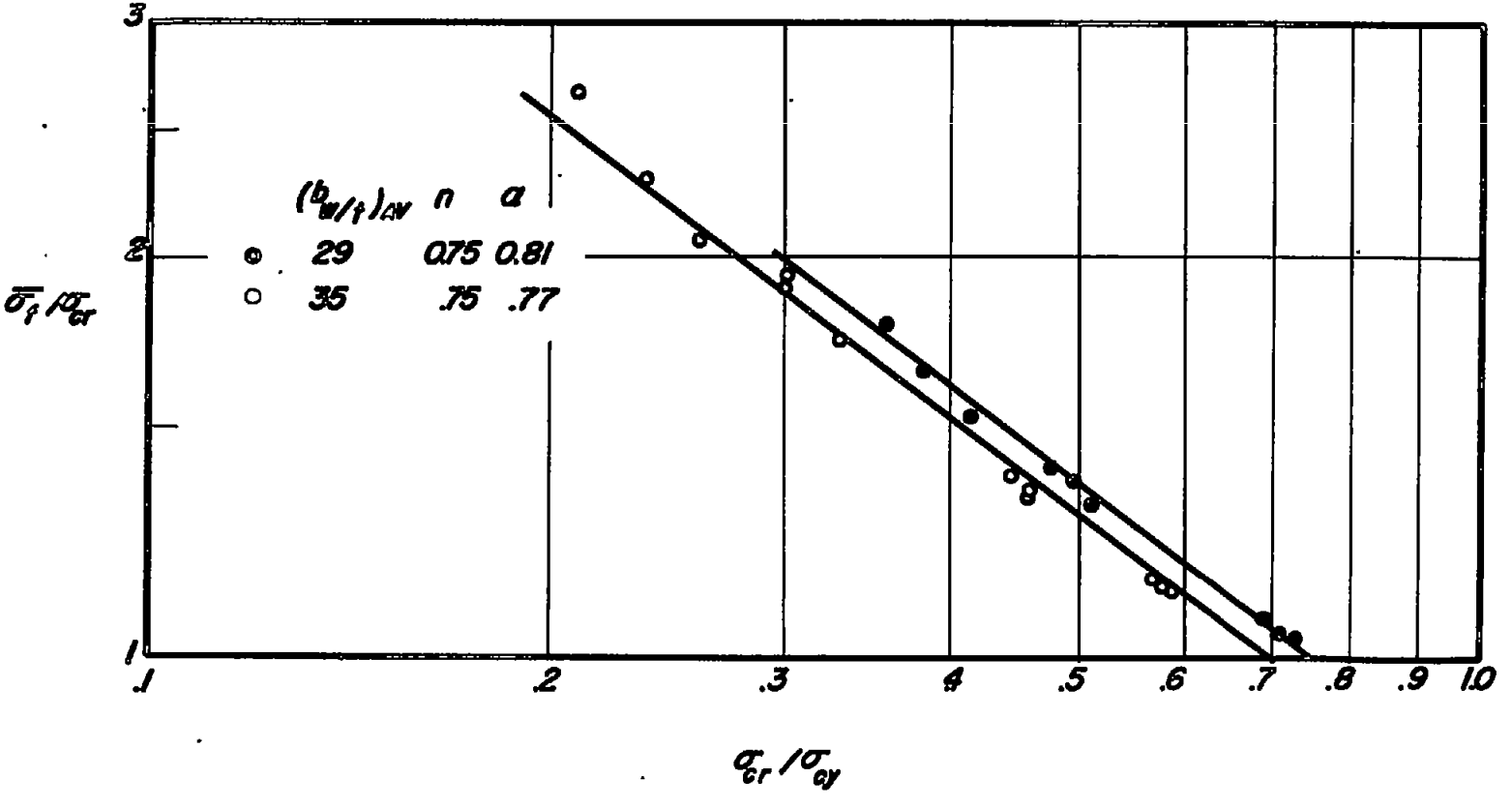

(d) Formed Z-sections of F8-1h magnesium alloy.

Figure 15.- Continued.

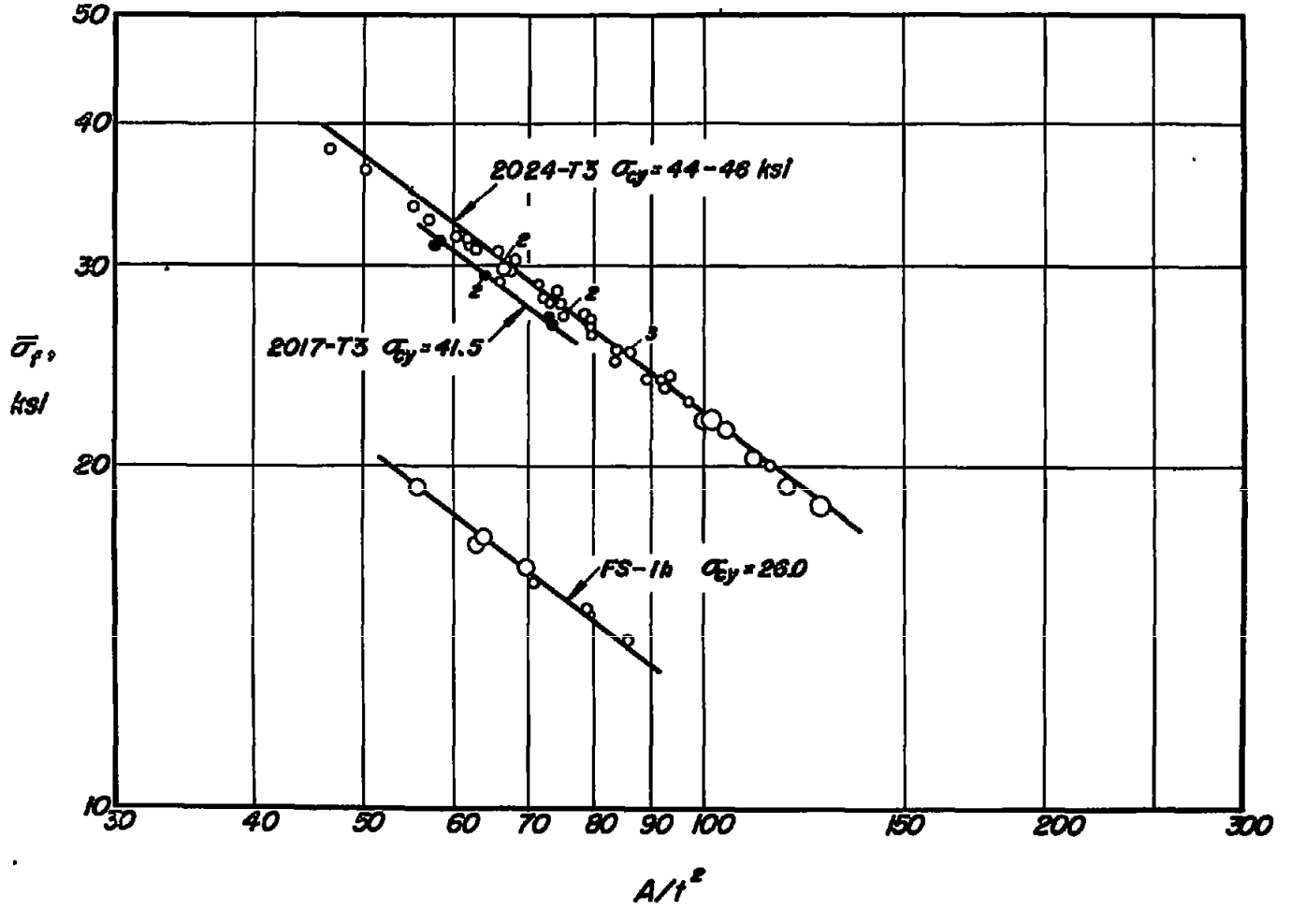

(e) Formed Z- and channel sections. Each circle represents three tests; size of circle indicates scatter of data in each group. Slope, m = 0.75.

Figure 15.- Concluded.

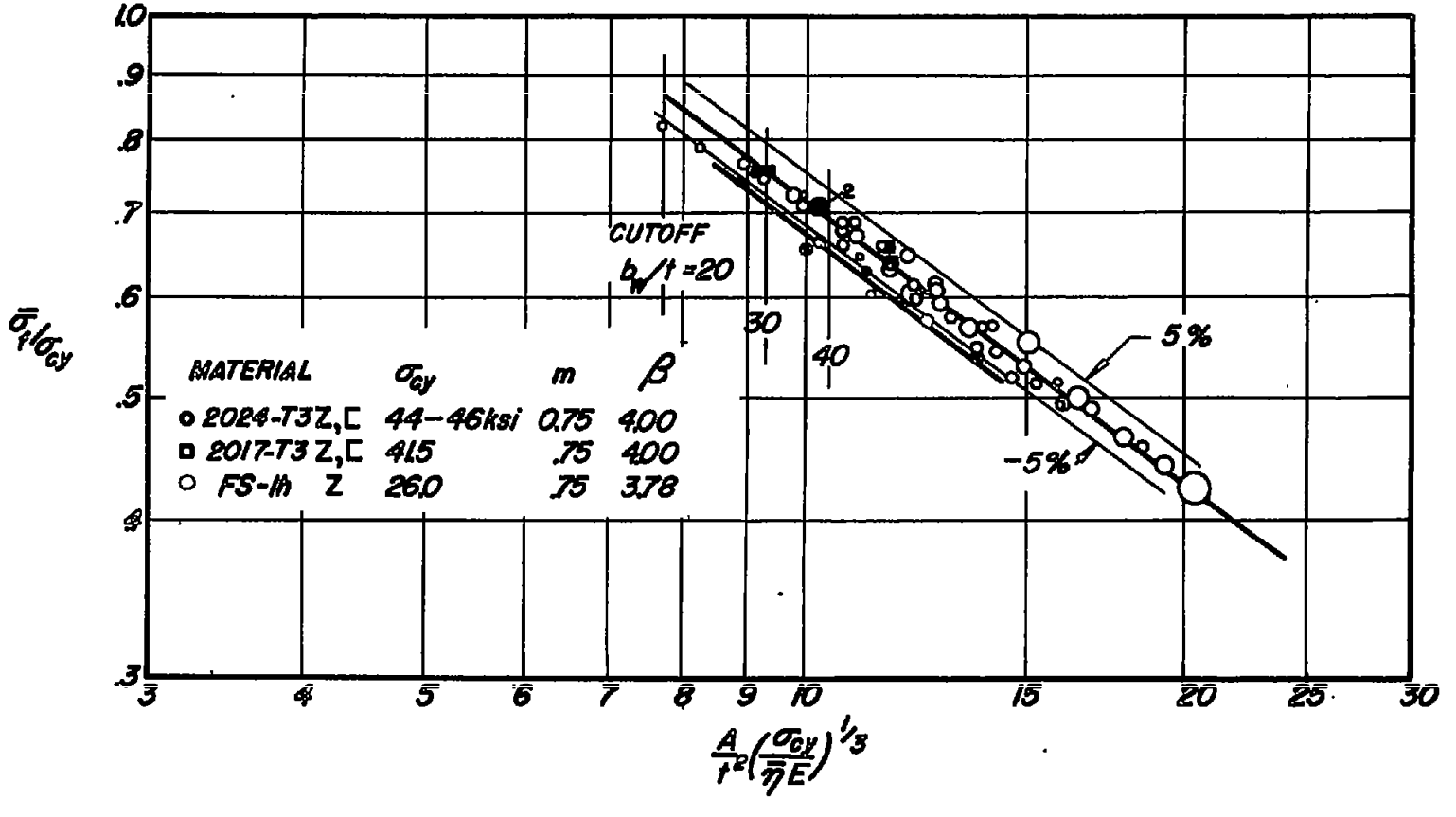

Figure 16.- Generalized crippling analysis of formed Z- and channel sections. Each symbol represents three tests; size of symbol indicates scatter of data in each group.

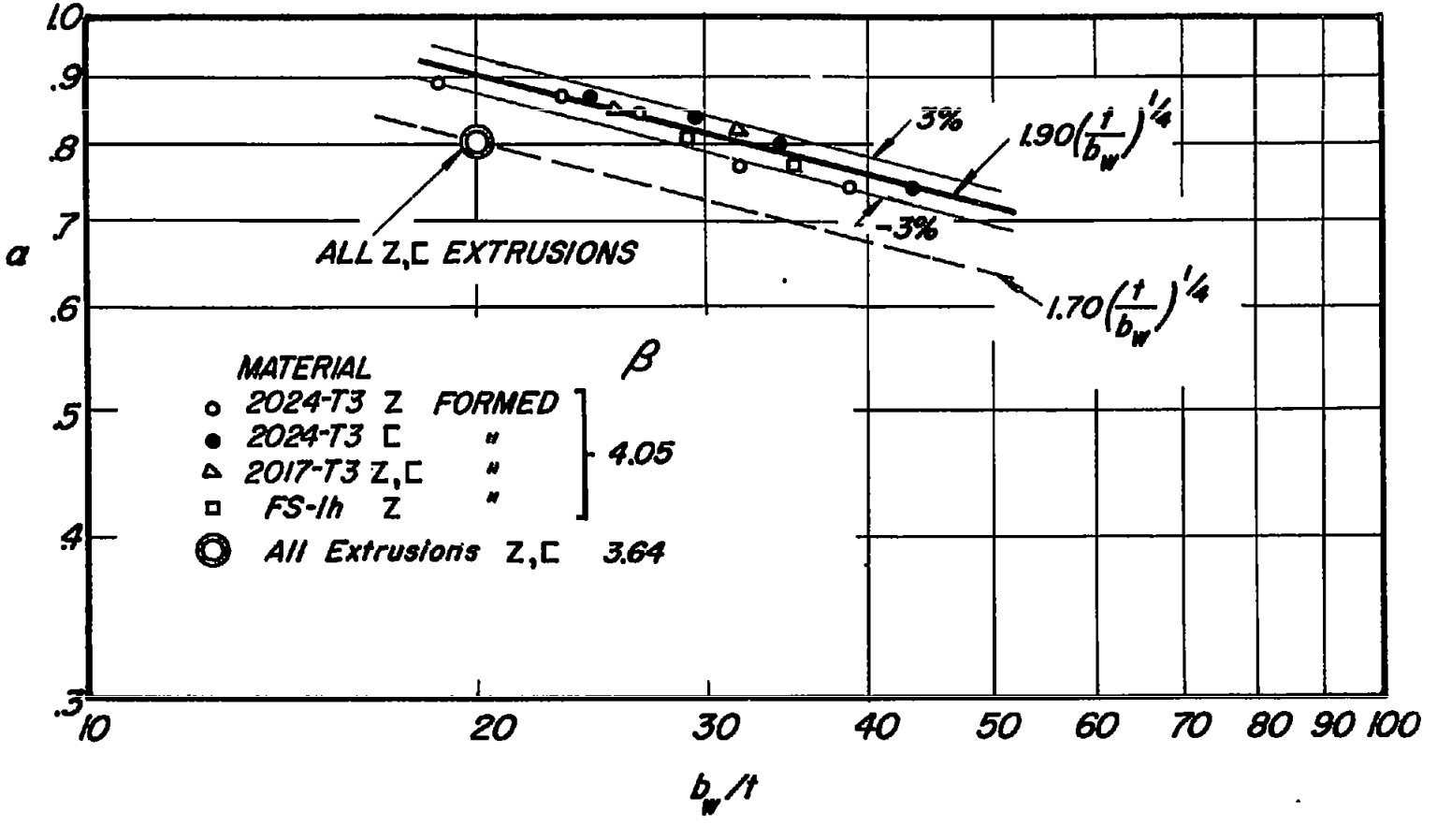

Figure 17.- Variation of crippling coefficient with parameter b_w/t.

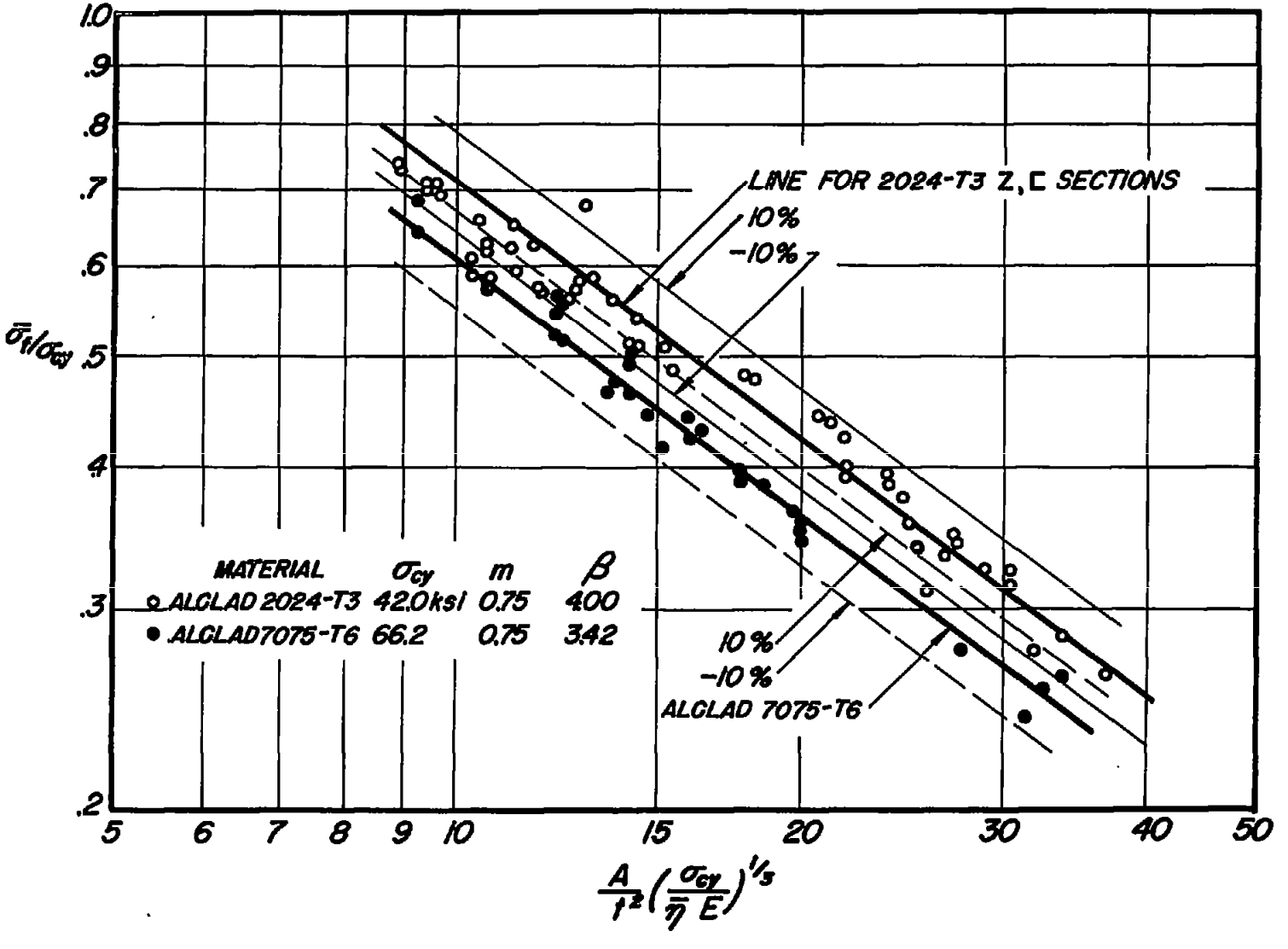

Figure 18.- Generalized crippling analysis of formed alclad channel sections.

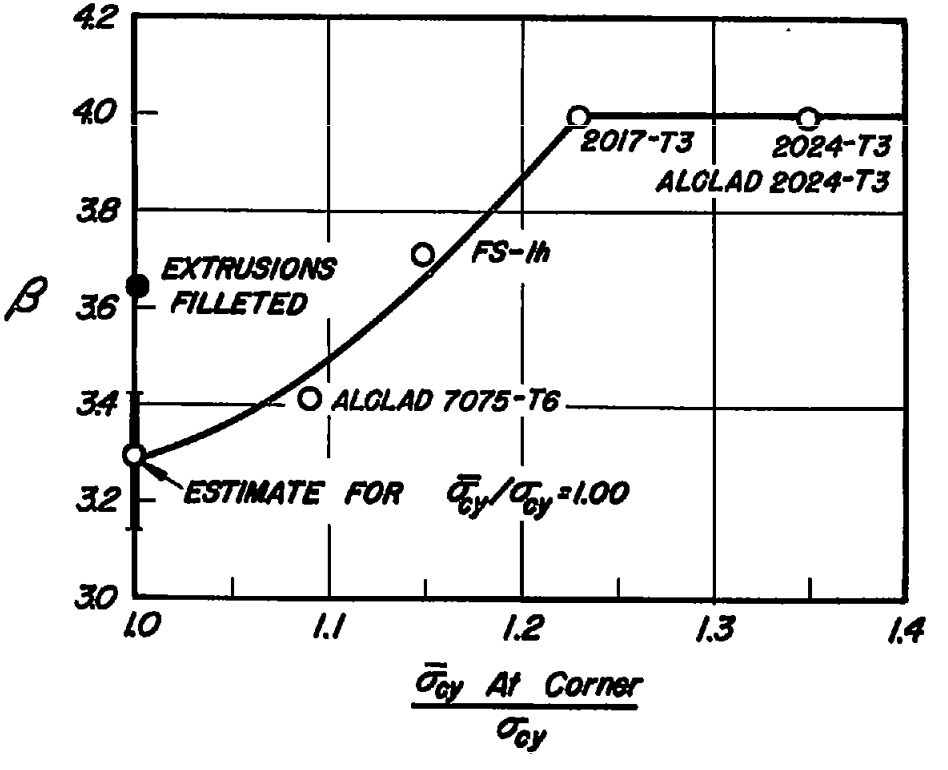

Figure 19.- Variation of generalized crippling coefficient with increased corner properties.

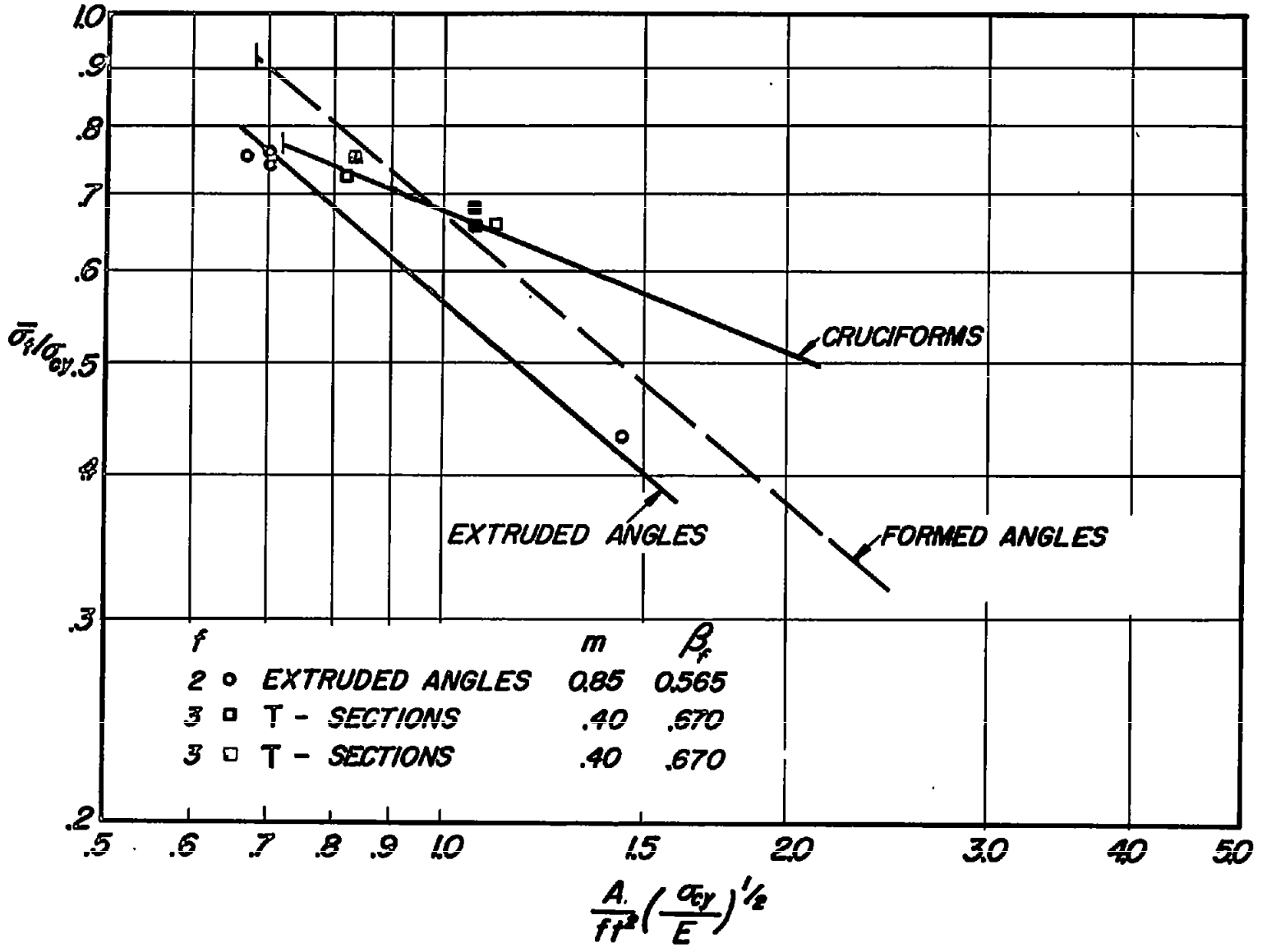

Figure 20.- Generalized crippling analysis of flanged one-corner extruded sections. f, number of flanges.

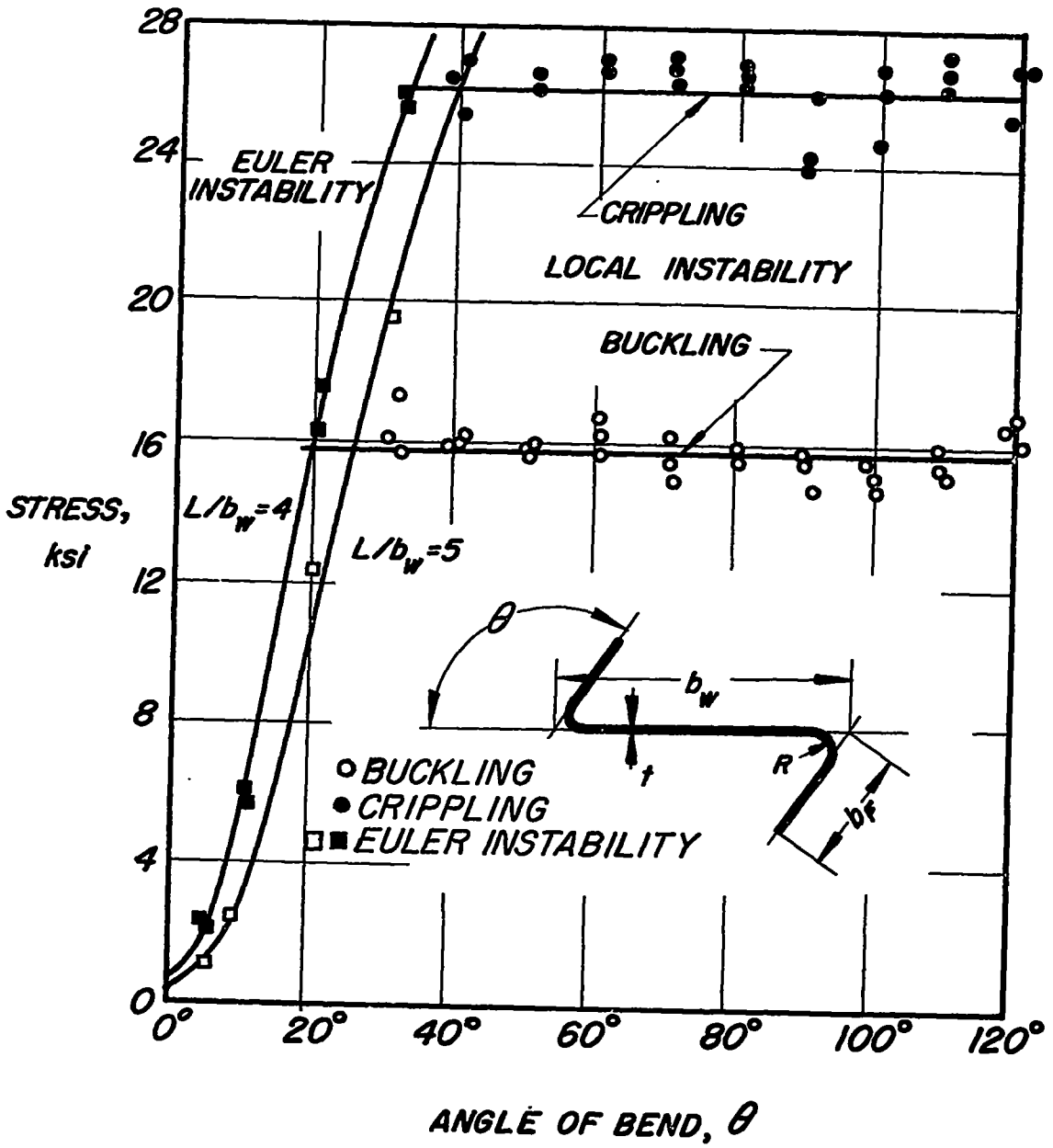

Figure 21.- Effect of bend angles on buckling and crippling of formed Z-sections. L, length; material, 2024-T3 aluminum alloy.

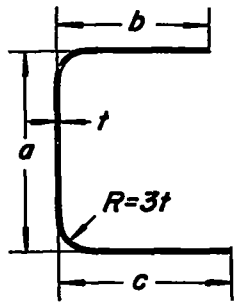

SOURCE: NEEDHAM SHAPE E

SHAPE	t,in.	a,in.	b,in.	c,in.
E1	0.0252	1.991	0.653	0.961
E2	.0253	1.032	.492	.844
E3	.0504	2.141	.418	1.028
E4	.0255	1.213	.408	.935

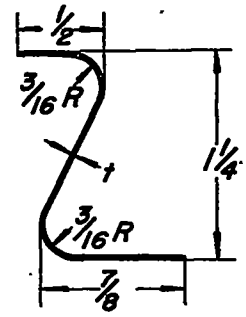

SOURCE: CROCKETT X785-C

t,in.
0.025
.040
.064

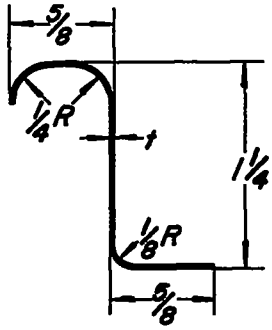

SOURCE: CROCKETT XLS-165

t,in.
0.025
.040

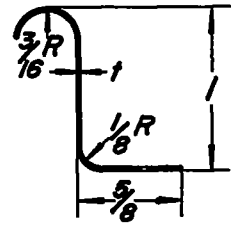

CROCKETT LS-160

t,in.
0.025
.040

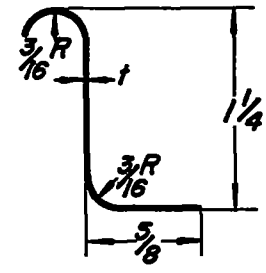

CROCKETT LS-161

t,in.
0.025
.040

Figure 22.- Dimensions of two-corner formed sections used for analysis. Needham, reference 7; Crockett, reference 19.

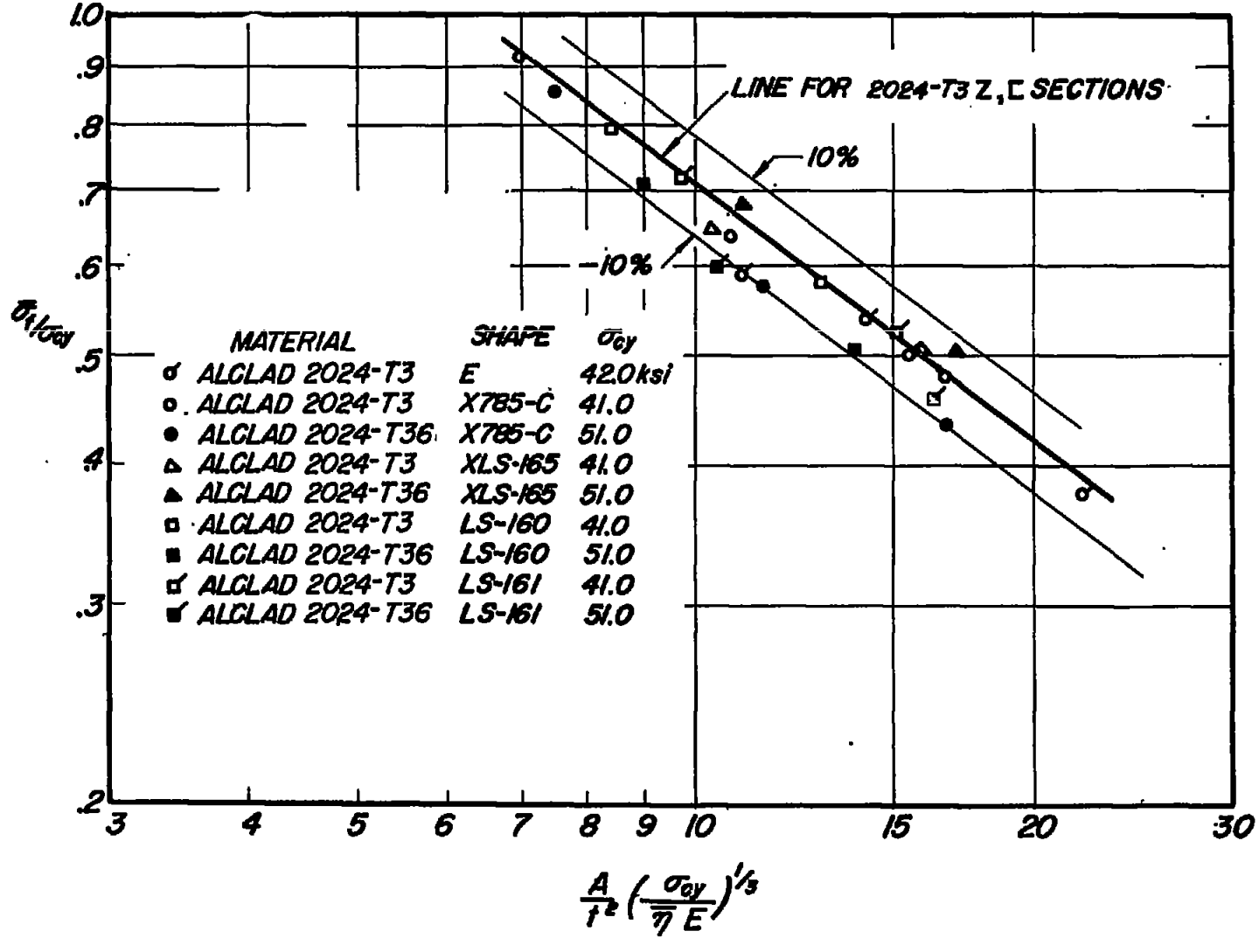

Figure 23.- Generalized crippling analysis of two-corner formed sections.

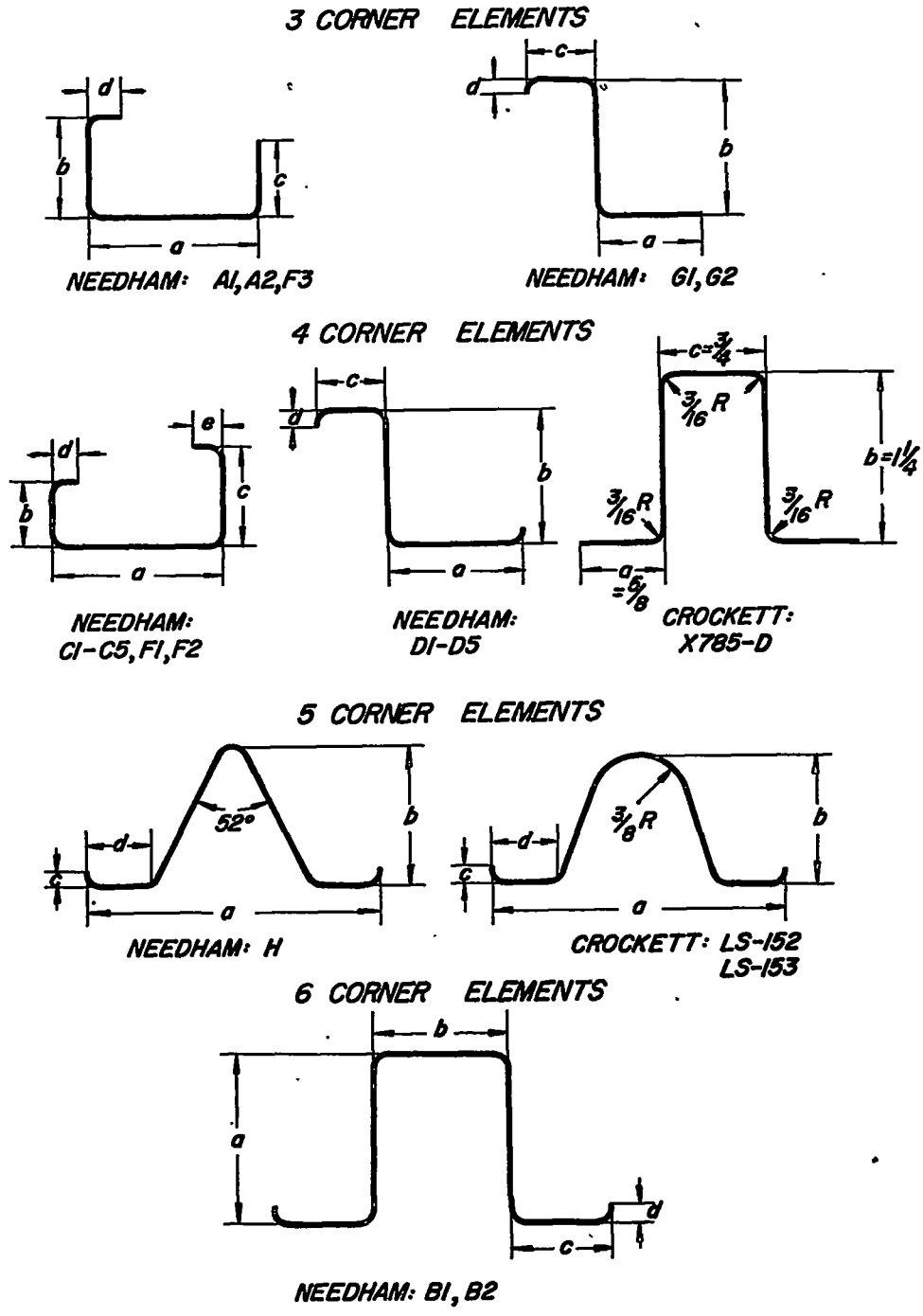

Figure 24.- Multicorner formed sections used for analysis. Bend radius, R = 3t except as noted. Needham, reference 7; Crockett, reference 19.

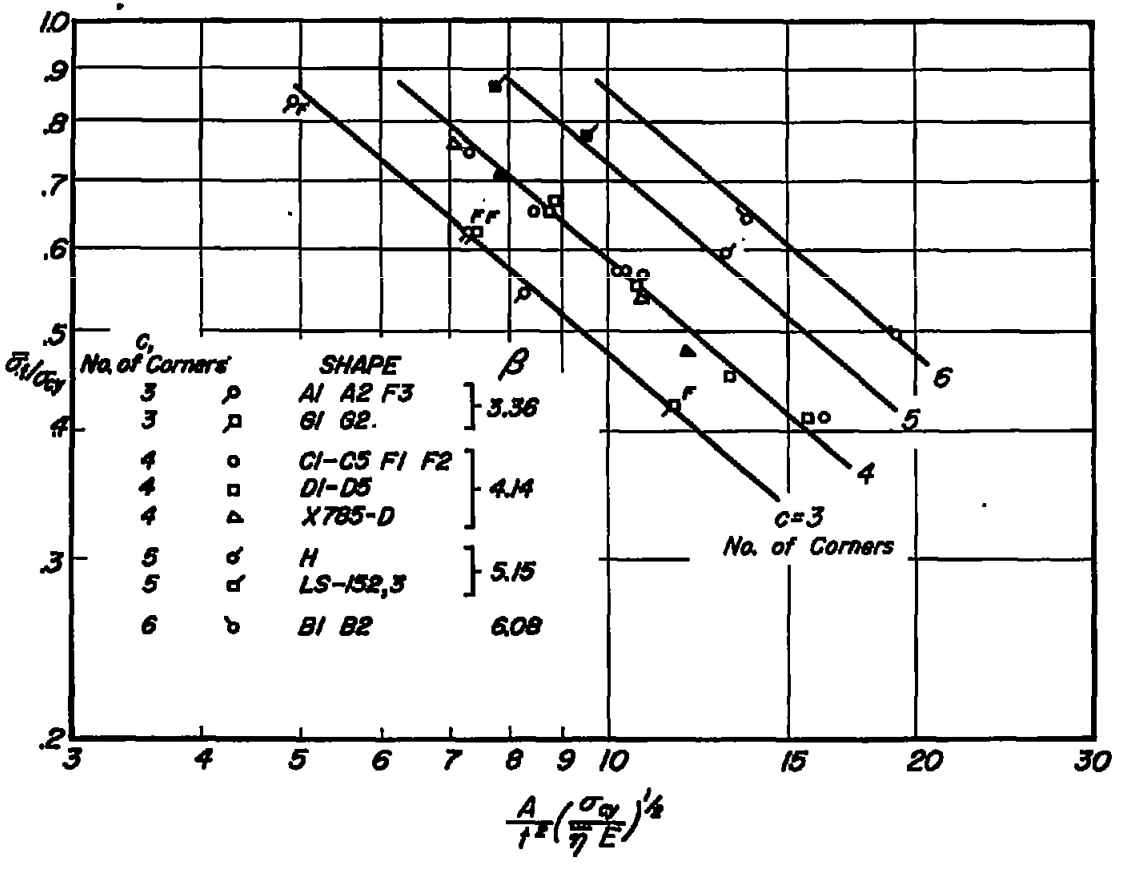

Figure 25.- Generalized crippling analysis of multicorner formed sections according to number of corners. Open symbols, alclad 2024-T3 alloy; solid symbols, alclad 2024-T36 alloy; F indicates flange buckled first.

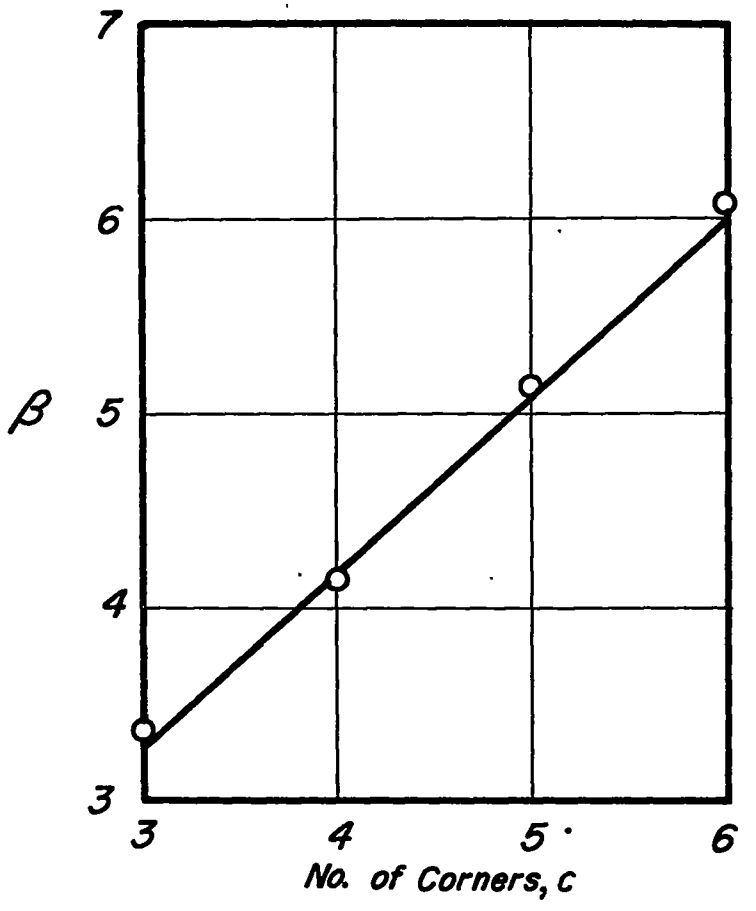

Figure 26.- Variation of generalized crippling coefficient with number of corners.

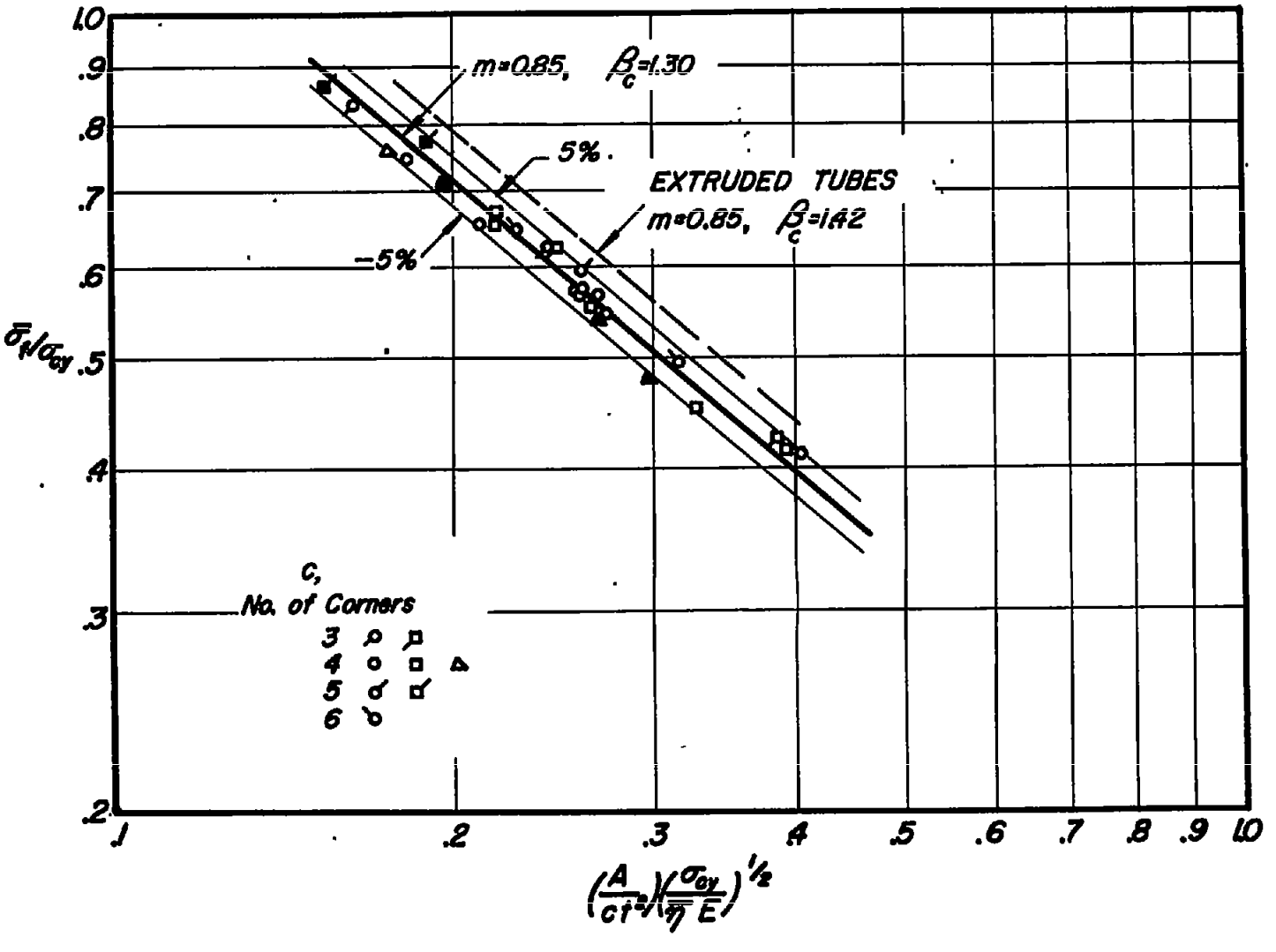

Figure 27.- Generalized crippling analysis of multicorner formed sections. Open symbols, alclad 2024-T3 alloy; solid symbols, alclad 2024-T36 alloy.

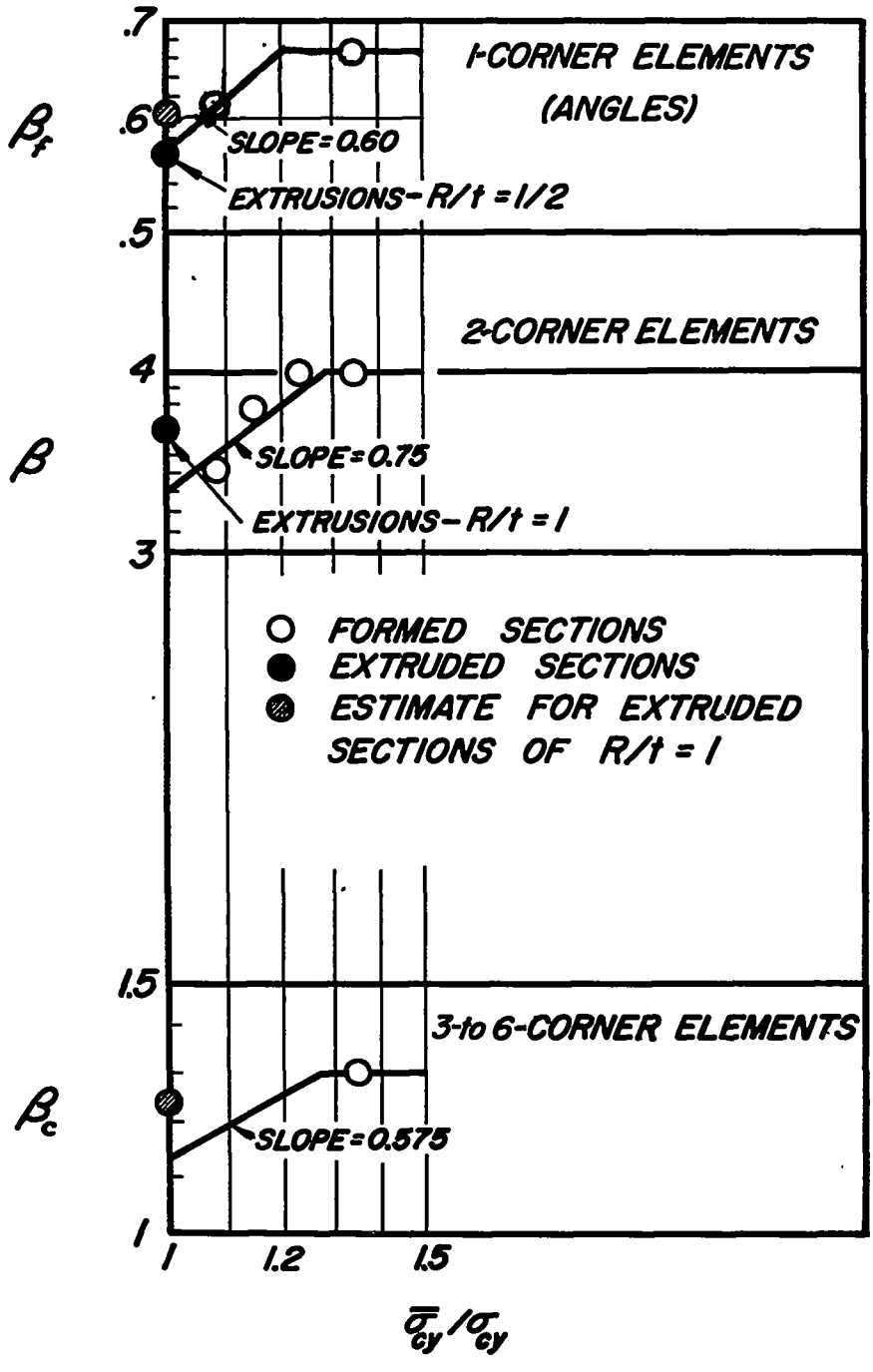

Figure 28.- Estimated variations of generalized crippling coefficient for various sections.